

Atomic Orbital Magnetic Moments in d and f Electron Systems

Tatsuya Shishidou

January 29, 1999

Department of Materials Science, Faculty of Science, Hiroshima
University, Higashi-Hiroshima 739-8526, Japan

Abstract

The orbital magnetic moment and related phenomena in the $3d$ and $5f$ electron systems are examined by the Hartree-Fock approximation (HFA). We will show that the faithful treatment for the exchange interaction is crucially important in describing the orbital magnetism in solids.

First, the atomic ground states of magnetic ions are summarized and the applications of HFA are given to examine its validity in describing magnetic quantities. It is shown that HFA reproduces Hund's first and second rules in the $3d$ and $4f$ systems. The third rule is not reproduced in the less than half filling case. In the $3d$ ions, however, the crystal-field effect, i.e., some kind of the solid-state effect, makes HFA to be a good approximation. In the uranium ions, where the $5f$ spin-orbit interaction is so large, HFA gives their ground state fairly reasonably.

Encouraged by these results, we apply the tight-binding HF method to the insulating CoO in order to study its possible antiferromagnetic structure and orbital state. CoO is well known to exhibit the second kind of antiferromagnetic structure, which is in general described by the four wave vectors $\{Q_i\}$. It is still an open question whether the single- Q structure or multiple- Q structure is realized in CoO. Our calculation, which takes into consideration the $3d$ spin-orbit interaction and the intra-atomic full $3d$ - $3d$ multipole interaction, shows interesting results; in addition to a collinear single- Q structure, a noncollinear quadruple- Q one, both of which are compatible with the neutron diffraction experiment, are obtained as stable HF solutions. The magnitude of the Co orbital magnetic moment is shown to be as large as $\sim 1\mu_B$. Relationship between the orbital magnetism and the band-gap formation is explained.

In free atoms, their ground states have no relation to the monopole Coulomb interaction represented by the Slater integral F^0 , and the other multipole terms determine their magnetic state. In solids, however, the orbital magnetic moment shows strong dependence on F^0 , even in metallic phase. By considering simple systems, the enhancement mechanism of the orbital moment through F^0 is discussed in detail.

Finally, the electronic structure of the ferromagnetic compound US is examined. The U $5f$ spin and orbital magnetic moments are calculated on the basis of the extended Hubbard model and HFA. Our tight-binding model includes the U $6p$, $5f$, $6d$ and $7s$ orbitals and the S $3s$, $3p$ and $3d$ ones, and the intra-atomic $5f$ - $5f$ multipole interaction and the spin-orbit interaction in the $5f$ state are taken into account. Most of parameters involved in the model are determined by fitting with the energy of Bloch electrons in the paramagnetic state obtained by a first-principles calculation based on the local density approximation (LDA). The calculated magnetic quantities are in good agreement with available experimental results. The magnetic circular dichroism spectrum at the U $3d \rightarrow 5f$ x-ray absorption is also calculated and agrees with the recent experiment. It is shown that the exact exchange potential, gained by HFA, can mix the spin up and down states and enhance the effect of the spin-orbit interaction. This feature is not seen in the LDA potential, and the problems of LDA in the estimation of the orbital moments are discussed.

Contents

1	Introduction	3
2	Hartree-Fock approximation	7
2.1	General principle	7
2.2	Second quantization	9
3	Atomic ground state	12
3.1	Hamiltonian	12
3.2	HF Hamiltonian	14
3.3	Magnetic quantities	16
3.4	$3d$ ion	20
3.4.1	Free ion — the Russell-Saunders case and LS -coupling scheme	20
3.4.2	$3d$ ion under O_h crystal field	27
3.5	$4f$ ion	33
3.5.1	Spherical symmetry	33
3.5.2	$4f$ ions in O_h symmetry — Weak crystal field	38
3.6	U ion	43
3.7	Summary	45
4	Tight-binding method	46
5	Antiferromagnetic structure and orbital magnetism in CoO	55
5.1	Introduction	55
5.2	Formulation	58
5.3	Results and Discussions	58
5.4	Conclusion	63
6	Orbital magnetism in metallic $3d$ systems	64
6.1	Introduction	64
6.2	Model	65
6.3	Calculated results	66
6.3.1	$n_{3d} = 7$	66
6.3.2	$n_{3d} = 2$	68
6.3.3	Another filling case	71
6.4	Discussions and Conclusions	71
7	Electronic structure of US	74
7.1	Introduction	74
7.2	Formulation	76
7.2.1	Hamiltonian	76
7.2.2	A test of HF approximation in the atomic limit	77

7.2.3	Determination of the parameter values	78
7.3	Results and Discussions	81
7.3.1	Magnetic ground state	81
7.3.2	U $M_{4,5}$ MCD spectrum	83
7.3.3	HF and LSDA	86
7.4	Conclusions	88
	References	90
	Acknowledgments	94

Chapter 1

Introduction

In recent years, orbital-related phenomena in the $3d$, $4f$, and $5f$ electron systems have been attracted much attention. One of the examples is the orbital ordering in manganites,[1] where the orbital degree of freedom of the $3d$ electrons is coupled with that of the lattice and further considered to be related to the spin ordering. In magnets, the spin-orbit interaction induces the orbital magnetism that is disclosed in phenomena such as magnetocrystalline anisotropy, magneto-optical effects, and x-ray magnetic circular dichroism (MCD). MCD, using the synchrotron-radiated x-ray, becomes a powerful tool for studying ferromagnetic substances, after the discovery of the so-called orbital and spin sum rules.[2, 3] The atomic orbital and spin magnetic moments (μ_{orb} and μ_{spin}) are considered to be the fundamental quantities in magnets, whereas the conventional bulk magnetization measurement just probes the total magnetic moment. The MCD experiment[4, 5, 6] combined with the sum rules enables one to measure the individual contributions of the spin and orbit to the specific-site total moment in ferromagnetic compounds though there are some limitations in the application of the sum rules.[7, 8, 9]

In a free atom or ion, μ_{spin} and μ_{orb} are typically comparable in magnitude. It is known that from Hund's rules one can predict the ground-state electron-configuration for atoms with an unfilled shell. According to them, the total spin angular momentum S and orbital angular momentum L of the open shell are described by the following three rules:

1. S has the largest value consistent with the Pauli exclusion principle.
2. L has the largest value consistent with the Pauli exclusion principle and the first rule.
3. The spin-orbit interaction couples the vectors \mathbf{L} and \mathbf{S} . The coupling is antiparallel way for the less than half filling case, and parallel for the more than half filling case.

The first and second rules are considered to be a consequence of the Pauli principle and Coulomb interaction. The Pauli principle states that the probability of finding two electrons with the same spin direction must vanish as they approach each other because of the antisymmetry of the wavefunction under exchange. Hence electrons with parallel spins tend to be farther apart from each other. The Coulomb repulsion also favors this tendency. The energy cost due to the Coulomb interaction is lower for the longer distance between electrons, resulting in the first rule. The maximum L is considered to be due to the multipole Coulomb interaction. The exceptional cases of the Hund rule LS -coupling scheme are heavy atoms, including the actinides, where the spin-orbit interaction is so strong that the jj coupling or intermediate coupling has priority. At the present day one can perform full quantum mechanical calculations for light atoms without any simplifying approximations, and it is found that μ_{spin} and μ_{orb} follow Hund's rules quite well. For heavy atoms such complete calculations are infeasible because of the large number of electrons. However we

alternatively have good approximate results for heavy atoms. Thus the formation of the atomic magnetic moments are well understood.[10]

In solids, the number of electrons involved is tremendously large and complete calculations like those for free atoms are never possible. Therefore it is convenient to have simplified models or methods that describe magnetism in solids to first approximation. Density functional theory (DFT), proposed first by Hohenberg and Kohn,[12] is in principle a rigorous theory for a system of interacting electrons, based on the electron density distribution $n(\mathbf{r})$, instead of the many-electron wave function $\Psi(\mathbf{r}_1, \mathbf{r}_2, \dots)$. [11] DFT states that the exchange-correlation energy of electrons E_{xc} , which is, in the atomic case, the driving force of the spin and orbital polarization that leads to Hund's rules, is to be expressed by a functional in terms of $n(\mathbf{r})$. This allows one to substitute the many-body problem for dealing with a non-interacting electron system which gives the exact $n(\mathbf{r})$. The true functional $E_{xc}[n(\mathbf{r})]$ is, however, not known, and this is the point where the major approximation is needed to proceed with DFT. Usually the so-called local density approximation (LDA) is applied with being guided by the results of analytical or Monte Carlo calculations for a homogeneous interacting electron gas. Thus, in the itinerant limit, LDA gives exact results. The standard procedure of this approximation is as follows. At each point in space the exchange-correlation properties are assumed to be determined by the *local* charge density of electrons. The exchange-correlation energy density ε_{xc} is simply assumed to be given by that of a homogeneous electron gas with the same charge density. The total exchange-correlation energy is gained by integrating over all space: $E_{xc} = \int n(\mathbf{r}) \varepsilon_{xc}(n(\mathbf{r})) d\mathbf{r}$. Extension to the spin-polarized case is gained analogously and known as the local spin density approximation (LSDA). In this case, the exchange-correlation energy density is assumed to be determined by the local spin-magnetization density $m(\mathbf{r}) = n_{\uparrow}(\mathbf{r}) - n_{\downarrow}(\mathbf{r})$ in addition to the charge density $n(\mathbf{r}) = n_{\uparrow}(\mathbf{r}) + n_{\downarrow}(\mathbf{r})$: $\varepsilon_{xc}(\mathbf{r}) = \varepsilon_{xc}(n(\mathbf{r}), m(\mathbf{r}))$. As the explicit form of ε_{xc} , again, the results of analytical or Monte Carlo calculations for a homogeneous electron gas, with the spin polarization, are usually referred to.

With the progress of computer facilities, the first-principles band-structure calculations based on L(S)DA, where there is no free parameter, have been carried out for several decades. It has been shown that LSDA yields good results about the electronic structure and μ_{spin} of itinerant magnetic materials containing the $3d$ transition-metal elements.[13] In the $4f$ and $5f$ systems, the contribution of μ_{orb} to the total moment is comparable with μ_{spin} in magnitude, even in solids. To handle the orbital magnetism, the effect of the spin-orbit interaction (SOI), i.e., one of the relativistic effects, has been included in the calculations, but still based on LSDA (hereafter we denote this scheme as LSDA+SOI). Such attempts are, however, not necessarily encouraging. In most cases, the calculated orbital moments are too small compared with experiments.[14, 15, 16, 17, 18, 19, 20, 21] Even in the $3d$ systems, where μ_{orb} is typically quite small, LSDA+SOI seriously underestimates its contribution.[14, 15, 16, 17, 18] Among the $5f$ systems, ferromagnetic uranium compounds are rather extensively studied.[18, 19, 20, 21] Due to the less than half filling in the $5f$ state, μ_{orb} and μ_{spin} of U site are aligned in the antiparallel way, and μ_{orb} is typically larger than μ_{spin} in magnitude, even in metallic substances. In the LSDA+SOI calculations for uranium compounds, the condition $|\mu_{\text{orb}}| > |\mu_{\text{spin}}|$ is successfully reproduced, but the calculated μ_{orb} is usually still small, leading to a too small magnitude of the total magnetic moment, $|\mu_{\text{orb}}| - |\mu_{\text{spin}}|$, compared with experiments.

Why does this method, LSDA+SOI, fails to describe the contribution of the orbital moment? It is supposed that the following reasons are crucial:

1. The homogeneous electron-gas picture, on which L(S)DA is based, clashes with the existence of the orbital moment. The orbital angular momentum comes from the rotational movement about a nucleus, whereas, in the homogeneous picture, there is no nucleus and hence electrons are unbounded.

2. The correlation of different orbital states, which leads to Hund's second rule in the case of free atoms, is considered to be *nonlocal* effect. The orbital state is characterized by the rotational properties of the electronic wave function about the nucleus. In other words, one needs to know the charge density of the electrons around the nucleus, and not just at the single point in question. On the other hand, in L(S)DA, it is a *local* potential that has been used to describe every exchange-correlation effect.
3. LSDA is based on the *spin* DFT, where the total energy is minimized with respect to $n(\mathbf{r})$ and the *spin*-magnetization density $m(\mathbf{r})$. Even if an exact functional is known, which is able to include implicitly all effects related to the orbital magnetism, DFT just guarantees the densities used in the variational process are to be reproduced exactly, in this case, the total and spin densities; not the orbital moment. So long as we are based on the spin DFT, there is no guarantee that the orbital-related quantities can be reproduced.

From these reasons, it can be said that, in LSDA, there is no theoretical framework to determine μ_{orb} self-consistently. Extension of LSDA, or another framework is necessary for describing the itinerant magnetism including the orbital contribution. The correlation needed here is atomic one, opposite to the homogeneous electron-gas picture.

Historically, discussions of the itinerant ferromagnetism, based on the band picture, go back to the pioneering work by Slater.[22] He stood in the tight-binding Hartree-Fock (HF) method, and showed that one can deduce the exchange splitting of $3d$ bands from the intra-atomic Coulomb interaction. In his theory the orbital magnetic effect was not taken into account; he considered only the spin polarization. It is supposed that the orbital polarization should be also related to the intra-atomic Coulomb interaction, not only driven by the relativistic spin-orbit coupling.

The effect of the Coulomb interaction between electrons is to be classified into the following three categories: (i) the classical Coulomb interaction; (ii) a correlation effect between electrons with the same spin orientation, which is a quantum-mechanical effect gained by Hartree-Fock approximation (HFA); (iii) the remaining correlation effect, which cannot be managed by HFA. For the sake of clear distinction, the effect (ii) is called the "exchange effect", and (iii) the "correlation effect". HFA is a well-known and well-defined approximation, where the many-body wave function is expressed by a single Slater determinant. By definition, although it cannot describe the correlation effect, one can obtain an exact exchange potential by HFA. In L(S)DA, both of the exchange and correlation effects are taken into consideration to some extent, but not completely, by referring to the homogeneous electron gas, and there is no guarantee that those effects in L(S)DA correspond well to the real ones.

The aim of this thesis is to examine the effect of the atomic correlation for the orbital magnetism in solids, featuring the effect of the exchange interaction based on model calculations. Our model is the so-called extended Hubbard model, where we consider the full degeneracy of relevant orbitals, the spin-orbit interaction, and the intra-atomic multipole Coulomb interaction which is treated within HFA. It is shown that the faithful treatment for the intra-atomic exchange interaction is crucially important for good descriptions of the orbital magnetism in the $3d$ or $5f$ systems.

Organization of this thesis is the following. Chapters 2-4 give introductory explanations concerned about the models and concepts used in this thesis. In Chap. 2, principles of HFA are represented in detail. In Chap. 3, we formulate the intra-atomic interactions and deduce the corresponding HF Hamiltonian. Atomic ground state is examined by HFA to investigate its validity and accuracy in describing the magnetic quantities. It is shown that HFA reproduces Hund's first and second rules for the $3d$ and $4f$ atoms and that it is a fairly good approximation for uranium atom where the spin-orbit interaction is strong. Limitations of HFA are also given. In Chap. 4, the tight-binding method, which is used in

this thesis to represent the electron kinetic energy, is explained. Using the tight-binding HF model, the orbital-related magnetic quantities and effects in solids are discussed in Chaps 5-7. In Chap. 5, possible magnetic structure of insulating CoO is discussed. Both of the facts that the orbital moment of the $3d$ state in CoO is so large and that CoO is an insulator, indicate that LSDA calculation is not suitable for CoO. We obtained interesting results by the present method. In Chap. 6, the orbital moment in the metallic $3d$ systems is discussed. It is shown that the monopole Coulomb interaction, to which the magnetic quantities in the free atoms are independent, plays an important role to enhance the orbital magnetic moment, not only in the *insulating* phase but also in the *metallic* phase. Finally in Chap. 7, discussions about the uranium $5f$ state and the role of the exact exchange potential are given with taking US as an example. US is known as an itinerant ferromagnetic compound, but its orbital moment is quite large. It is shown that the exact exchange potential will enhance the effect of the $5f$ spin-orbit interaction and mix the spin up and down states. MCD spectrum and a detailed comparison between the potentials in LSDA and HFA are also given.

Chapter 2

Hartree-Fock approximation

2.1 General principle

Mean-field approximation is often used as the first approach to understand interacting-electron system. It provides us a simple picture that each electron is moving independently in the one-electron potential which comes from the averaged interaction with all other electrons. The Hartree-Fock approximation (HFA) is one of the well known approach in this direction and is based on the variational method. In HFA, the ground-state wavefunction for N -electron system is expressed by a single Slater determinant:

$$\Psi^{\text{HF}} = \frac{1}{\sqrt{N!}} \begin{vmatrix} \psi_1(\mathbf{x}_1) & \psi_2(\mathbf{x}_1) & \cdots & \psi_N(\mathbf{x}_1) \\ \psi_1(\mathbf{x}_2) & \psi_2(\mathbf{x}_2) & \cdots & \psi_N(\mathbf{x}_2) \\ \vdots & \vdots & & \vdots \\ \psi_1(\mathbf{x}_N) & \psi_2(\mathbf{x}_N) & \cdots & \psi_N(\mathbf{x}_N) \end{vmatrix} \quad (2.1)$$

The single-electron states $\psi_k(\mathbf{x})$'s ($k = 1, \dots, N$) are to be determined by the variational method. Here in Eq. (2.1), \mathbf{x}_j stands for both of the coordinate in the real space \mathbf{r} , and the spin variable σ , of the j -th electron. $\psi_k(\mathbf{x})$'s include the spin function and they are orthonormalized with each other;

$$\int \psi_k^*(\mathbf{x})\psi_{k'}(\mathbf{x}) d\mathbf{x} = \delta_{kk'}. \quad (2.2)$$

We consider the following Hamiltonian which consists of 2 parts:

$$H = \sum_{i=1}^N h(\mathbf{x}_i) + \frac{1}{2} \sum_{i=1}^N \sum_{j=1, (i \neq j)}^N v(\mathbf{x}_i, \mathbf{x}_j), \quad (2.3)$$

where h includes any kind of one-body Hamiltonian, for instance, the kinetic energy, the spin-orbit interaction, the Zeeman energy, the potential energy in the periodic crystal lattice, etc. The second term represents the Coulomb interaction between electrons, $v(\mathbf{x}_1, \mathbf{x}_2) = 1/|\mathbf{r}_1 - \mathbf{r}_2|$. The expectation value of (2.3) in the ground state (2.1) is calculated as follows:

$$\langle \Psi^{\text{HF}} | H | \Psi^{\text{HF}} \rangle = \sum_{k=1}^N \langle k | h | k \rangle + \frac{1}{2} \sum_{k=1}^N \sum_{k'=1}^N \{ \langle k k' | v | k k' \rangle - \langle k k' | v | k' k \rangle \}, \quad (2.4)$$

where we have used the relation (2.2) and defined the following expressions,

$$\langle k | h | k \rangle = \int \psi_k^*(\mathbf{x}) h(\mathbf{x}) \psi_k(\mathbf{x}) d\mathbf{x} \quad (2.5)$$

and

$$\langle kk'|v|k_1k_1'\rangle = \int \int \psi_k^*(\mathbf{x})\psi_{k'}^*(\mathbf{x}')v(\mathbf{x},\mathbf{x}')\psi_{k_1}(\mathbf{x})\psi_{k_1'}(\mathbf{x}') d\mathbf{x}d\mathbf{x}'. \quad (2.6)$$

The interaction matrix elements in Eq. (2.4), $\langle kk'|v|kk'\rangle$ and $\langle kk'|v|k'k\rangle$, are called the Coulomb integral and the exchange integral, respectively. The minimization problem of $\langle \Psi^{\text{HF}}|H|\Psi^{\text{HF}}\rangle$ in terms of ψ_k 's under the condition of (2.2) yields the following equation with Lagrange's undetermined multiplier $\epsilon_{kk'}$:

$$\frac{\partial}{\partial \psi_k^*} \left[\langle \Psi^{\text{HF}}|H|\Psi^{\text{HF}}\rangle - \sum_{k_1=1}^N \sum_{k_1'=1}^N \epsilon_{k_1k_1'} \langle \psi_{k_1}|\psi_{k_1'}\rangle \right] = 0. \quad (2.7)$$

This becomes

$$\begin{aligned} h(\mathbf{x})\psi_k(\mathbf{x}) + \sum_{k'=1}^N \left\{ \int |\psi_{k'}(\mathbf{x}')|^2 v(\mathbf{x},\mathbf{x}') d\mathbf{x}' \right\} \psi_k(\mathbf{x}) \\ - \int \psi_{k'}^*(\mathbf{x}')v(\mathbf{x},\mathbf{x}')\psi_k(\mathbf{x}') d\mathbf{x}' \psi_{k'}(\mathbf{x}) \Big\} = \sum_{k'=1}^N \epsilon_{kk'}\psi_{k'}(\mathbf{x}). \end{aligned} \quad (2.8)$$

For the summation over k' in the left-hand side of this equation, the term of $k'=k$, which means the self interaction, is automatically excluded by the canceling out between the Coulomb and exchange parts. This is one of the important aspects of HFA; *nonphysical self interaction is automatically removed in HFA*. The one-body density matrix in the ground state (2.1) can be defined as follows:

$$\rho(\mathbf{x},\mathbf{x}') = \sum_{k=1}^N \psi_k^*(\mathbf{x})\psi_k(\mathbf{x}'). \quad (2.9)$$

Making use of this expression, Eq. (2.8) is rewritten as

$$\{h(\mathbf{x}) + v_{\text{eff}}(\mathbf{x}) - A(\mathbf{x})\} \psi_k(\mathbf{x}) = \sum_{k'=1}^N \epsilon_{kk'}\psi_{k'}(\mathbf{x}), \quad (2.10)$$

where $v_{\text{eff}}(\mathbf{x})$ and $A(\mathbf{x})$ are defined by

$$v_{\text{eff}}(\mathbf{x}) = \int v(\mathbf{x},\mathbf{x}')\rho(\mathbf{x}',\mathbf{x}') d\mathbf{x}', \quad (2.11)$$

$$A(\mathbf{x})\psi(\mathbf{x}) = \int v(\mathbf{x},\mathbf{x}')\psi(\mathbf{x}')\rho(\mathbf{x}',\mathbf{x}) d\mathbf{x}'. \quad (2.12)$$

The operators in the brackets of Eq. (2.10), which act on ψ_k , are the Hermitian operators and independent of k , so that we can take ψ_k as the eigenfunction of these operators. Then $\epsilon_{kk'}$ in the right-hand side becomes zero for $k \neq k'$, namely,

$$\{h(\mathbf{x}) + v_{\text{eff}}(\mathbf{x}) - A(\mathbf{x})\} \psi_k(\mathbf{x}) = \epsilon_k\psi_k(\mathbf{x}). \quad (2.13)$$

This is called 'Hartree-Fock equation'. More explicit form like (2.8) is given by

$$\begin{aligned} h(\mathbf{x})\psi_k(\mathbf{x}) + \sum_{k'=1}^N \left[\int v(\mathbf{x},\mathbf{x}')|\psi_{k'}(\mathbf{x}')|^2 d\mathbf{x}' \right] \psi_k(\mathbf{x}) \\ - \sum_{k'=1}^N \left[\int v(\mathbf{x},\mathbf{x}')\psi_{k'}^*(\mathbf{x}')\psi_k(\mathbf{x}') d\mathbf{x}' \right] \psi_{k'}(\mathbf{x}) = \epsilon_k\psi_k(\mathbf{x}). \end{aligned} \quad (2.14)$$

The single determinant Ψ^{HF} is constructed by these eigenfunctions ψ_k 's ($k=1, \dots, N$) of Eq. (2.13), which are in order of the energy from the lowest eigenvalue ϵ . In general, this procedure of HFA is rather difficult because v_{eff} and A in Eq. (2.13) contains ψ_k 's ($k=1, \dots, N$) and this is a nonlinear problem by nature. Usually, the following iterative way is employed to deal with this problem. First, assuming an appropriate form for v_{eff} and A , one will solve Eq. (2.13). Then with this solution ψ_k 's one will calculate v_{eff} and A and examine whether the obtained v_{eff} and A are the same as the assumed ones or not. If the agreement is not obtained, one should go further with the calculated v_{eff} and A to get new solution ψ_k 's and recalculate v_{eff} and A . This cycle is to be iterated until the sufficient convergence is seen for v_{eff} and A . Thus converged potential, v_{eff} plus A , is called 'self-consistent field'.

Equation (2.14) multiplied by $\psi_k^*(\mathbf{x})$ from the left side and integrated with respect to \mathbf{x} yields the one-electron energy of the state k ;

$$\epsilon_k = \langle k|h|k \rangle + \sum_{k'=1}^N \{ \langle kk'|v|kk' \rangle - \langle kk'|v|k'k \rangle \}. \quad (2.15)$$

The total energy, Eq. (2.4), can be rewritten with this one-electron energy ϵ_k as follows:

$$W = \langle \Psi^{\text{HF}}|H|\Psi^{\text{HF}} \rangle = \sum_{k=1}^N \epsilon_k - \frac{1}{2} \sum_{k=1}^N \sum_{k'=1}^N \{ \langle kk'|v|kk' \rangle - \langle kk'|v|k'k \rangle \}, \quad (2.16)$$

where it should be noted that the second term prevents the double-counting of the electron-electron interaction.

2.2 Second quantization

In general, the second-quantization method is more convenient than using the Slater determinant. In this section, we would formulate the Hamiltonian by the second quantization and examine its form in HFA. This procedure provides us with an insight about what is missing in HFA and it can help us to go further into a higher order approximation. We consider the following Hamiltonian which is the same as Eq. (2.3) but is expressed by the second quantization,

$$H = \sum_{k,k'} \langle k|h|k' \rangle a_k^\dagger a_{k'} + \frac{1}{2} \sum_{k_1, k_2, k_1', k_2'} \langle k_1 k_2 | v | k_1' k_2' \rangle a_{k_1}^\dagger a_{k_2}^\dagger a_{k_2'} a_{k_1'}, \quad (2.17)$$

here note that there is no restriction about the single-electron states k 's except that they construct an orthonormal complete set. a_k^\dagger (a_k) is the creation (annihilation) operator of the k -th state. We express the HF ground-state wavefunction for N -electron system as

$$\Psi^{\text{HF}} = a_{k_1}^\dagger a_{k_2}^\dagger \cdots a_{k_N}^\dagger |0\rangle, \quad (2.18)$$

where $|0\rangle$ represents the vacuum state. We should try to minimize $\langle \Psi^{\text{HF}}|H|\Psi^{\text{HF}} \rangle$, which is calculated as follows:

$$\begin{aligned} W &= \langle \Psi^{\text{HF}}|H|\Psi^{\text{HF}} \rangle \\ &= \sum_{i=1}^N \langle k_i|h|k_i \rangle + \frac{1}{2} \sum_{i=1}^N \sum_{j=1}^N \{ \langle k_i k_j | v | k_i k_j \rangle - \langle k_i k_j | v | k_j k_i \rangle \}. \end{aligned} \quad (2.19)$$

This is the same as (2.4) and the states k 's should satisfy the HF equation (2.13) from the condition of minimizing W . The HF ground state Ψ^{HF} is realized by filling these states

with N electrons in order of the energy from the lowest eigenvalue ϵ . The story up to now is completely the same as the previous one discussed in sec. 2.1.

Let us examine the original Hamiltonian (2.17) in detail, provided that the states k 's in (2.17) satisfy the HF equation (2.13). It is convenient to stand in the hole picture for the occupied states in the HF ground state Ψ^{HF} ;

$$b_{k_i} = a_{k_i}^+, \quad b_{k_i}^+ = a_{k_i}, \quad \{b_{k_i}, b_{k_j}^+\} = b_{k_i} b_{k_j}^+ + b_{k_j}^+ b_{k_i} = \delta_{ij}, \quad (2.20)$$

namely, b_k^+ (b_k) represents an operator to create (annihilate) a hole in the state k . Hereinafter the occupied states of Ψ^{HF} are labeled as $k \leq k_F$, and the unoccupied states, $k > k_F$, and we would stand in the hole picture for $k \leq k_F$ with using operators b_k^+ and b_k , while electron picture for $k > k_F$ with a_k^+ and a_k . Then

$$a_k \Psi^{\text{HF}} = 0 \quad (k > k_F), \quad b_k \Psi^{\text{HF}} = 0 \quad (k \leq k_F), \quad (2.21)$$

namely, Ψ^{HF} behaves like vacuum state for the operators a and b .

Utilizing this new scheme of the electron-hole picture, we would rewrite the Hamiltonian (2.17) in terms of a and b and furthermore in terms of the normal product. After a cumbersome procedure, the Hamiltonian becomes as follows:

$$H = \sum_{k \leq k_F} \langle k|h|k \rangle + \frac{1}{2} \sum_{k, k' \leq k_F} \{ \langle kk'|v|kk' \rangle - \langle kk'|v|k'k \rangle \} \quad (2.22)$$

$$+ \sum_{k, k'} (a_k^+ a_{k'} - b_k^+ b_k) \otimes \left[\langle k|h|k' \rangle + \sum_{k_1 \leq k_F} \{ \langle kk_1|v|k'k_1 \rangle - \langle kk_1|v|k_1k' \rangle \} \right] \quad (2.23)$$

$$+ \sum_{k, k'} (a_k^+ b_{k'}^+ + b_k a_{k'}) \otimes \left[\langle k|h|k' \rangle + \sum_{k_1 \leq k_F} \{ \langle kk_1|v|k'k_1 \rangle - \langle kk_1|v|k_1k' \rangle \} \right] \quad (2.24)$$

$$+ \frac{1}{2} \sum_{1,2,3,4} [\langle 12|v|34 \rangle a_1^+ a_2^+ b_4^+ b_3^+ + \{ \langle 12|v|34 \rangle - \langle 12|v|43 \rangle \} (a_1^+ a_2^+ b_4^+ a_3 + a_1^+ b_4^+ b_3^+ b_2) + \langle 12|v|34 \rangle (a_1^+ a_2^+ a_4 a_3 + b_4^+ b_3^+ b_1 b_2) - 2 \{ \langle 12|v|34 \rangle - \langle 12|v|43 \rangle \} a_1^+ b_4^+ b_2 a_3 + \{ \langle 12|v|34 \rangle - \langle 12|v|43 \rangle \} (a_1^+ b_2 a_4 a_3 + b_4^+ b_1 b_2 a_3) + \langle 12|v|34 \rangle b_1 b_2 a_4 a_3], \quad (2.25)$$

where it should be noted that the summation over k is to be taken as $k > k_F$ when k is the subscript of a or a^+ , while $k \leq k_F$ for b or b^+ . In (2.23) and (2.24), one can recognize that the equation within the square brackets $[\]$ is the matrix element of the mean-field Hamiltonian of (2.13) between the states k and k' . Since the state k' satisfies the HF equation (2.13), this matrix element becomes $\epsilon_k \delta_{kk'}$. The equation (2.24) is, however, to be zero since the subscript of a should be different from that of b . The equation (2.22), which is a constant term, is equal to the ground-state energy in HFA, namely, Eq. (2.19). Hence the original Hamiltonian (2.17) can be written in the form

$$H = W + \sum_k \epsilon_k (a_k^+ a_k - b_k^+ b_k) + H_2, \quad (2.26)$$

here H_2 represents the interaction term, which contains four operators, and is described by Eq. (2.25). The characteristic feature of (2.26) is that the one-body term, which contains two operators, is already diagonalized. Operating H to Ψ^{HF} leads to

$$\begin{aligned} H\Psi^{\text{HF}} &= W\Psi^{\text{HF}} + H_2\Psi^{\text{HF}} \\ &= W\Psi^{\text{HF}} + \frac{1}{2} \sum_{1,2,3,4} \langle 12|v|34\rangle a_1^\dagger a_2^\dagger b_4^\dagger b_3^\dagger \Psi^{\text{HF}}, \end{aligned} \quad (2.27)$$

here note that we have utilized Eq. (2.21). The second term becomes the summation over the excited states, in which two electron-hole pairs are excited from Ψ^{HF} . To go beyond HFA, we should take into account this term.

Chapter 3

Atomic ground state

In this chapter, we summarize the magnetic ground state of an atom or ion, which has an incomplete shell such as $3d$, $4f$, or $5f$ orbital outside closed shells, and examine how properly the HF method can describe the magnetic quantities of such system. In Sec. 3.1, we prepare an appropriate Hamiltonian for an isolated ion. In Sec. 3.2, a corresponding HF Hamiltonian is derived. Magnetic quantities, to which we should pay attention, are introduced in Sec. 3.3. Calculated results and discussions for the $3d$, $4f$, and U ions are given in Sec. 3.4, 3.5, and 3.6, respectively. Sec. 3.7 is devoted to conclusion.

3.1 Hamiltonian

The ground state of an ion with an incomplete shell nl (n and l are the principal quantum number and the azimuthal quantum number of the atomic orbital, respectively) may be described by the following Hamiltonian:

$$H = H_{ee} + H_{\text{kin}} + H_{\text{so}} + H_{\text{cry}} + H_{\text{m}}, \quad (3.1)$$

where H_{ee} is the electrostatic Coulomb interaction between the equivalent electrons in the nl shell; H_{kin} is the kinetic energy; H_{so} is the spin-orbit interaction; H_{cry} is the crystalline field; H_{m} is the infinitesimal molecular field, which is added to lift degeneracy and obtain a magnetically polarized solution.

The one-electron state of the nl shell can be specified by the orbital magnetic quantum number m and the spin magnetic quantum number σ :

$$|\nu\rangle = |nlm\sigma\rangle = R_{nl}(r)Y_{lm}(\theta\phi)\chi_{\sigma}, \quad (3.2)$$

where ν is the abbreviation for all of the one-electron quantum numbers; R_{nl} is the radial wave function; Y_{lm} is the spherical harmonics; χ is the spin function. For R_{nl} , we would use the *ab initio* HF numerical result with multiplet-averaged configuration and limit our discussion to only the angular and spin parts. This simplification has been justified by a number of calculations based on the same approximation. With fixing R_{nl} , H_{kin} becomes constant and we will omit it from the following discussions.

The interaction term H_{ee} is written as follows:

$$H_{ee} = \frac{1}{2} \sum_{i=1}^N \sum_{j=1(i \neq j)}^N v(\mathbf{x}_i, \mathbf{x}_j) \quad (3.3)$$

$$= \frac{1}{2} \sum_{\nu_1, \nu_2, \nu_3, \nu_4} \langle \nu_1 \nu_2 | v | \nu_3 \nu_4 \rangle a_{\nu_1}^{\dagger} a_{\nu_2}^{\dagger} a_{\nu_4} a_{\nu_3}, \quad (3.4)$$

where N in the first line is the electron number in the nl shell, and we have used the second-quantization method in the second line. The interaction matrix element is given by

$$\begin{aligned} \langle \nu_1 \nu_2 | v | \nu_3 \nu_4 \rangle &= \delta_{\sigma_1 \sigma_3} \delta_{\sigma_2 \sigma_4} \delta_{m_1+m_2, m_3+m_4} \\ &\times \sum_{k=0,2,4,\dots,2l} c^k(lm_1, lm_3) c^k(lm_4, lm_2) F^k(nl). \end{aligned} \quad (3.5)$$

Here, c^k and F^k are called the Gaunt coefficient and Slater integral, respectively, and their explicit forms are

$$c^k(lm, l'm') = \sqrt{\frac{4\pi}{2k+1}} \int d\Omega Y_{lm}^* Y_{k(m-m')} Y_{l'm'}, \quad (3.6)$$

$$F^k(nl) = \int dr_1 dr_2 \frac{r_{<}^{k+2}}{r_{>}^{k-1}} |R_{nl}(r_1)|^2 |R_{nl}(r_2)|^2, \quad (3.7)$$

where $r_{<}$ ($r_{>}$) denotes the smaller (larger) of r_1 and r_2 . As can be seen from Eq. (3.5), the electron-electron interaction within an atom is in general *multipole* interaction. The monopole part ($k=0$ term) is trivial in the case of an isolated atom because it only gives a shift in the total energy according to the electron number and has no effect on the magnetic quantities or wavefunction. In the interaction matrix element, the monopole part is

$$\begin{aligned} \langle \nu_1 \nu_2 | v | \nu_3 \nu_4 \rangle_{(k=0)} &= \delta_{\sigma_1 \sigma_3} \delta_{\sigma_2 \sigma_4} \delta_{m_1+m_2, m_3+m_4} c^0(lm_1, lm_3) c^0(lm_4, lm_2) F^0(nl) \\ &= \delta_{\sigma_1 \sigma_3} \delta_{\sigma_2 \sigma_4} \delta_{m_1 m_3} \delta_{m_2 m_4} F^0(nl) \\ &= \delta_{\nu_1 \nu_3} \delta_{\nu_2 \nu_4} F^0(nl), \end{aligned} \quad (3.8)$$

where we have used the relation $c^0(lm, lm') = \delta_{mm'}$. Then the monopole part of the interaction Hamiltonian (3.4) is

$$\begin{aligned} H_{ee} (k=0) &= \frac{1}{2} F^0(nl) \sum_{\nu} \sum_{\nu'} a_{\nu}^{\dagger} a_{\nu'}^{\dagger} a_{\nu'} a_{\nu} \\ &= \frac{1}{2} F^0(nl) \sum_{\nu \neq \nu'} \hat{n}_{\nu} \hat{n}_{\nu'} \\ &= \frac{1}{2} F^0(nl) N(N-1), \end{aligned} \quad (3.9)$$

here \hat{n}_{ν} is the number operator; $\hat{n}_{\nu} = a_{\nu}^{\dagger} a_{\nu}$. The other multipole parts ($k \neq 0$ terms) determine the ground state of an isolated ion.¹ In the case of solid, F^0 plays an important role as will be discussed in the following chapters.

The spin-orbit interaction and molecular field are written as

$$H_{so} = \zeta_{nl} \sum_{i=1}^N \mathbf{l}_i \cdot \mathbf{s}_i = \zeta_{nl} \sum_{\nu_1 \nu_2} \langle \nu_1 | \mathbf{l} \cdot \mathbf{s} | \nu_2 \rangle a_{\nu_1}^{\dagger} a_{\nu_2}, \quad (3.10)$$

$$H_m = \Delta_m \sum_{i=1}^N s_{iz} = \Delta_m \sum_{\nu_1 \nu_2} \langle \nu_1 | s_z | \nu_2 \rangle a_{\nu_1}^{\dagger} a_{\nu_2}, \quad (3.11)$$

where ζ_{nl} is the coupling constant and Δ_m is infinitesimal. \mathbf{l}_i and \mathbf{s}_i are the orbital and spin angular momentum operators, respectively, of the i -th electron. The parameter values

¹In HFA, however, a finite F^0 larger than an appropriate critical value, usually several electron volts, is needed to converge calculations even for an atom. In the mean-field approximation, it is necessary to draw a distinction between occupied and unoccupied states, and F^0 takes the role of it. Once F^0 goes beyond the critical value, calculated results for an atom do not depend on the value of F^0 .

that we encounter in (3.1) and the explicit form of the crystal field H_{cry} will be given later in the course of each calculation.

The exact eigenfunction of the Hamiltonian (3.1) can be obtained numerically with the configuration-interaction (CI) method. For a given electron configuration, setting up all the possible many-body bases, *i.e.*, all the possible Slater determinants, we calculate the Hamiltonian matrix in this space and diagonalize it numerically. For instance, in the case of $3d^3$ configuration, there are ${}_{10}C_3 = 120$ Slater determinants as the bases and we should construct the (120×120) Hamiltonian matrix to be diagonalized. The ground-state wavefunction Ψ is given by a linear combination of these 120 bases.

3.2 HF Hamiltonian

The Hamiltonian for an isolated atom (3.1) is solvable within the CI scheme, whereas we shall apply HFA and derive the explicit form of the mean-field Hamiltonian in accordance with the prescription of Sec. 2.1.

The HF ground-state wavefunction is written by a single product

$$\Psi^{\text{HF}} = a_{k_1}^+ a_{k_2}^+ \cdots a_{k_N}^+ |0\rangle, \quad (3.12)$$

where N is the electron number in the incomplete nl shell. From the variational method, the HF equation has been derived as Eq. (2.14) to determine the one-electron states k 's :

$$\begin{aligned} h(\mathbf{x})\psi_k(\mathbf{x}) + \sum_{k'=1}^N \left[\int v(\mathbf{x}, \mathbf{x}') |\psi_{k'}(\mathbf{x}')|^2 d\mathbf{x}' \right] \psi_k(\mathbf{x}) \\ - \sum_{k'=1}^N \left[\int v(\mathbf{x}, \mathbf{x}') \psi_{k'}^*(\mathbf{x}') \psi_k(\mathbf{x}') d\mathbf{x}' \right] \psi_{k'}(\mathbf{x}) = \epsilon_k \psi_k(\mathbf{x}), \end{aligned} \quad (3.13)$$

where $h(\mathbf{x})$ is sum of the one-body Hamiltonian, namely, it corresponds to $H_{\text{so}} + H_{\text{cry}} + H_{\text{m}}$ in the present case, but note that the sum over the electron index i ($i = 1, \dots, N$) has been dropped and we would formally represent this point as follows:

$$h(\mathbf{x}) = H_{\text{so}}^{(1)}(\mathbf{x}) + H_{\text{cry}}^{(1)}(\mathbf{x}) + H_{\text{m}}^{(1)}(\mathbf{x}). \quad (3.14)$$

Since we are dealing with atomic orbitals, each one-electron state k can be represented by a linear combination of the spin-orbit function ν defined by Eq. (3.2);

$$\psi_k(\mathbf{x}) = \sum_{\nu} C_{k\nu} \phi_{\nu}(\mathbf{x}). \quad (3.15)$$

The matrix form of (3.15) is

$$(\psi_{k_1}, \dots, \psi_{k_{N_l}}) = (\phi_{\nu_1}, \dots, \phi_{\nu_{N_l}}) \mathbf{C}, \quad (3.16)$$

where \mathbf{C} is a unitary matrix whose size is $N_l \times N_l$. N_l is the degeneracy of the nl orbital, $N_l = 2(2l + 1)$. From this relation between ψ_k and ϕ_{ν} , we can define the following creation and annihilation operators;

$$a_k^+ = \sum_{\nu} C_{k\nu} a_{\nu}^+, \quad a_k = \sum_{\nu} C_{k\nu}^* a_{\nu} \quad (3.17)$$

or

$$a_{\nu}^+ = \sum_k C_{k\nu}^* a_k^+, \quad a_{\nu} = \sum_k C_{k\nu} a_k. \quad (3.18)$$

In the HF equation (3.13), there appear summations over k . Using the relation (3.15), these summations is rewritten as

$$\begin{aligned} \sum_{k=1}^N |\psi_k|^2 &= \sum_{k=1}^N \left(\sum_{\nu} C_{k\nu} \phi_{\nu} \right)^* \left(\sum_{\nu'} C_{k\nu'} \phi_{\nu'} \right) \\ &= \sum_{\nu\nu'} \left[\sum_{k=1}^N C_{k\nu}^* C_{k\nu'} \right] \phi_{\nu}^* \phi_{\nu'} \end{aligned} \quad (3.19)$$

$$\sum_{k=1}^N \psi_k^*(\mathbf{x}') \psi_k(\mathbf{x}) = \sum_{\nu\nu'} \left[\sum_{k=1}^N C_{k\nu}^* C_{k\nu'} \right] \phi_{\nu}^*(\mathbf{x}') \phi_{\nu'}(\mathbf{x}). \quad (3.20)$$

In Eqs. (3.19) and (3.20), the summation over k in the square brackets has a significant meaning in HFA. To see this, let us consider the following expectation value:

$$\begin{aligned} \langle a_{\nu}^{\dagger} a_{\nu'} \rangle &\equiv \langle \Psi^{\text{HF}} | a_{\nu}^{\dagger} a_{\nu'} | \Psi^{\text{HF}} \rangle \\ &= \langle \Psi^{\text{HF}} | \left(\sum_{k=1}^{N_i} C_{k\nu}^* a_k^{\dagger} \right) \left(\sum_{k'=1}^{N_i} C_{k'\nu'} a_{k'} \right) | \Psi^{\text{HF}} \rangle \\ &= \sum_{k=1}^{N_i} \sum_{k'=1}^{N_i} C_{k\nu}^* C_{k'\nu'} \langle \Psi^{\text{HF}} | a_k^{\dagger} a_{k'} | \Psi^{\text{HF}} \rangle \end{aligned} \quad (3.21)$$

where we have used Eq. (3.18) in the second line. The expectation value $\langle \Psi^{\text{HF}} | a_k^{\dagger} a_{k'} | \Psi^{\text{HF}} \rangle$ becomes zero unless $k = k'$ and $k \leq N$. Then

$$\langle a_{\nu}^{\dagger} a_{\nu'} \rangle = \sum_{k=1}^N C_{k\nu}^* C_{k\nu'}. \quad (3.22)$$

Now we recognize that the quantity in the square brackets in (3.19) and (3.20) happens to be the ground-state expectation value of a pair of operators $\langle a_{\nu}^{\dagger} a_{\nu'} \rangle$. This is called *HF order parameter*. Rewriting Eq. (3.13) with making use of the HF order parameter, we get

$$\begin{aligned} h(\mathbf{x}) \psi_k(\mathbf{x}) + \sum_{\nu_1 \nu'_1} \langle a_{\nu_1}^{\dagger} a_{\nu'_1} \rangle \int v(\mathbf{x}, \mathbf{x}') d\mathbf{x}' \\ \times \left[\phi_{\nu_1}^*(\mathbf{x}') \phi_{\nu'_1}(\mathbf{x}') \psi_k(\mathbf{x}) - \phi_{\nu_1}^*(\mathbf{x}') \phi_{\nu'_1}(\mathbf{x}) \psi_k(\mathbf{x}') \right] = \epsilon_k \psi_k(\mathbf{x}). \end{aligned} \quad (3.23)$$

The insertion of (3.15) yields

$$\begin{aligned} h(\mathbf{x}) \sum_{\nu'} C_{k\nu'} \phi_{\nu'}(\mathbf{x}) + \sum_{\nu_1 \nu'_1} \langle a_{\nu_1}^{\dagger} a_{\nu'_1} \rangle \int v(\mathbf{x}, \mathbf{x}') d\mathbf{x}' \\ \times \sum_{\nu'} C_{k\nu'} \left[\phi_{\nu_1}^*(\mathbf{x}') \phi_{\nu'_1}(\mathbf{x}') \phi_{\nu'}(\mathbf{x}) - \phi_{\nu_1}^*(\mathbf{x}') \phi_{\nu'_1}(\mathbf{x}) \phi_{\nu'}(\mathbf{x}') \right] \\ = \epsilon_k \sum_{\nu'} C_{k\nu'} \phi_{\nu'}(\mathbf{x}). \end{aligned} \quad (3.24)$$

By multiplying $\phi_{\nu}^*(\mathbf{x})$ from the left side and integrating with respect to \mathbf{x} , one can obtain the following secular equation:

$$\sum_{\nu'} \langle \nu | h | \nu' \rangle C_{k\nu'} +$$

$$\begin{aligned}
& \sum_{\nu_1 \nu'_1} \langle a_{\nu_1}^\dagger a_{\nu'_1} \rangle \sum_{\nu'} [\langle \nu \nu_1 | v | \nu' \nu'_1 \rangle - \langle \nu \nu_1 | v | \nu'_1 \nu' \rangle] C_{k\nu'} \\
& = \epsilon_k \sum_{\nu'} C_{k\nu'}.
\end{aligned} \tag{3.25}$$

This equation reduces to a matrix form:

$$\mathbf{H}^{\text{HF}} \mathbf{C}_k = \epsilon_k \mathbf{C}_k, \tag{3.26}$$

with

$$\begin{aligned}
(\mathbf{H}^{\text{HF}})_{\nu\nu'} & = \langle \nu | h | \nu' \rangle \\
& + \sum_{\nu_1 \nu'_1} \langle a_{\nu_1}^\dagger a_{\nu'_1} \rangle [\langle \nu \nu_1 | v | \nu' \nu'_1 \rangle - \langle \nu \nu_1 | v | \nu'_1 \nu' \rangle]
\end{aligned} \tag{3.27}$$

and

$$\mathbf{C}_k = (\dots, C_{k\nu}, \dots). \tag{3.28}$$

The matrix \mathbf{H}^{HF} is the HF Hamiltonian matrix in the ν space, whose size is $N_l \times N_l$. An alternative form of the HF Hamiltonian can be written as follows by using the creation and annihilation operators:

$$\begin{aligned}
H^{\text{HF}} & = \sum_{\nu\nu'} a_\nu^\dagger a_{\nu'} \\
& \times \left\{ \langle \nu | h | \nu' \rangle + \sum_{\nu_1 \nu'_1} \langle a_{\nu_1}^\dagger a_{\nu'_1} \rangle [\langle \nu \nu_1 | v | \nu' \nu'_1 \rangle - \langle \nu \nu_1 | v | \nu'_1 \nu' \rangle] \right\}.
\end{aligned} \tag{3.29}$$

Obviously this is a mean-field Hamiltonian, which contains only one pair of creation and annihilation operators. Self-consistent iterative procedure to solve Eq. (3.26) is as follows: Furnishing appropriate order parameters $\langle a_\nu^\dagger a_{\nu'} \rangle$ as an initial input, one will construct the Hamiltonian matrix in the ν space, (3.27), and numerically diagonalize it. From the obtained eigenvector \mathbf{C}_k 's, new order parameters are computed by Eq. (3.22), and with them, a new Hamiltonian matrix is calculated for the next step. One should iterate this cycle until a sufficient convergence is obtained for the order parameters.

The total energy given by Eq. (2.16) reduces to the following simple form with the order parameters:

$$\begin{aligned}
W & = \langle \Psi^{\text{HF}} | H | \Psi^{\text{HF}} \rangle \\
& = \sum_{k=1}^N \epsilon_k - \frac{1}{2} \sum_{k=1}^N \sum_{k'=1}^N \{ \langle k k' | v | k k' \rangle - \langle k k' | v | k' k \rangle \} \\
& = \sum_{k=1}^N \epsilon_k - \frac{1}{2} \sum_{\nu\nu'} \sum_{\nu_1 \nu'_1} \langle a_\nu^\dagger a_{\nu'} \rangle \langle a_{\nu_1}^\dagger a_{\nu'_1} \rangle \{ \langle \nu \nu_1 | v | \nu' \nu'_1 \rangle - \langle \nu \nu_1 | v | \nu'_1 \nu' \rangle \}.
\end{aligned} \tag{3.30}$$

3.3 Magnetic quantities

In examining the ground state of an ion, we concentrate on the resultant spin angular momentum $\mathbf{S} = \sum_{i=1}^N \mathbf{s}_i$, the resultant orbital angular momentum $\mathbf{L} = \sum_{i=1}^N \mathbf{l}_i$, the total

angular momentum $\mathbf{J} = \mathbf{S} + \mathbf{L}$, and their squares, \mathbf{S}^2 , \mathbf{L}^2 , and \mathbf{J}^2 . Note that these momenta and their squares are *operators*; for instance,

$$\mathbf{S} = \sum_{\nu\nu'} \langle \nu | \mathbf{s} | \nu' \rangle a_\nu^\dagger a_{\nu'} \quad (3.31)$$

$$\mathbf{S}^2 = S_x^2 + S_y^2 + S_z^2 = \frac{1}{2}(S_+ S_- + S_- S_+) + S_z^2, \quad (3.32)$$

where

$$S_+ = S_x + iS_y = \sum_{\nu\nu'} \langle \nu | s_x + is_y | \nu' \rangle a_\nu^\dagger a_{\nu'} = \sum_{\nu\nu'} \langle \nu | s_+ | \nu' \rangle a_\nu^\dagger a_{\nu'} \quad (3.33)$$

$$S_- = S_x - iS_y = \sum_{\nu\nu'} \langle \nu | s_x - is_y | \nu' \rangle a_\nu^\dagger a_{\nu'} = \sum_{\nu\nu'} \langle \nu | s_- | \nu' \rangle a_\nu^\dagger a_{\nu'}. \quad (3.34)$$

We should calculate the ground-state expectation values of them such as $\langle \Psi | S_z | \Psi \rangle$ or $\langle \Psi^{\text{HF}} | S_z | \Psi^{\text{HF}} \rangle$. The spin magnetic moment ($\boldsymbol{\mu}_{\text{spin}}$) and orbital magnetic moment ($\boldsymbol{\mu}_{\text{orb}}$) are related to the spin and orbital angular momenta by

$$\boldsymbol{\mu}_{\text{spin}} = -2\mu_B \langle \mathbf{S} \rangle, \quad \boldsymbol{\mu}_{\text{orb}} = -\mu_B \langle \mathbf{L} \rangle. \quad (3.35)$$

The other important magnetic quantity is the so-called spin magnetic dipole

$$\mathbf{T} = \sum_{i=1}^N \left[\mathbf{s}_i - 3\mathbf{r}_i \frac{(\mathbf{r}_i \cdot \mathbf{s}_i)}{r_i^2} \right]. \quad (3.36)$$

With defining the following function

$$c_m^{(k)}(\hat{\mathbf{r}}) = \sqrt{\frac{4\pi}{2k+1}} Y_{km}(\theta, \phi), \quad (3.37)$$

each component of \mathbf{T} is rewritten as

$$\begin{aligned} T_+ &= \sum_{\nu\nu'} a_\nu^\dagger a_{\nu'} \langle \nu | c_0^{(2)} s_+ - \sqrt{6} c_2^{(2)} s_- + \sqrt{6} c_1^{(2)} s_z | \nu' \rangle \\ T_- &= \sum_{\nu\nu'} a_\nu^\dagger a_{\nu'} \langle \nu | -\sqrt{6} c_{-2}^{(2)} s_+ + c_0^{(2)} s_- - \sqrt{6} c_{-1}^{(2)} s_z | \nu' \rangle \\ T_z &= \sum_{\nu\nu'} a_\nu^\dagger a_{\nu'} \langle \nu | -\sqrt{\frac{3}{2}} c_{-1}^{(2)} s_+ + \sqrt{\frac{3}{2}} c_1^{(2)} s_- - 2 c_0^{(2)} s_z | \nu' \rangle. \end{aligned} \quad (3.38)$$

The expectation value $\langle \mathbf{T} \rangle$ gives an insight about the anisotropy of the spin magnetic field when the atomic cloud is distorted due to the spin-orbit interaction or crystal field effect. If the system is in cubic symmetry, a nonzero value of $\langle \mathbf{T} \rangle$ is driven only by the spin-orbit interaction.

In HFA, the ground-state expectation values of those operators given above are easily calculated if one knows corresponding one-body matrix elements in addition to the converged HF order parameter. For instance, the expectation value of the spin angular momentum \mathbf{S} , (3.31), turns out to be

$$\begin{aligned} \langle \mathbf{S} \rangle^{\text{HF}} &= \langle \Psi^{\text{HF}} | \mathbf{S} | \Psi^{\text{HF}} \rangle \\ &= \sum_{\nu\nu'} \langle \nu | \mathbf{s} | \nu' \rangle \langle a_\nu^\dagger a_{\nu'} \rangle. \end{aligned} \quad (3.39)$$

Terms in Eq. (3.32), such as S_+S_- , need attention because they contain four operators;

$$\begin{aligned}
S_+S_- &= \sum_{\nu_1\nu'_1} \sum_{\nu_2\nu'_2} \langle \nu_1|s_+|\nu'_1\rangle \langle \nu_2|s_-|\nu'_2\rangle a_{\nu_1}^+ a_{\nu'_1} a_{\nu_2}^+ a_{\nu'_2} \\
&= \sum_{\nu_1\nu'_1} \sum_{\nu_2\nu'_2} \langle \nu_1|s_+|\nu'_1\rangle \langle \nu_2|s_-|\nu'_2\rangle \\
&\quad \times \sum_{k_1=1}^{N_l} \sum_{k'_1=1}^{N_l} \sum_{k_2=1}^{N_l} \sum_{k'_2=1}^{N_l} C_{k_1\nu_1}^* C_{k'_1\nu'_1} C_{k_2\nu_2}^* C_{k'_2\nu'_2} a_{k_1}^+ a_{k'_1} a_{k_2}^+ a_{k'_2}, \quad (3.40)
\end{aligned}$$

where the relation (3.18) has been used. We should concentrate on $G \equiv \langle a_{k_1}^+ a_{k'_1} a_{k_2}^+ a_{k'_2} \rangle^{\text{HF}}$. Since the HF ground-state wavefunction is a single product in terms of $\{k\}$ ($k = 1, \dots, N$), nonvanishing value of G is restricted to the following k -combinations:

(i) $k_1 = k'_1$ and $k_2 = k'_2$

(ii) $k_1 = k'_2$ and $k_2 = k'_1$.

Then the set of operators comes to be the number operators \hat{n}_k . In the case (i), G reduces to

$$\begin{aligned}
G &= \langle \hat{n}_{k_1} \hat{n}_{k_2} \rangle^{\text{HF}} \\
&= \begin{cases} 1 & \text{if both } k_1 \text{ and } k_2 \text{ belong to occupied states} \\ 0 & \text{otherwise.} \end{cases} \quad (3.41)
\end{aligned}$$

For the expectation value of (3.40), the term corresponding to (i) is

$$\begin{aligned}
\langle S_+S_- \rangle^{\text{HF}}|_{(i)} &= \sum_{\nu_1\nu'_1} \sum_{\nu_2\nu'_2} \langle \nu_1|s_+|\nu'_1\rangle \langle \nu_2|s_-|\nu'_2\rangle \sum_{k_1=1}^N C_{k_1\nu_1}^* C_{k_1\nu'_1} \sum_{k_2=1}^N C_{k_2\nu_2}^* C_{k_2\nu'_2} \\
&= \left[\sum_{\nu_1\nu'_1} \langle \nu_1|s_+|\nu'_1\rangle \langle a_{\nu_1}^+ a_{\nu'_1} \rangle \right] \left[\sum_{\nu_2\nu'_2} \langle \nu_2|s_-|\nu'_2\rangle \langle a_{\nu_2}^+ a_{\nu'_2} \rangle \right] \\
&= \langle S_+ \rangle^{\text{HF}} \langle S_- \rangle^{\text{HF}}. \quad (3.42)
\end{aligned}$$

In (ii), using the commutation relation, G becomes

$$\begin{aligned}
G &= \langle \hat{n}_{k_1} (1 - \hat{n}_{k_2}) \rangle^{\text{HF}} \\
&= \begin{cases} 1 & \text{if } k_1 \text{ is being occupied and } k_2 \text{ unoccupied} \\ 0 & \text{otherwise,} \end{cases} \quad (3.43)
\end{aligned}$$

where note that a case $k_1 = k'_1 = k_2 = k'_2$ is not considered here because it can be included in (i). A schematic diagram for the process (ii) is depicted in Fig. 3.1. The corresponding term in the expectation value of S_+S_- is

$$\begin{aligned}
\langle S_+S_- \rangle^{\text{HF}}|_{(ii)} &= \sum_{\nu_1\nu'_1} \sum_{\nu_2\nu'_2} \langle \nu_1|s_+|\nu'_1\rangle \langle \nu_2|s_-|\nu'_2\rangle \sum_{k_1=1}^N \sum_{k_2=N+1}^{N_l} C_{k_1\nu_1}^* C_{k_2\nu'_1} C_{k_2\nu_2}^* C_{k_1\nu'_2} \\
&= \sum_{\nu_1\nu'_1} \sum_{\nu_2\nu'_2} \langle \nu_1|s_+|\nu'_1\rangle \langle \nu_2|s_-|\nu'_2\rangle \left[\sum_{k_1=1}^N C_{k_1\nu_1}^* C_{k_1\nu'_2} \right] \left[\sum_{k_2=N+1}^{N_l} C_{k_2\nu_2}^* C_{k_2\nu'_1} \right] \\
&= \sum_{\nu_1\nu'_1} \sum_{\nu_2\nu'_2} \langle \nu_1|s_+|\nu'_1\rangle \langle \nu_2|s_-|\nu'_2\rangle
\end{aligned}$$

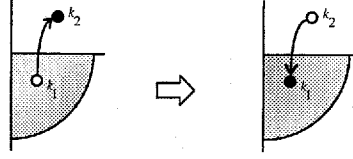


Figure 3.1: One of the processes that appear in the calculation of the HF ground-state expectation value of Eq. (3.40), $a_{k_1}^+ a_{k_2} a_{k_2}^+ a_{k_1}$. The hatched area represents occupied states in the HF ground state.

$$\begin{aligned}
& \times \left[\sum_{k_1=1}^N C_{k_1 \nu_1}^* C_{k_1 \nu_2}' \right] \left[\sum_{k_2=1}^{N_1} C_{k_2 \nu_2}^* C_{k_2 \nu_1}' - \sum_{k_2=1}^N C_{k_2 \nu_2}^* C_{k_2 \nu_1}' \right] \\
& = \sum_{\nu_1 \nu_1'} \sum_{\nu_2 \nu_2'} \langle \nu_1 | s_+ | \nu_1' \rangle \langle \nu_2 | s_- | \nu_2' \rangle \langle a_{\nu_1}^+ a_{\nu_2} \rangle \left[\delta_{\nu_2 \nu_1'} - \langle a_{\nu_2}^+ a_{\nu_1}' \rangle \right] \\
& = \sum_{\nu_1 \nu_2'} \langle \nu_1 | s_+ s_- | \nu_2' \rangle \langle a_{\nu_1}^+ a_{\nu_2} \rangle \\
& \quad - \sum_{\nu_1 \nu_1'} \sum_{\nu_2 \nu_2'} \langle \nu_1 | s_+ | \nu_1' \rangle \langle \nu_2 | s_- | \nu_2' \rangle \langle a_{\nu_1}^+ a_{\nu_2} \rangle \langle a_{\nu_2}^+ a_{\nu_1}' \rangle, \tag{3.44}
\end{aligned}$$

where we have used the relation

$$\sum_k C_{k\nu}^* C_{k\nu'} = \delta_{\nu\nu'}, \tag{3.45}$$

which is derived from the following relation for the complete system:

$$\delta(\mathbf{x} - \mathbf{x}') = \sum_k \psi_k^*(\mathbf{x}) \psi_k(\mathbf{x}') = \sum_\nu \phi_\nu^*(\mathbf{x}) \phi_\nu(\mathbf{x}'). \tag{3.46}$$

Thus we obtain

$$\begin{aligned}
\langle S_+ S_- \rangle^{\text{HF}} & = \langle S_+ \rangle^{\text{HF}} \langle S_- \rangle^{\text{HF}} + \sum_{\nu_1 \nu_2'} \langle \nu_1 | s_+ s_- | \nu_2' \rangle \langle a_{\nu_1}^+ a_{\nu_2} \rangle \\
& \quad - \sum_{\nu_1 \nu_1'} \sum_{\nu_2 \nu_2'} \langle \nu_1 | s_+ | \nu_1' \rangle \langle \nu_2 | s_- | \nu_2' \rangle \langle a_{\nu_1}^+ a_{\nu_2} \rangle \langle a_{\nu_2}^+ a_{\nu_1}' \rangle. \tag{3.47}
\end{aligned}$$

In the CI scheme, to calculate the expectation value of magnetic operators we need not only $\langle a_{\nu_1}^+ a_{\nu_2} \rangle$ but also $\langle a_{\nu_1}^+ a_{\nu_2} a_{\nu_3}^+ a_{\nu_4} \rangle$, and in the course of calculating these quantities we need to pay attention to *signs* that originate from the commutation relation.

3.4 3d ion

We survey the ground state of ions with having a 3d orbit as an incomplete shell. First, the free 3d ions, with the crystal field H_{cry} being either zero or spherical, are investigated. Numerical CI calculation shows that their ground states are described by a simple picture; the spin-orbit interaction among 3d electrons is weak compared with the Coulomb interaction (the Russell-Saunders case) and a perturbative treatment for the spin-orbit interaction is justified (LS -coupling limit). In addition to the spherical case, we will discuss the 3d ions under the crystal field with O_h symmetry, to simulate the solid-state effect. For each case we give results gained by the CI scheme, and they are compared with those by HFA. It is shown that HFA reproduces the atomic Hund rules.

3.4.1 Free ion — the Russell-Saunders case and LS -coupling scheme

First of all, we deal with the 3d ions with spherical symmetry. The Hamiltonian without the spin-orbit interaction commutes with all components of \mathbf{L} , \mathbf{S} , and \mathbf{J} . Hence this Hamiltonian has no matrix elements between the states labeled by two different sets of eigenvalues of \mathbf{S}^2 , \mathbf{L}^2 , \mathbf{J}^2 , S_z , L_z , and J_z . For the sake of labeling states, we introduce quantum numbers S , L , J , M_S , M_L , and M according to the following scheme

$$\begin{aligned} \mathbf{S}^{2'} &= S(S+1) & S'_z &= M_S \\ \mathbf{L}^{2'} &= L(L+1) & L'_z &= M_L \\ \mathbf{J}^{2'} &= J(J+1) & J'_z &= M, \end{aligned} \quad (3.48)$$

where the prime stands for manipulation to take precise value of these observables.

The electrostatic interaction produces the energy difference among terms, which are characterized by S and L , the LS multiplets, but leaves these terms degenerate with regard to $[J$ and $M]$, or, $[J, M_S, \text{ and } M_L]$. The ground-state S and L are given by empirical Hund's rules; S takes the maximum value (Hund's 1st rule); among the maximum- S multiplets the term of largest L is lowest in energy (Hund's 2nd rule). The maximum S is well understood as a consequence of the exchange interaction to align the spin of each single electron. The maximum L is on the basis of the multipole Coulomb interaction represented by the Gaunt coefficient (See Eq. (3.5)).

For a given LS multiplet, the total angular momentum J can take the following value from the principle of coupling of two angular momenta:

$$J = |L - S|, |L - S| + 1, \dots, L + S. \quad (3.49)$$

The degeneracy among J 's is lifted by the spin-orbit coupling. We shall treat it by a perturbative manner. In the Russell-Saunders case the energy interval between different LS multiplets is large compared with the spin-orbit interaction, and we can ignore its off-diagonal matrix elements connecting different LS multiplets. Then an effective Hamiltonian in a specific (L, S) space can be written in the form

$$(H_{\text{so}})_{LS} \equiv H_{LS} = \lambda \mathbf{L} \cdot \mathbf{S}. \quad (3.50)$$

For the Hund-rule LS multiplet, the coupling constant λ becomes

$$\lambda = \begin{cases} \zeta_{nl}/N & \text{if } N < N_l/2 \\ -\zeta_{nl}/(N_l - N) & \text{if } N > N_l/2 \\ 0 & \text{otherwise,} \end{cases} \quad (3.51)$$

here $N_l = 2(2l + 1)$. The Hamiltonian (3.50) commutes with \mathbf{J} . Even if we go back to the original Hamiltonian (3.10), it also commutes with \mathbf{J} . This permits the levels to be

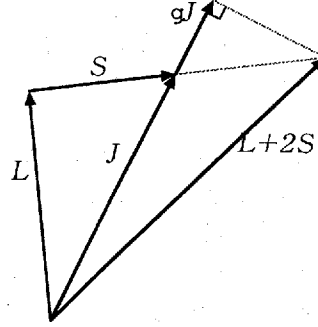


Figure 3.2: Vector-model analysis of the component of $L + 2S$ in the direction of J , under the LS -coupling limit.

labeled by J . It should be noted that S and L do not commute with H_{LS} and that these are no longer good quantum numbers. However, in the weak spin-orbit coupling limit, it is permissible to label states by a set of quantum numbers $SLJM$. The Hamiltonian (3.50) reduces to

$$\begin{aligned} H_{LS} &= \lambda \mathbf{L} \cdot \mathbf{S} \\ &= \frac{\lambda}{2} [(\mathbf{L} + \mathbf{S})^2 - \mathbf{L}^2 - \mathbf{S}^2] \\ &= \frac{\lambda}{2} [\mathbf{J}^2 - \mathbf{L}^2 - \mathbf{S}^2], \end{aligned}$$

and its matrix element within a given SLJ term is given by

$$\langle SLJM | H_{LS} | SLJM' \rangle = \frac{\lambda}{2} [J(J+1) - L(L+1) - S(S+1)] \delta_{MM'}. \quad (3.52)$$

For the individual levels separated by H_{LS} , we use the standard notation $^{2S+1}L_J$. The sign of the coupling constant λ determines the lowest J term in energy. In the Hund-rule LS multiplet the coupling constant λ given by Eq. (3.51) is positive (negative) for the less (more) than half filling so that the ground-state J -value is $|L - S|$ ($L + S$).

Finally the degeneracy about M is lifted by the infinitesimal molecular field (3.11); either $M = -J$ or $M = J$ term will be lowest in energy.

Under H_{LS} , the angular momenta S and L interact with each other; they offers a twisting force to one another. In consequence, they show precession around J and components of them perpendicular to J vanish if we take the time average. Hence the magnetic moments, $\boldsymbol{\mu}_{\text{spin}} = -2\mu_B \langle \mathbf{S} \rangle$, $\boldsymbol{\mu}_{\text{orb}} = -\mu_B \langle \mathbf{L} \rangle$, and $\boldsymbol{\mu} = \boldsymbol{\mu}_{\text{spin}} + \boldsymbol{\mu}_{\text{orb}}$, are proportional to J and can be written by

$$\begin{aligned} (\boldsymbol{\mu})_J &= (\boldsymbol{\mu}_{\text{spin}} + \boldsymbol{\mu}_{\text{orb}})_J \equiv -g_J \mu_B \mathbf{J} \\ (\boldsymbol{\mu}_{\text{spin}})_J &\equiv -g_J^s \mu_B \mathbf{J} \\ (\boldsymbol{\mu}_{\text{orb}})_J &\equiv -g_J^o \mu_B \mathbf{J}, \end{aligned} \quad (3.53)$$

where the proportional constants are given by

$$\begin{aligned} g_J &= \frac{3}{2} + \frac{S(S+1) - L(L+1)}{2J(J+1)} \\ g_J^s &= 1 + \frac{S(S+1) - L(L+1)}{J(J+1)} \\ g_J^o &= \frac{1}{2} - \frac{S(S+1) - L(L+1)}{2J(J+1)}. \end{aligned} \quad (3.54)$$

These factors are easily obtained by making the scalar product between Eq. (3.53) and J (See Fig. 3.2). The factor g_J is known as the Landé g -factor.

Table 3.1: Parameter values used in the calculation for the $3d$ ions. F^k and ζ_{3d} were obtained by Cowan's *ab initio* atomic HF program with relativistic correction.[23] This calculation was done for the average of the $3d^N$ configuration with all lower shells filled. The Slater integrals were reduced to 80% of their *ab initio* values, to account for intra-atomic CI. (The listed ones have already been renormalized.) All values are in unit of eV.

$3d^N$		F^2	F^4	ζ_{3d}	Δ_m
d^1	(Ti ³⁺)	—	—	0.019	1.0×10^{-4}
d^2	(V ³⁺)	8.1018	5.0825	0.027	1.0×10^{-4}
d^3	(Cr ³⁺)	8.6210	5.4029	0.035	1.0×10^{-4}
d^4	(Cr ²⁺)	7.7193	4.7997	0.030	5.0×10^{-6}
d^5	(Mn ²⁺)	8.2523	5.1292	0.040	1.0×10^{-4}
d^6	(Fe ²⁺)	8.7729	5.4507	0.052	1.0×10^{-4}
d^7	(Co ²⁺)	9.2837	5.7655	0.066	1.0×10^{-4}
d^8	(Ni ²⁺)	9.7868	6.0770	0.083	1.0×10^{-4}
d^9	(Cu ²⁺)	10.2840	6.3838	0.102	1.0×10^{-4}

Table 3.2: Calculated results for the $3d$ ions with spherical symmetry, based on the CI method. The second column "Term", such as ${}^2D_{3/2}$, is representing the ground-state multiplet deduced from the *LS*-coupling scheme. S , L , and J are evaluated by calculating $\langle \mathbf{S}^2 \rangle$ etc. and solving equations such as $S(S+1) = \langle \mathbf{S}^2 \rangle$. The magnetic moments μ , μ_{spin} , and μ_{orb} are in unit of μ_B . R_μ is the ratio of μ_{orb} to μ_{spin} ; $R_\mu = \mu_{\text{orb}}/\mu_{\text{spin}}$. One can see that these results fit in well with those resolved by the *LS*-coupling scheme.

$3d^N$	Term	S	L	J	μ	μ_{spin}	μ_{orb}	R_μ	$\langle J_z \rangle$	$\langle T_z \rangle$
d^1 (Ti ³⁺)	${}^2D_{3/2}$	1/2	2	3/2	-1.20	0.60	-1.80	-3.00	3/2	-0.60
d^2 (V ³⁺)	3F_2	1	3	2	-1.33	1.34	-2.67	-2.00	2	-0.26
d^3 (Cr ³⁺)	${}^4F_{3/2}$	3/2	3	3/2	-0.60	1.81	-2.40	-1.33	3/2	0.19
d^4 (Cr ²⁺)	5D_0	2	2	0	0.00	0.00	0.00	—	0	0.00
d^5 (Mn ²⁺)	${}^6S_{5/2}$	5/2	0	5/2	5.00	5.00	0.00	0.00	-5/2	0.00
d^6 (Fe ²⁺)	5D_4	2	2	4	6.00	4.00	2.00	0.50	-4	0.27
d^7 (Co ²⁺)	${}^4F_{9/2}$	3/2	3	9/2	6.00	3.00	3.00	1.00	-9/2	0.10
d^8 (Ni ²⁺)	3F_4	1	3	4	5.00	2.00	3.00	1.50	-4	-0.17
d^9 (Cu ²⁺)	${}^2D_{5/2}$	1/2	2	5/2	3.00	1.00	2.00	2.00	-5/2	-0.29

Calculated results and discussions — Numerical calculations based on the CI scheme show that the *LS*-coupling scheme well holds in the $3d$ ions with spherical symmetry. Used parameters are given in Table 3.1. Figures 3.3-3.8 show comparison between the CI and HF results as a function of the occupation number of the $3d$ orbital. Numerical values of calculated quantities are listed in Table 3.2 for the CI method and in Table 3.3 for the HF method. In all calculations the quantization axis was taken as z axis.

Figure 3.3 demonstrates the energy difference between the HF total energy and the true eigenvalue of the ground state gained by the CI method. It can be seen that the HF result agrees well with the CI one for the more than half filling case. On the other hand, significant deviations are observed in the less than half filling ($N=2, 3$, and 4). Figure 3.4 shows the calculated S and L . They are evaluated by calculating $\langle \mathbf{S}^2 \rangle$ etc. and solving equations such as $S(S+1) = \langle \mathbf{S}^2 \rangle$. Excellent agreements are seen between the CI and HF results, showing that the HF method can reproduce the Hund-rule S and L . The calculated J displayed in Fig. 3.5 shows that HFA overestimates J in the less than half filling case. Figure 3.6 gives the total magnetic moment $\mu = \mu_{\text{spin}} + \mu_{\text{orb}}$ and the individual moments' ratio $R_\mu = \mu_{\text{orb}}/\mu_{\text{spin}}$.

Table 3.3: Results of the HF calculation for the free $3d$ ions. The second column ΔE is the HF total energy in unit of meV, measured from the ground-state energy gained by the CI method. The other columns are the same as Table 3.2.

$3d^N$	ΔE	S	L	J	μ	μ_{spin}	μ_{orb}	R_μ	$\langle J_z \rangle$	$\langle T_z \rangle$
d^1 (Ti^{3+})	0	1/2	2	3/2	-1.20	0.60	-1.80	-3.00	3/2	-0.60
d^2 (V^{3+})	12.6	1	3	2.33	-1.00	1.99	-3.00	-1.50	2	-0.18
d^3 (Cr^{3+})	17.5	3/2	3	2.13	-0.00	3.00	-3.00	-1.00	3/2	0.13
d^4 (Cr^{2+})	15.6	2	2	1.54	2.00	4.00	-2.00	-0.50	0	0.30
d^5 (Mn^{2+})	0	5/2	0	5/2	5.00	5.00	0.00	0.00	-5/2	0.00
d^6 (Fe^{2+})	0.1	2	2	4	6.00	4.00	2.00	0.50	-4	0.27
d^7 (Co^{2+})	0	3/2	3	9/2	6.00	2.99	3.00	1.00	-9/2	0.10
d^8 (Ni^{2+})	0	1	3	4	5.00	2.00	3.00	1.50	-4	-0.17
d^9 (Cu^{2+})	0	1/2	2	5/2	3.00	1.00	2.00	2.00	-5/2	-0.29

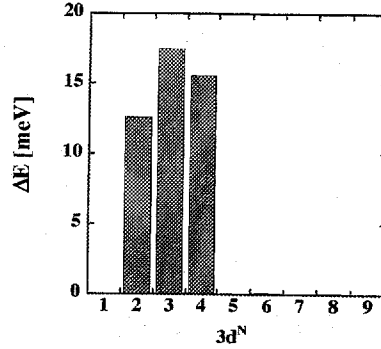


Figure 3.3: The HF total energy of the free $3d$ ions, measured from the ground-state eigenvalue obtained by the CI method.

Similar tendency of these quantities, as a function of the number of $3d$ electron, can be seen between the CI and HF results, although noticeable disagreement appears in the less than half filling. The individual moments themselves, μ_{spin} and μ_{orb} , are given in Fig. 3.7. $\langle J_z \rangle$ and $\langle T_z \rangle$ are in Fig. 3.8. $\langle J_z \rangle$ in HFA is completely identical with that of the CI method. As for $\langle T_z \rangle$, deviation is small. However, μ_{spin} and μ_{orb} in HFA show serious deviation from those of CI in the filling $N = 2, 3$, and 4.

To see the reason why some of the HF results deviate from CI's in the less than half filling case, we demonstrate the way of electron occupation into the $m\sigma$ basis in Fig. 3.9. First, in more than half filling case ($N \geq 5$) we can see that the HF results are wholly or almost the same as those by CI; the down-spin states are fully occupied, and the up-spin states come to be occupied from the smallest m basis as we increase the electron number. Since the LS -coupling constant λ , defined in Eqs. (3.50) and (3.51), is negative for $N > 5$, S and L are coupled in a parallel way so as to realize the maximum J . This leads to a *stretched* state where $\langle S_z \rangle$ and $\langle L_z \rangle$ take minimum values, $-S$ and $-L$, respectively, which are obtained by the way of occupation demonstrated in the lower panel of Fig. 3.9; one-electron states specified by $m\sigma$ come to be occupied one by one from the down spin state and further from the smallest m state. Such a stretched state is represented by a single determinant, which is achievable by HFA. This fact results in the excellent agreement between the CI and HF results. Secondly, let us examine the less than half filling case ($N = 2, 3$, and 4). In the CI scheme the electrons are distributed not only in the down-spin states but also in the up-spin states, to realize the minimum J resulting from the positive value of λ . In

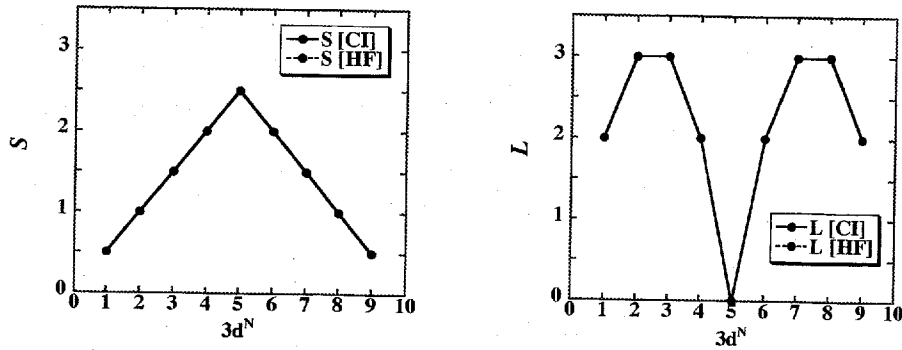


Figure 3.4: Calculated S and L of the free $3d$ ions. Solid and broken lines correspond to the results by the CI and HF method, respectively, although they are overlapping so that we can not tell one from another.

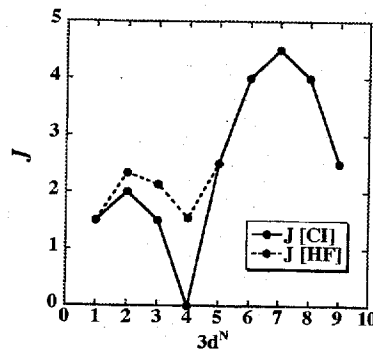


Figure 3.5: Calculated J of the free $3d$ ions.

HFA, however, the stretched states still hold as in the case of the more than half filling; the electron population is restricted to the down-spin states. The Hund-rule LS multiplets, deduced by H_{ee} alone, degenerate by $(2S+1)(2L+1)$ -fold. Among them, single-determinant states, which are accessible by HFA, are limited to only a few states: $[|M_S| = S, |M_L| = L]$ states, namely, the stretched states. In the Russell-Saunders case the Coulomb interaction is large compared with the spin-orbit interaction. Thus the HF procedure selects one of the stretched states as the lowest state in energy, even if it loses some energy from the spin-orbit interaction.

In summary, when the Coulomb interaction is so large compared with other one-body interactions, HFA is not a good approximation of the electronic state of the free $3d$ ions with less than half filling. In the real crystal, however, a large crystal field should act on the $3d$ electrons and moreover the $3d$ orbital should hybridize with orbitals of surrounding atoms. Hence it is expected that, in the real crystal, the description by HFA will be closer to the true one. In the next section, we will make a close study of this point by introducing a crystal field Hamiltonian with O_h symmetry.

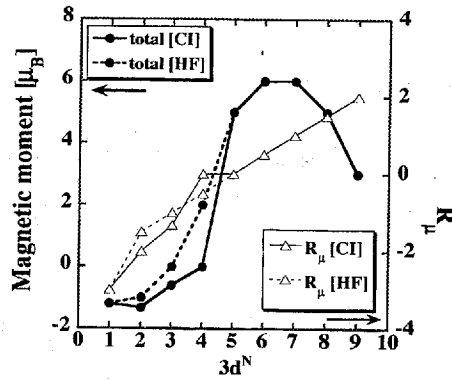


Figure 3.6: Calculated total magnetic moment $\mu = \mu_{\text{spin}} + \mu_{\text{orb}}$ (thick line with circle) and $R_\mu = \mu_{\text{orb}}/\mu_{\text{spin}}$ (thin line with triangle) in the free $3d$ ions. Solid line is by the CI method, and broken line by HFA.

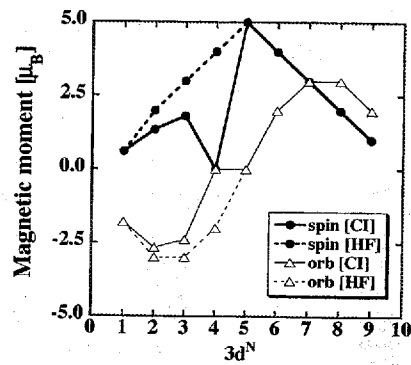


Figure 3.7: Calculated μ_{spin} (thick line with circle) and μ_{orb} (thin line with triangle) of the free $3d$ ions. Solid line is by the CI method, and broken line by HFA.

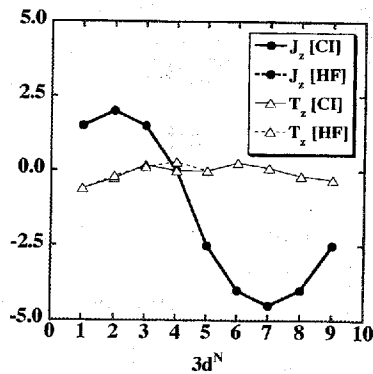


Figure 3.8: Calculated $\langle J_z \rangle$ (thick line with circle) and $\langle T_z \rangle$ (thin line with triangle) of the free $3d$ ions. Solid line is by the CI method, and broken line by HFA.

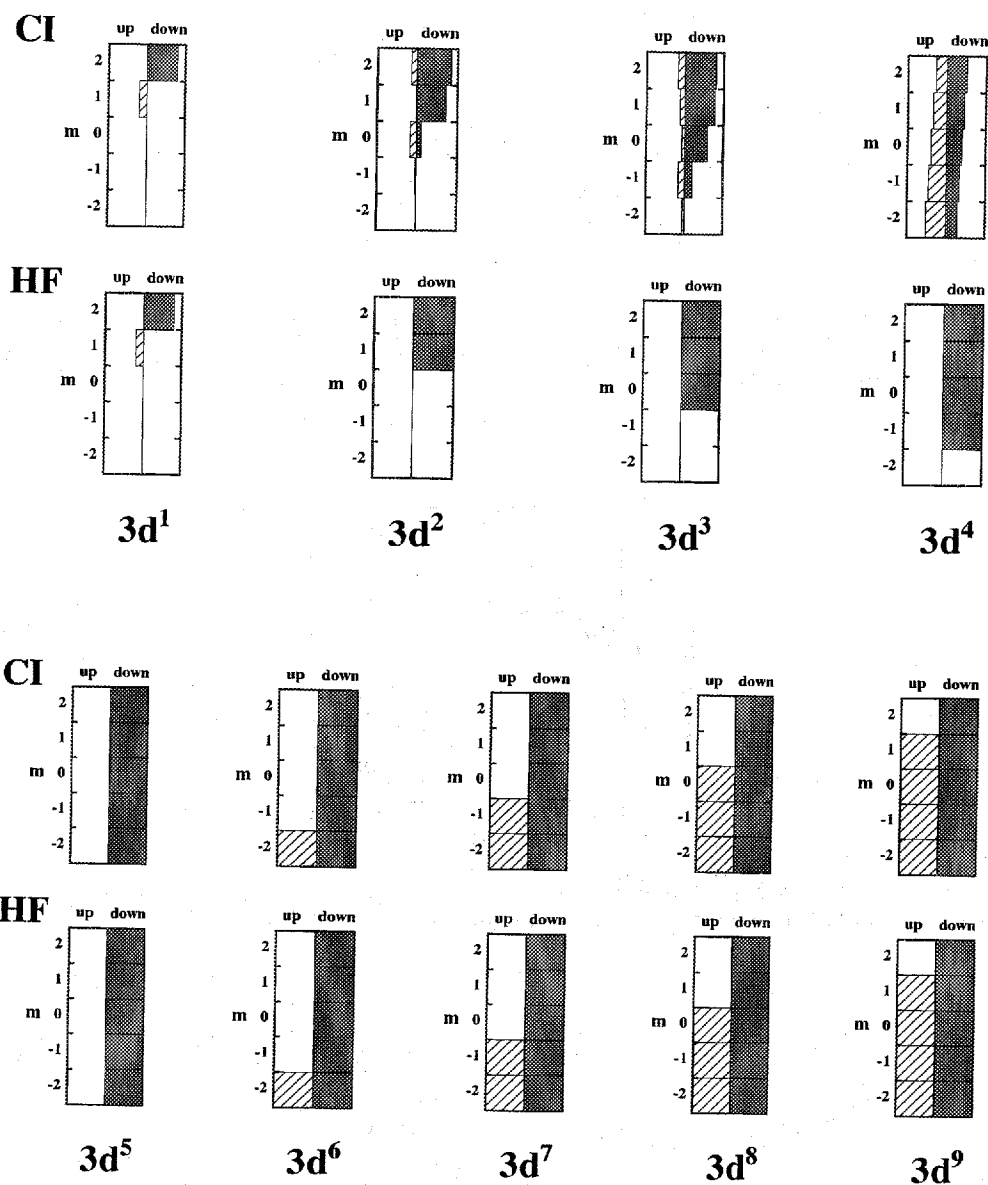


Figure 3.9: The way of electron occupation in the $m\sigma$ basis, for the free $3d$ ions. In each configuration the upper panel represents the result by the CI method, and lower by the HF method; the shaded or hatched area shows the probability of electron occupation of each $m\sigma$ state.

3.4.2 3d ion under O_h crystal field

In ionic crystals, 3d ions are often surrounded octahedrally by negatively charged ions such as O^{2-} (See Fig. 3.10). In such cases, 3d electrons feel a crystal field with O_h symmetry, and the five-fold degenerate orbital states of a single 3d electron split into three-fold T_{2g} state (ϕ_{xy} , ϕ_{yz} , and ϕ_{zx}) and two-fold E_g state ($\phi_{x^2-y^2}$ and $\phi_{3z^2-r^2}$). Functions in parentheses, such as ϕ_{xy} , are called the cubic harmonics which is given by an appropriate linear combination of the spherical harmonics Y_{2m} . The crystal-field splitting of one-electron state, $\epsilon(E_g) - \epsilon(T_{2g})$, is denoted by $10Dq$. The explicit form of H_{cry} is given by the following matrix whose basis is the orbital magnetic quantum number m ($m = -2, \dots, 2$):

$$H_{\text{cry}} = \begin{pmatrix} Dq & 0 & 0 & 0 & 5Dq \\ 0 & -4Dq & 0 & 0 & 0 \\ 0 & 0 & 6Dq & 0 & 0 \\ 0 & 0 & 0 & -4Dq & 0 \\ 5Dq & 0 & 0 & 0 & Dq \end{pmatrix}. \quad (3.55)$$

Typical value of $10Dq$ is about 1 eV for insulating oxides. This order of energy is smaller than that of the multipole interaction, but fairly larger than that of the spin-orbit interaction. We represent this situation by the following conceptual relation: $|H_{ee}| \gg |H_{\text{cry}}| \gg |H_{so}|$ (Note that this relation has no strict meaning). When this condition holds, the ground state of the 3d ion is approximately given by a simple picture. To begin with, H_{ee} realizes the Hund-rule S and L as in the case of the free ions. Then H_{cry} reduces the orbital state L to several irreducible representations of the O_h point group. The term energy of each irreducible representation can be gained by the method of equivalent operator.[24] For these procedures, a considerable knowledge of group theory is needed. We just show the outcomes of these processes. Fig. 3.11 manifests the way of splitting of each L , and in the following, the eigenvalues and eigenfunctions of the crystal field Hamiltonian effective for the Hund-rule LS multiplet are given:

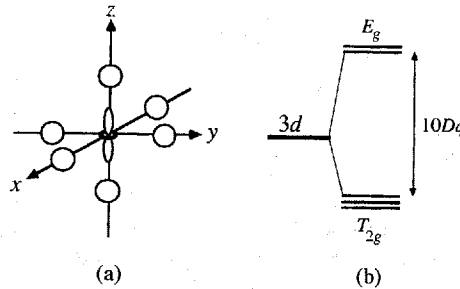


Figure 3.10: (a) Octahedral coordination. (b) Splitting of the 3d one-electron states due to the O_h crystal field.

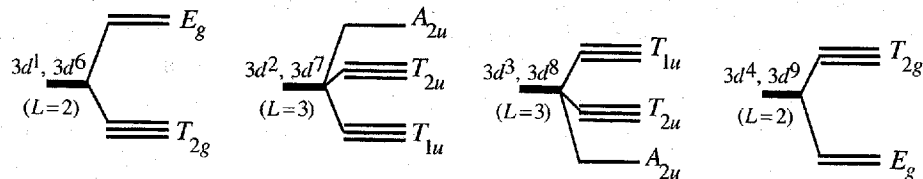


Figure 3.11: Splitting of the Hund-rule L state due to the O_h crystal field.

$$\begin{aligned}
 \underline{L = 2} \\
 \epsilon = -\frac{12}{5}\beta c \quad T_{2g} \quad \begin{cases} \phi_{xy} = \frac{i}{\sqrt{2}}(Y_{2-2} - Y_{22}) \\ \phi_{yz} = \frac{i}{\sqrt{2}}(Y_{2-1} + Y_{21}) \\ \phi_{zx} = \frac{i}{\sqrt{2}}(Y_{2-1} - Y_{21}) \end{cases} \\
 \epsilon = \frac{18}{5}\beta c \quad E_g \quad \begin{cases} \phi_{x^2-y^2} = \frac{1}{\sqrt{2}}(Y_{2-2} + Y_{22}) \\ \phi_{3z^2-r^2} = Y_{20} \end{cases}
 \end{aligned} \tag{3.56}$$

$$\begin{aligned}
 \underline{L = 3} \\
 \epsilon = 18\beta c \quad T_{1u} \\
 \begin{cases} \phi_{x(5x^2-3r^2)} = -\frac{1}{4}[\sqrt{3}(Y_{3-1} - Y_{31}) - \sqrt{5}(Y_{3-3} - Y_{33})] \\ \phi_{y(5y^2-3r^2)} = -\frac{i}{4}[\sqrt{3}(Y_{3-1} + Y_{31}) + \sqrt{5}(Y_{3-3} + Y_{33})] \\ \phi_{z(5z^2-3r^2)} = Y_{30} \end{cases} \\
 \epsilon = -6\beta c \quad T_{2u} \\
 \begin{cases} \phi_{x(y^2-z^2)} = -\frac{1}{4}[\sqrt{5}(Y_{3-1} - Y_{31}) + \sqrt{3}(Y_{3-3} - Y_{33})] \\ \phi_{y(z^2-x^2)} = +\frac{i}{4}[\sqrt{5}(Y_{3-1} + Y_{31}) - \sqrt{3}(Y_{3-3} + Y_{33})] \\ \phi_{z(x^2-y^2)} = \frac{1}{\sqrt{2}}(Y_{3-2} + Y_{32}) \end{cases} \\
 \epsilon = -36\beta c \quad A_{2u} \\
 \phi_{xyz} = \frac{i}{\sqrt{2}}(Y_{3-2} - Y_{32})
 \end{aligned} \tag{3.57}$$

Note that the used spherical harmonics in these expressions is the eigenfunction of the total orbital angular momentum \mathbf{L} and is not necessarily corresponding to the genuine wavefunction of the $3d^N$ electron system, which is given by a linear combination of Slater determinants. The factors c and β are defined as follows:

$$c = \frac{21}{4}(10Dq) \tag{3.58}$$

$$\beta = \pm \frac{2}{63} \frac{\{7S(2S-5) + 15\}(5-4S)}{(L-1)(2L-1)(2L-3)} \tag{3.59}$$

Here the upper sign refers to $N < 5$, and lower, $N > 5$.

Finally, H_{so} is taken into account by a perturbative treatment in the space of the Hund-rule spin S and the split orbital states. As shown in Fig. 3.11, the lowest orbital state in $3d^3$ and $3d^8$ configurations has no degeneracy. Its eigenstate, $|0\rangle$, is given by a real function because H_{ee} and H_{cry} , both of which have an origin in electrostatic interaction, are represented by real functions. On the other hand, \mathbf{L} is a pure imaginary operator and the expectation value $\langle 0|\mathbf{L}|0\rangle$ is also pure imaginary. This contradicts the fact that \mathbf{L} is a Hermitian operator and its diagonal element should be real. Then $\langle 0|\mathbf{L}|0\rangle=0$, *i.e.*, quenching of the orbital moment occurs when the crystal-field splitting state of the lowest energy has no degeneracy. This quenched moment will be partially recovered by H_{so} perturbation higher than or equal to the second order. When T_1 or T_2 is lowest in energy, both of which degenerate by three-fold, the first order perturbation of H_{so} is enough to induce the orbital moment, and this can be done by the method of pseudo orbital. See Refs. [25, 26] for details.

In the following, calculated results, obtained by a numerical calculation but not by the perturbative treatment described above, are summarized. Used parameters are $10Dq = 1.5$ eV and $\Delta_m = 0.02$ eV. F^k and ζ_{3d} are the same as those in Table 3.1. Figure 3.12 shows the way of electron population into the cubic basis. Compared with the free ion case, the agreement between the CI and HF results is fairly good for all electron filling. It should be noted that in the $3d^4$ and $3d^9$ configurations the displayed state degenerates

Table 3.4: Magnetic quantities of $3d$ ions under the crystal field with O_h symmetry, calculated by the CI method. $10Dq = 1.5$ eV and $\Delta_m = 0.02$ eV. The second column "Term", such as ${}^2T_{2g}$, is deduced by Hund's rules and the point group theory. S , L , and J are evaluated by solving equations such as $S(S+1) = \langle S^2 \rangle$. Magnetic moments μ , μ_{spin} , and μ_{orb} are in unit of μ_B . $R_\mu = \mu_{\text{orb}}/\mu_{\text{spin}}$.

$3d^N$	Term	S	L	J	μ	μ_{spin}	μ_{orb}	R_μ	$\langle J_z \rangle$	$\langle T_z \rangle$
d^1 (Ti^{3+})	${}^2T_{2g}$	1/2	2	1.93	-0.00	1.00	-1.00	-1.00	0.50	0.14
d^2 (V^{3+})	${}^3T_{1u}$	1	2.93	2.78	0.55	2.00	-1.45	-0.73	0.45	-0.13
d^3 (Cr^{3+})	${}^4A_{2u}$	3/2	3	3.44	2.91	3.00	-0.09	-0.03	-1.41	0
d^4 (Cr^{2+})	5E_g	2	2	2.95	3.92	3.99	-0.08	-0.02	-1.92	0.30
d^5 (Mn^{2+})	${}^6S_{5/2}$	5/2	0	5/2	5.00	5.00	0.00	0.00	-5/2	0.00
d^6 (Fe^{2+})	${}^5T_{2g}$	2	2	3.74	4.53	3.67	0.86	0.23	-2.69	-0.02
d^7 (Co^{2+})	${}^4T_{1u}$	3/2	2.95	4.25	3.43	2.37	1.05	0.44	-2.24	0.01
d^8 (Ni^{2+})	${}^3A_{2u}$	1	3	3.39	2.21	1.99	0.22	0.11	-1.21	-0.00
d^9 (Cu^{2+})	2E_g	1/2	2	2.22	1.25	1.00	0.26	0.26	-0.76	-0.26

Table 3.5: Same as Table 3.4, but calculated by HFA. The second column ΔE is the total energy in unit of meV, measured from the ground-state eigenvalue by the CI method.

$3d^N$	ΔE	S	L	J	μ	μ_{spin}	μ_{orb}	R_μ	$\langle J_z \rangle$	$\langle T_z \rangle$
d^1 (Ti^{3+})	0	1/2	2	1.93	-0.00	1.00	-1.00	-1.00	0.50	0.14
d^2 (V^{3+})	86.8	1	2.83	2.55	0.15	2.00	-1.85	-0.92	0.85	-0.16
d^3 (Cr^{3+})	0.2	3/2	3	3.45	2.91	3.00	-0.09	-0.03	-1.41	0
d^4 (Cr^{2+})	0.2	2	2	2.95	3.92	4.00	-0.08	-0.02	-1.92	0.30
d^5 (Mn^{2+})	0	5/2	0.01	5/2	5.00	5.00	0.00	0.00	-5/2	0.00
d^6 (Fe^{2+})	7.8	2	2	3.54	5.00	4.00	1.00	0.25	-3.00	-0.15
d^7 (Co^{2+})	111.3	3/2	2.86	4.09	5.00	2.99	2.01	0.67	-3.51	0.09
d^8 (Ni^{2+})	1.0	1	3	3.36	2.21	2.00	0.22	0.11	-1.21	-0.00
d^9 (Cu^{2+})	0	1/2	2	2.22	1.25	1.00	0.26	0.26	-0.76	-0.26

with $(\phi_{xy}\phi_{yz}\phi_{zx})^3(\phi_{x^2-y^2})^1$ state. This is related to the recent topic of the orbital ordering in manganites. Figures 3.13-3.17, which display various calculated quantities, also indicate that the ground-state properties of the $3d$ ions are well described by HFA. Numerical values of the calculated quantities are listed in Tables 3.4 and 3.5.

In summary we have introduced the O_h crystal field as an additional one-body term to examine the solid-state effect. The agreement between the CI and HF results has been improved compared with the free ion case. This suggests that HFA increases its accuracy with reinforcement of the one-body term. In Sec. 3.6 we would confirm this point by exploring the ground state of free uranium ion, where the one-body term is only H_{so} but the condition $|H_{\text{ee}}| \gg |H_{\text{so}}|$ is no longer satisfied. As for the real crystal, there exists hybridization (electron hopping) between orbitals of different atoms. This contributes considerably to the one-body term, especially in metals, prompting an expectation that HFA becomes a good approximation in crystals. In metallic substances, however, there is another problem concerned about F^0 , which has nothing to do with the present ionic case. Discussion about it will be given in the next chapter.

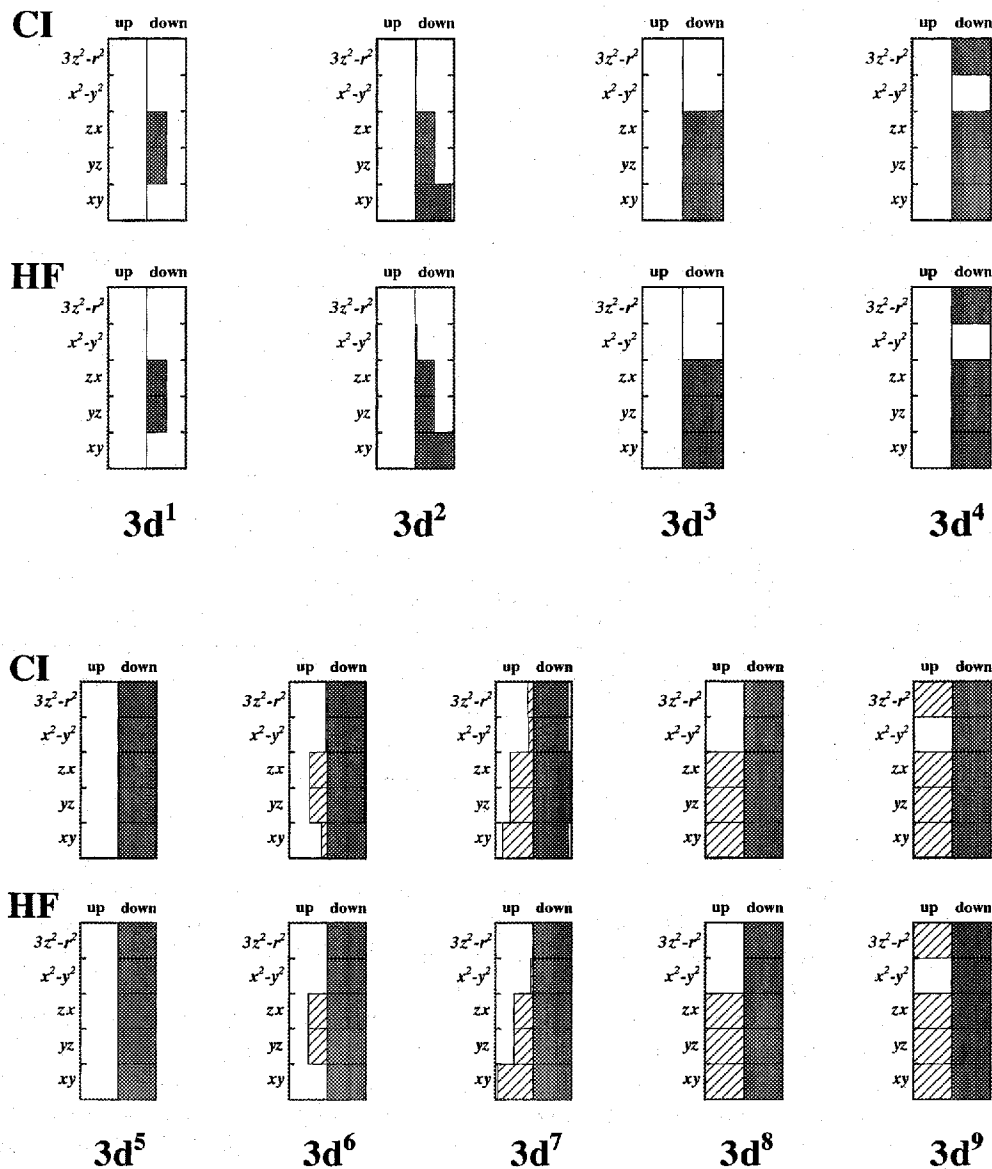


Figure 3.12: The way of electron occupation in the cubic basis, for the 3d ions in the O_h crystal field ($10Dq = 1.5$ eV). In each configuration the upper panel represents the result by the CI method, and lower by the HF method; the shaded or hatched area shows the probability of electron occupation of each state.

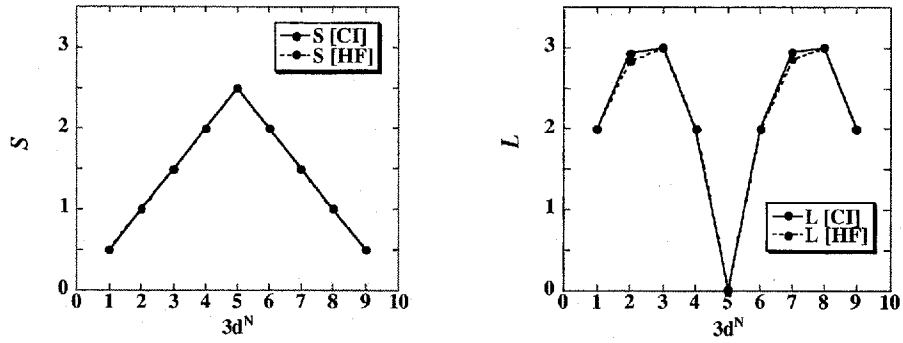


Figure 3.13: Calculated S and L of the 3d ions in the O_h crystal field ($10Dq = 1.5$ eV). Solid and broken lines correspond to the results by the CI and HF method, respectively.

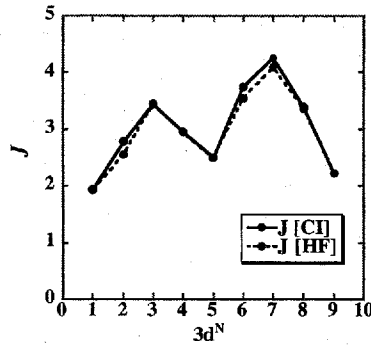


Figure 3.14: Calculated J of the 3d ions in the O_h crystal field ($10Dq = 1.5$ eV).

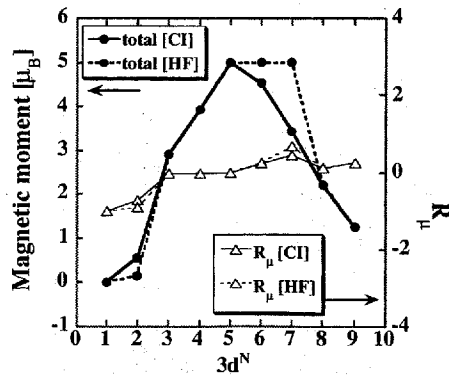


Figure 3.15: Calculated total magnetic moment $\mu = \mu_{\text{spin}} + \mu_{\text{orb}}$ (thick line with circle) and $R_\mu = \mu_{\text{orb}}/\mu_{\text{spin}}$ (thin line with triangle) of the 3d ions in the O_h crystal field ($10Dq = 1.5$ eV). Solid line is by the CI method, and broken line by HFA.

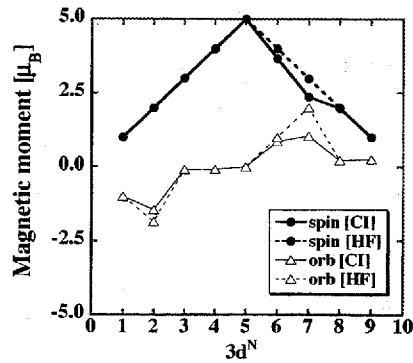


Figure 3.16: Calculated μ_{spin} (thick line with circle) and μ_{orb} (thin line with triangle) of the $3d$ ions in the O_h crystal field ($10Dq = 1.5$ eV). Solid line is by the CI method, and broken line by HFA.

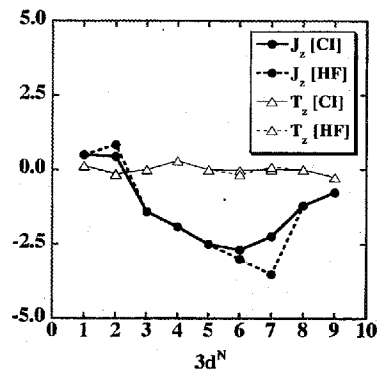


Figure 3.17: Calculated $\langle J_z \rangle$ (thick line with circle) and $\langle T_z \rangle$ (thin line with triangle) of the $3d$ ions in the O_h crystal field ($10Dq = 1.5$ eV). Solid line is by the CI method, and broken line by HFA.

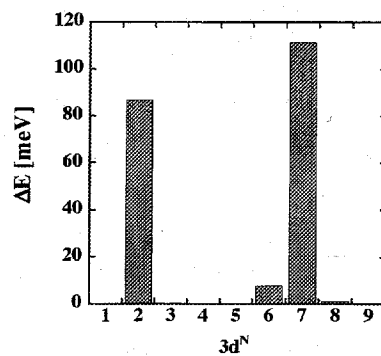


Figure 3.18: The HF total energy of the $3d$ ions in the O_h crystal field ($10Dq = 1.5$ eV), measured from the ground-state eigenvalue obtained by the CI method.

3.5 4f ion

We examine the ground state of 4f ions. In the spherical symmetry, the situation is completely the same as that of the 3d ions. The condition $|H_{ee}| \gg |H_{so}|$ holds, and the ground state is described by Hund's rules and the LS -coupling scheme. Thus determined ionic 4f states are usually valid even in solids in most cases. Even if we can not ignore the effect of the crystal field, it is considered to be very small compared with the spin-orbit interaction; the condition $|H_{ee}| \gg |H_{so}| \gg |H_{cry}|$ is satisfied in most cases. The effect of a weak O_h crystal field is examined.

In either spherical or O_h symmetry, the degree of appropriateness of HFA is investigated.

3.5.1 Spherical symmetry

The 4f ions are being in the Russell-Saunders case as in the case of the 3d ions. Their ground state is represented by the quantum numbers SL deduced from Hund's rules, and J from the LS coupling. HFA gives precise results in more than half filling but fails in less than half filling.

Figures 3.19-3.24 show the calculated results based on the CI and HF method. Numerical values of the calculated quantities are given in Tables 3.7 and 3.8, and used parameters are listed in Table 3.6.

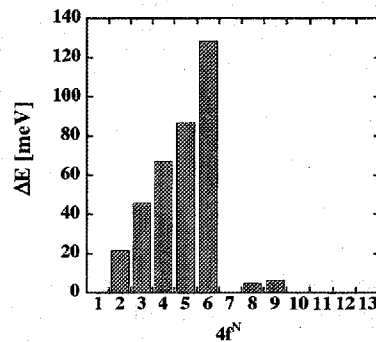


Figure 3.19: The HF total energy of the free 4f ions, measured from that obtained by the CI method.

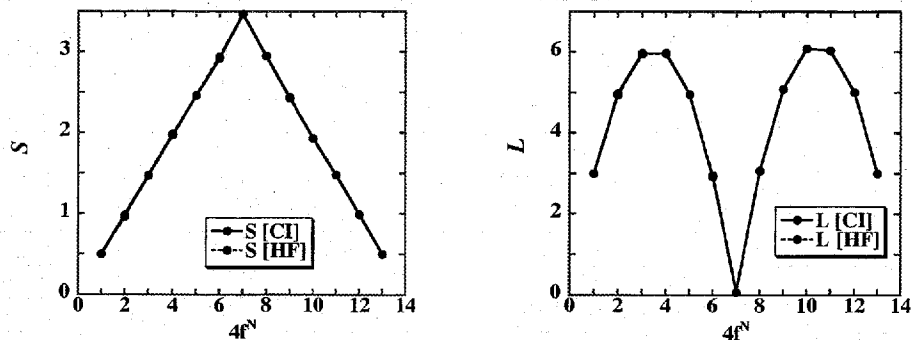


Figure 3.20: Calculated S and L of the free 4f ions. Solid and broken lines correspond to the results by the CI and HF method, respectively, although they are overlapping so that we can not tell one from another.

Table 3.6: Parameter values used in the calculation for the $4f$ ions. F^k and ζ_{4f} were obtained by Cowan's *ab initio* atomic HF program with relativistic correction.[23] This calculation was done for the average of the $4f^N$ configuration with all lower shells filled. The Slater integrals were reduced to 80% of their *ab initio* values, to account for intra-atomic CI. (The listed ones have already been renormalized.) All values are in unit of eV.

$4f^N$		F^2	F^4	F^6	ζ_{4f}	Δ_m
f^1	(Ce ³⁺)	—	—	—	0.087	1.0×10^{-4}
f^2	(Pr ³⁺)	9.7808	6.1355	4.3538	0.102	1.0×10^{-4}
f^3	(Nd ³⁺)	10.1789	6.3869	4.5496	0.119	1.0×10^{-4}
f^4	(Pm ³⁺)	10.5574	6.6243	4.7173	0.136	1.0×10^{-4}
f^5	(Sm ³⁺)	10.9187	6.8518	4.9171	0.155	1.0×10^{-4}
f^6	(Eu ³⁺)	11.2668	7.0703	5.0468	0.175	2.0×10^{-6}
f^7	(Gd ³⁺)	11.6040	7.2816	5.2079	0.197	1.0×10^{-4}
f^8	(Tb ³⁺)	11.9324	7.4875	5.3661	0.221	1.0×10^{-4}
f^9	(Dy ³⁺)	12.2530	7.6880	5.4422	0.246	1.0×10^{-4}
f^{10}	(Ho ³⁺)	12.5664	7.8832	5.5965	0.273	1.0×10^{-4}
f^{11}	(Er ³⁺)	12.8736	8.0744	5.7452	0.302	1.0×10^{-4}
f^{12}	(Tm ³⁺)	13.1761	8.2633	5.8871	0.333	1.0×10^{-4}
f^{13}	(Yb ³⁺)	13.4745	8.4489	5.9922	0.366	1.0×10^{-4}

Table 3.7: Calculated results for the free $4f$ ions, based on the CI method. The column "Term", such as $^2F_{5/2}$, is the ground-state multiplet deduced by the Hund rules and *LS*-coupling scheme. S , L , and J are evaluated by solving equations such as $S(S+1) = \langle S^2 \rangle$. The magnetic moments μ , μ_{spin} , and μ_{orb} are in unit of μ_B . $R_\mu = \mu_{\text{orb}}/\mu_{\text{spin}}$. It is seen that the *LS*-coupling scheme holds well as in the case of the free $3d$ ions.

$4f^N$	Term	S	L	J	μ	μ_{spin}	μ_{orb}	R_μ	$\langle J_z \rangle$	$\langle T_z \rangle$
f^1 (Ce ³⁺)	$^2F_{5/2}$	1/2	3	5/2	-2.14	0.71	-2.86	-4.00	5/2	-0.57
f^2 (Pr ³⁺)	3H_4	0.98	4.97	4	-3.23	1.54	-4.77	-3.10	4	-0.67
f^3 (Nd ³⁺)	$^4I_{9/2}$	1.47	5.97	9/2	-3.30	2.40	-5.70	-2.38	9/2	-0.39
f^4 (Pm ³⁺)	5I_4	1.97	5.97	4	-2.43	3.15	-5.57	-1.77	4	0.03
f^5 (Sm ³⁺)	$^6H_{5/2}$	2.46	4.95	5/2	-0.75	3.50	-4.25	-1.21	5/2	0.39
f^6 (Eu ³⁺)	7F_0	2.92	2.92	0	0	0	0	—	0	0
f^7 (Gd ³⁺)	$^8S_{7/2}$	3.47	0.07	7/2	6.97	6.93	0.03	0.005	-7/2	0.01
f^8 (Tb ³⁺)	7F_6	2.95	3.07	6	8.94	5.89	3.06	0.52	-6	0.24
f^9 (Dy ³⁺)	$^6H_{15/2}$	2.43	5.09	15/2	9.92	4.83	5.08	1.05	-15/2	0.13
f^{10} (Ho ³⁺)	5I_8	1.93	6.09	8	9.92	3.83	6.08	1.59	-8	-0.14
f^{11} (Er ³⁺)	$^4I_{15/2}$	1.48	6.04	15/2	8.97	2.93	6.03	2.06	-15/2	-0.31
f^{12} (Tm ³⁺)	3H_6	0.99	5.01	6	6.99	1.98	5.01	2.53	-6	-0.41
f^{13} (Yb ³⁺)	$^2F_{7/2}$	1/2	3	7/2	4	1	3	3	-7/2	-0.33

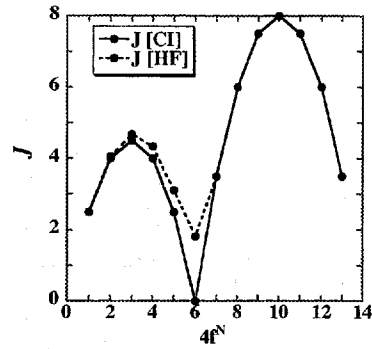


Figure 3.21: Calculated J of the free $4f$ ions. Solid line is by the CI method, and broken line by HFA.

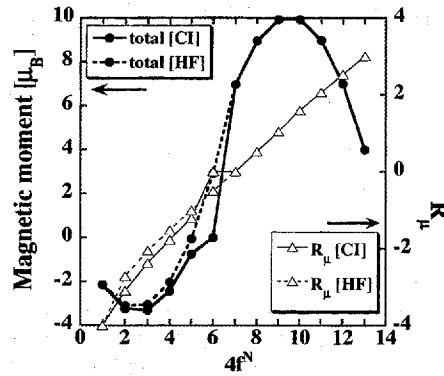


Figure 3.22: Calculated total magnetic moment $\mu = \mu_{\text{spin}} + \mu_{\text{orb}}$ (thick line with circle) and $R_\mu = \mu_{\text{orb}}/\mu_{\text{spin}}$ (thin line with triangle) in the free $4f$ ions. Solid line is by the CI method, and broken-line by HFA.

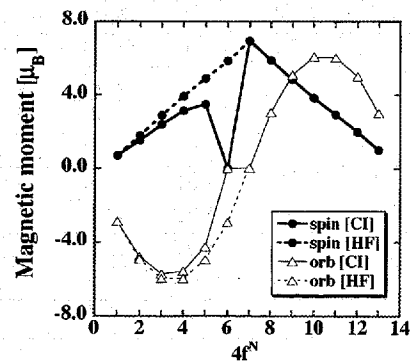


Figure 3.23: Calculated μ_{spin} (thick line with circle) and μ_{orb} (thin line with triangle) of the free $4f$ ions. Solid line is by the CI method, and broken line by HFA.

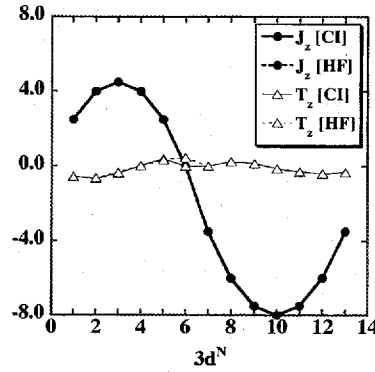


Figure 3.24: Calculated $\langle J_z \rangle$ (thick line with circle) and $\langle T_z \rangle$ (thin line with triangle) of the free 4f ions. Solid line is by the CI method, and broken line by HFA.

Table 3.8: Calculated results for the free 4f ions, based on HFA. The second column ΔE is the deviation of the HF total energy from the CI ground-state energy, in unit of meV. The other columns are the same as Table 3.7.

f^N	ΔE	S	L	J	μ	μ_{spin}	μ_{orb}	R_μ	$\langle J_z \rangle$	$\langle T_z \rangle$
f^1 (Ce ³⁺)	0	1/2	3	5/2	-2.14	0.71	-2.86	-4.00	5/2	-0.57
f^2 (Pr ³⁺)	21.6	0.96	4.94	4.06	-3.10	1.80	-4.90	-2.72	4	-0.63
f^3 (Nd ³⁺)	45.9	1.47	5.96	4.68	-3.06	2.89	-5.95	-2.06	9/2	-0.34
f^4 (Pm ³⁺)	67.3	1.98	5.97	4.34	-2.03	3.93	-5.97	-1.52	4	0.02
f^5 (Sm ³⁺)	87.1	2.46	4.96	3.11	-0.05	4.90	-4.95	-1.01	5/2	0.33
f^6 (Eu ³⁺)	128.4	2.94	2.95	1.82	2.93	5.86	-2.93	-0.50	0	0.47
f^7 (Gd ³⁺)	0.3	3.47	0.07	3.50	6.97	6.93	0.03	0.005	-7/2	0.01
f^8 (Tb ³⁺)	4.9	2.95	3.06	6.00	8.95	5.89	3.05	0.52	-6	0.24
f^9 (Dy ³⁺)	6.5	2.44	5.09	7.50	9.92	4.85	5.08	1.05	-15/2	0.13
f^{10} (Ho ³⁺)	0.5	1.93	6.09	8.00	9.92	3.83	6.08	1.59	-8	-0.14
f^{11} (Er ³⁺)	0.0	1.48	6.04	7.50	8.97	2.93	6.03	2.06	-15/2	-0.31
f^{12} (Tm ³⁺)	0	0.99	5.01	6	6.99	1.98	5.01	2.53	-6	-0.41
f^{13} (Yb ³⁺)	0	1/2	3	7/2	4	1	3	3	-7/2	-0.33

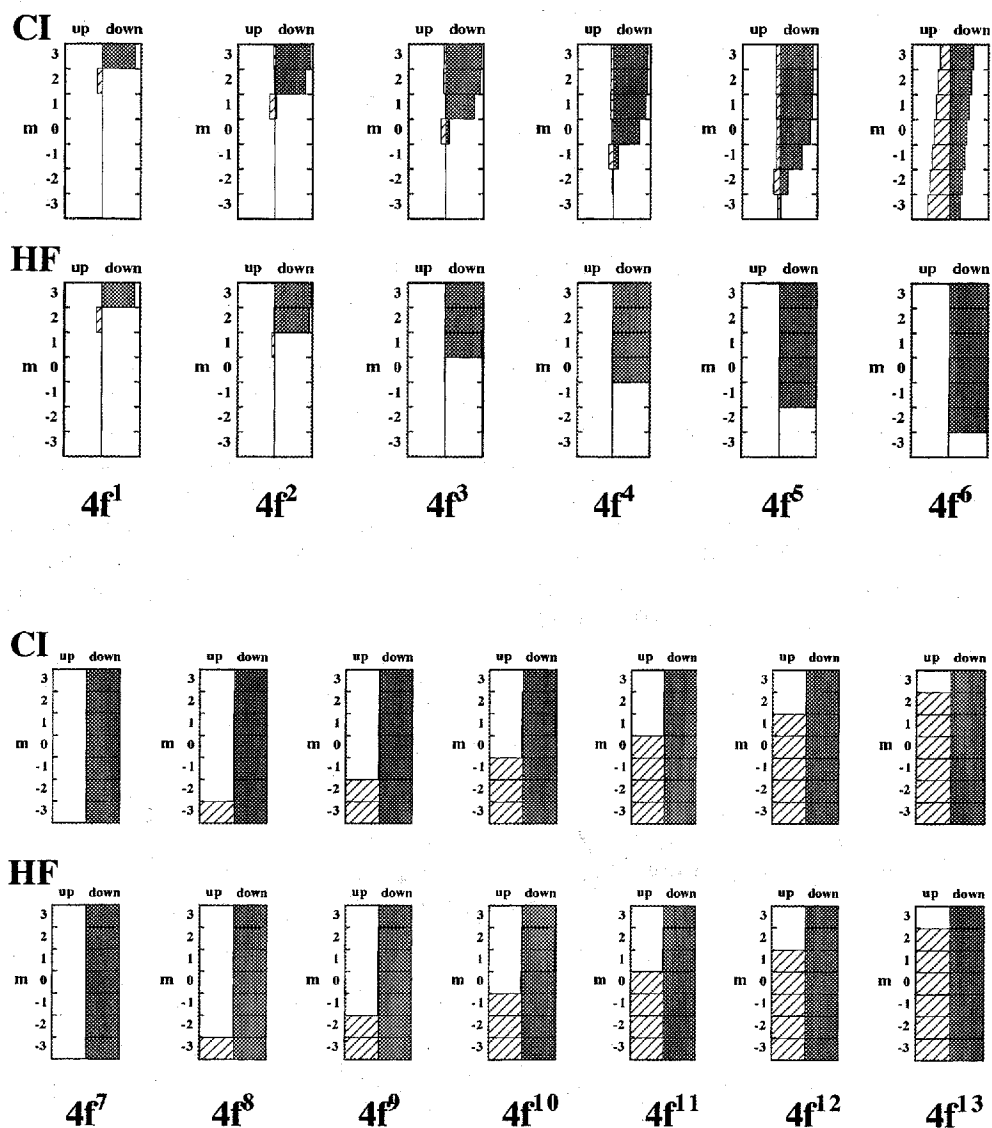


Figure 3.25: Electron population in the $m\sigma$ basis, for the $4f$ ions with spherical symmetry. In each configuration the upper panel represents the result by the CI method, and lower by the HF method. The shaded or hatched area shows the probability of electron occupation of each $m\sigma$ state.

3.5.2 $4f$ ions in O_h symmetry — Weak crystal field

We consider the effect of a small crystal field with O_h symmetry on the $4f$ ions. Figure 3.26 demonstrates the assumed crystal field, where the splitting energy is represented by only one parameter B for simplicity (This corresponds to an approximation that the sixth-order of r in the crystal field is ignored). The explicit form of the assumed H_{cry} is given by the following matrix whose basis is the orbital magnetic quantum number m ($m = -3, \dots, 3$):

$$H_{\text{cry}} = \frac{B}{2} \begin{pmatrix} 3 & 0 & 0 & 0 & \sqrt{15} & 0 & 0 \\ 0 & -7 & 0 & 0 & 0 & 5 & 0 \\ 0 & 0 & 1 & 0 & 0 & 0 & \sqrt{15} \\ 0 & 0 & 0 & 6 & 0 & 0 & 0 \\ \sqrt{15} & 0 & 0 & 0 & 1 & 0 & 0 \\ 0 & 5 & 0 & 0 & 0 & -7 & 0 \\ 0 & 0 & \sqrt{15} & 0 & 0 & 0 & 3 \end{pmatrix}. \quad (3.60)$$

For the numerical calculations we take $B = 2.0 \times 10^{-3}$ eV and $\Delta_m = 1.0 \times 10^{-4}$ eV. The other parameters are the same as in Table 3.6. Then the condition $|H_{\text{ee}}| \gg |H_{\text{so}}| \gg |H_{\text{cry}}|$ is satisfied and we can simulate a realistic situation of the $4f$ ions in solid. The calculated results are displayed in Figs. 3.27-3.33, and listed in Tables 3.9 and 3.10. One can see that the HF results for the magnetic moments μ_{spin} and μ_{orb} considerably deviate from those by the CI method, for all configuration except $N = 1, 7$, and 13. The crystal field applied now is not sufficiently large for HFA to be a good approximation. Since the present parameter set is a realistic one, it can be said that HFA is not suited for describe electronic structure of crystals which contain rare-earth atoms.

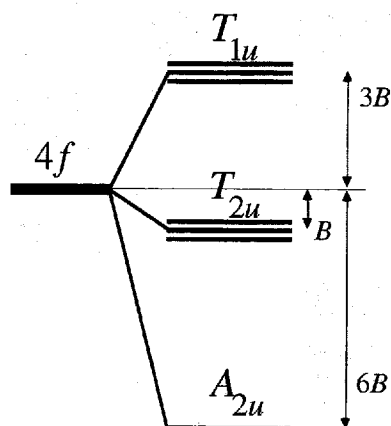


Figure 3.26: O_h crystal field splitting of the $4f$ one-electron orbital state.

Table 3.9: Magnetic quantities of 4f ions under the crystal field with O_h symmetry, calculated by the CI method. See text for the explicit form of H_{cry} . $B = 0.002$ eV and $\Delta_m = 1.0 \times 10^{-4}$ eV. Conceptually speaking, the present parameter set corresponds to $|H_{\text{ee}}| \gg |H_{\text{so}}| \gg |H_{\text{cry}}|$. The column "Term" represents the free-ion's ground-state multiplet. S , L , and J are evaluated by solving equations such as $S(S+1) = \langle S^2 \rangle$. The magnetic moments μ , μ_{spin} , and μ_{orb} are in unit of μ_B . $R_\mu = \mu_{\text{orb}}/\mu_{\text{spin}}$.

$4f^N$	Term	S	L	J	μ	μ_{spin}	μ_{orb}	R_μ	$\langle J_z \rangle$	$\langle T_z \rangle$
f^1 (Ce ³⁺)	$^2F_{5/2}$	1/2	3	5/2	-0.71	0.26	-0.97	-3.71	0.84	-0.19
f^2 (Pr ³⁺)	3H_4	0.98	4.97	4	-0.08	0.04	-0.12	-3.04	0.10	-0.02
f^3 (Nd ³⁺)	$^4I_{9/2}$	1.47	5.97	9/2	-1.47	1.07	-2.53	-2.38	2.00	-0.17
f^4 (Pm ³⁺)	5I_4	1.97	5.97	4	-1.53	1.99	-3.53	-1.77	2.53	0.02
f^5 (Sm ³⁺)	$^6H_{5/2}$	2.46	4.95	5/2	-0.23	1.37	-1.61	-1.17	0.92	0.14
f^6 (Eu ³⁺)	7F_0	2.92	2.92	0	0.01	0.03	-0.01	-0.50	0.00	0.00
f^7 (Gd ³⁺)	$^8S_{7/2}$	3.47	0.07	7/2	6.97	6.93	0.03	0.005	-7/2	0.01
f^8 (Tb ³⁺)	7F_6	2.95	3.07	6	2.20	1.45	0.75	0.52	-1.48	0.06
f^9 (Dy ³⁺)	$^6H_{15/2}$	2.43	5.09	15/2	6.45	3.15	3.31	1.05	-4.88	0.08
f^{10} (Ho ³⁺)	5I_8	1.93	6.09	8	6.73	2.60	4.13	1.59	-5.43	-0.09
f^{11} (Er ³⁺)	$^4I_{15/2}$	1.48	6.04	15/2	5.62	1.84	3.78	2.05	-4.70	-0.20
f^{12} (Tm ³⁺)	3H_6	0.99	5.01	6	0.44	0.13	0.32	2.52	-0.38	-0.03
f^{13} (Yb ³⁺)	$^2F_{7/2}$	1/2	3	7/2	1.36	0.34	1.02	3.00	-1.19	-0.11

Table 3.10: Same as Table 3.9, but calculated by HFA. ΔE , the energy difference between the HF and CI methods, is in unit of meV.

$4f^N$	ΔE	S	L	J	μ	μ_{spin}	μ_{orb}	R_μ	$\langle J_z \rangle$	$\langle T_z \rangle$
f^1 (Ce ³⁺)	0	1/2	3	5/2	-0.71	0.26	-0.97	-3.71	0.84	-0.19
f^2 (Pr ³⁺)	23.2	0.96	4.94	4.06	-3.10	1.80	-4.90	-2.72	4.00	-0.63
f^3 (Nd ³⁺)	45.7	1.47	5.96	4.68	-3.05	2.89	-5.95	-2.06	4.50	-0.34
f^4 (Pm ³⁺)	129.9	1.97	5.97	4.65	-1.04	3.91	-4.96	-1.27	3.00	0.01
f^5 (Sm ³⁺)	93.0	2.46	4.96	3.11	-0.05	4.90	-4.95	-1.01	2.50	0.33
f^6 (Eu ³⁺)	125.3	2.94	2.95	1.82	2.93	5.86	-2.93	-0.50	-0.00	0.47
f^7 (Gd ³⁺)	0.2	3.47	0.07	7/2	6.97	6.93	0.03	0.005	-7/2	0.01
f^8 (Tb ³⁺)	11.3	2.95	3.06	6	8.95	5.89	3.05	0.52	-6.00	0.24
f^9 (Dy ³⁺)	6.7	2.44	5.09	15/2	9.92	4.85	5.08	1.05	-15/2	0.13
f^{10} (Ho ³⁺)	0.6	1.93	6.09	8	9.92	3.83	6.08	1.59	-8.00	-0.14
f^{11} (Er ³⁺)	5.9	1.48	6.04	15/2	8.97	2.93	6.03	2.06	-15/2	-0.31
f^{12} (Tm ³⁺)	8.9	0.99	5.01	6	6.99	1.98	5.01	2.53	-6.00	-0.41
f^{13} (Yb ³⁺)	0	1/2	3	7/2	1.36	0.34	1.02	3.00	-1.19	-0.11

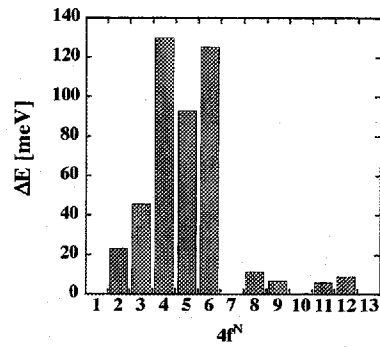


Figure 3.27: The HF total energy of the $4f$ ions in the weak O_h crystal field, measured from the ground-state eigenvalue obtained by the CI method.

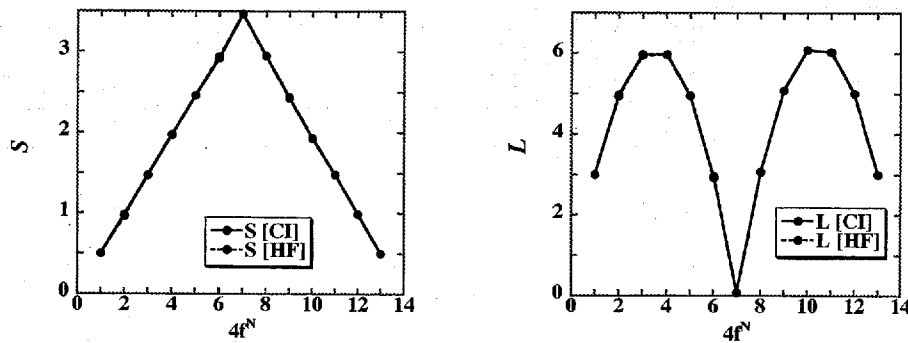


Figure 3.28: Calculated S and L of the $4f$ ions in the weak O_h crystal field. Solid and broken lines correspond to the results by the CI and HF method, respectively.

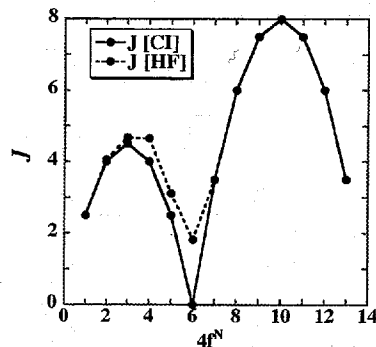


Figure 3.29: Calculated J of the $4f$ ions in the weak O_h crystal field.

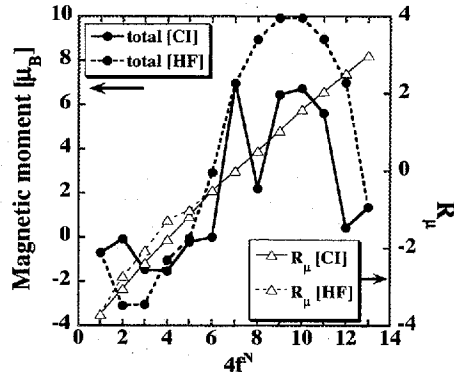


Figure 3.30: Calculated total magnetic moment $\mu = \mu_{\text{spin}} + \mu_{\text{orb}}$ (thick line with circle) and $R_\mu = \mu_{\text{orb}}/\mu_{\text{spin}}$ (thin line with triangle) of the 4f ions in the weak O_h crystal field. Solid line is by the CI method, and broken line by HFA.

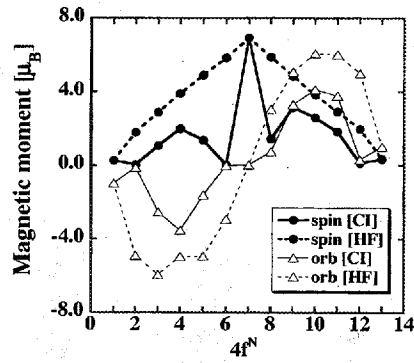


Figure 3.31: Calculated μ_{spin} (thick line with circle) and μ_{orb} (thin line with triangle) of the 4f ions in the weak O_h crystal field. Solid line is by the CI method, and broken line by HFA.

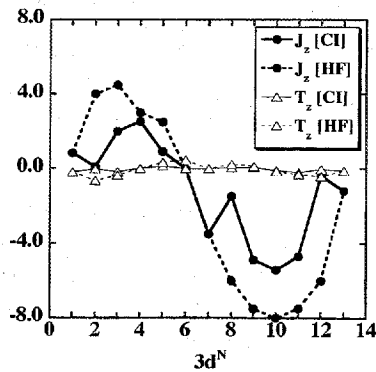


Figure 3.32: Calculated $\langle J_z \rangle$ (thick line with circle) and $\langle T_z \rangle$ (thin line with triangle) of the 4f ions in the weak O_h crystal field. Solid line is by the CI method, and broken line by HFA.

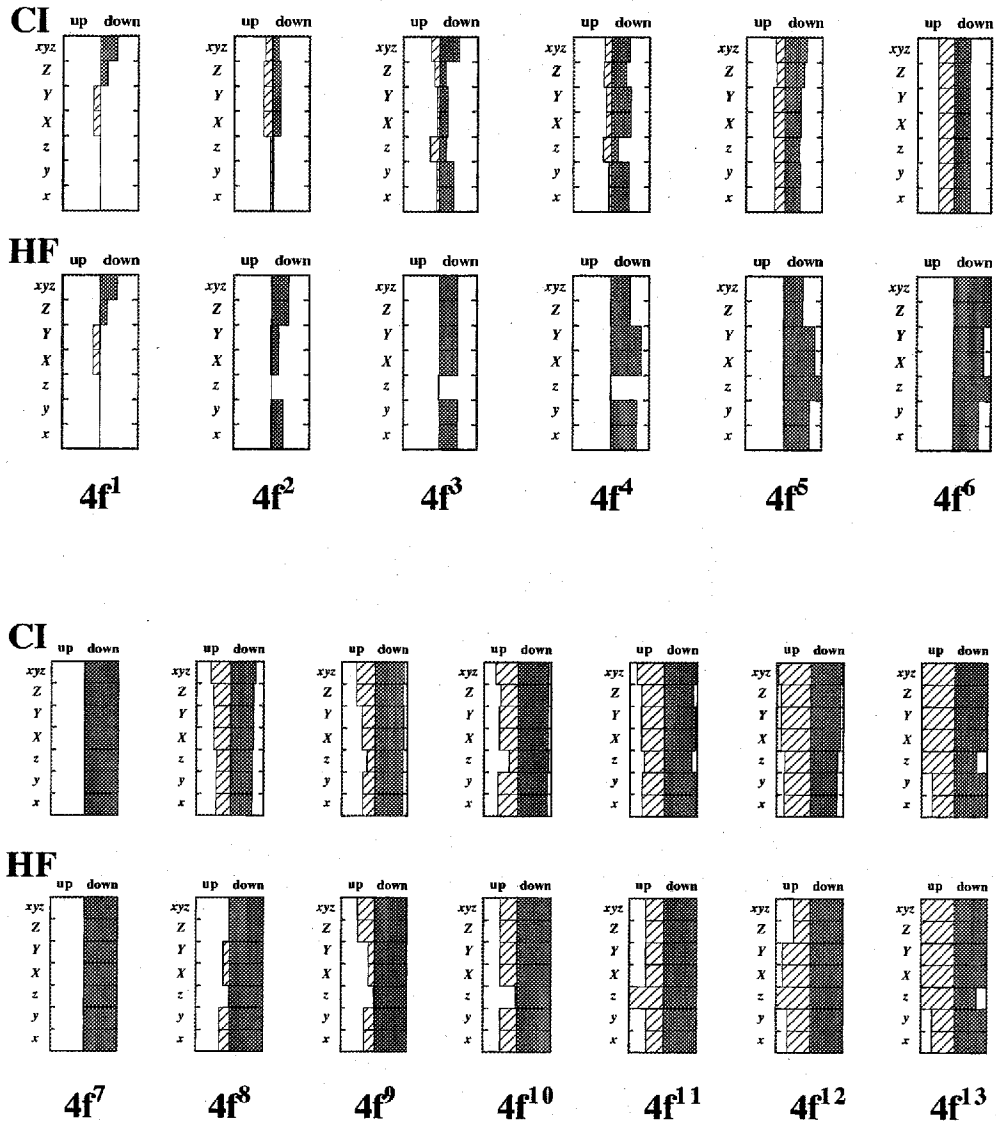


Figure 3.33: The way of electron population in the cubic basis, for the $4f$ ions in the weak O_h crystal field. In each configuration the upper panel represents the result by the CI method, and lower by the HF method. In the figures, x , y , and z denote the bases of T_{1u} representation; X , Y , and Z are the T_{2u} bases; xyz is the A_{2u} basis. The shaded or hatched area shows the probability of electron occupation of each state.

3.6 U ion

The ground state of uranium ions, which have the $5f$ shell as an incomplete shell, is investigated in this section. Radial wavefunction of the $5f$ orbital, $R_{5f}(r)$, has a distinct difference from the $4f$ one; R_{5f} spreads rather outside with possessing one node, in order to satisfy the orthogonalization with the core-state's R_{4f} . Consequently, the Slater integrals are smaller than those of rare-earth elements (For comparison, see Tables 3.11 and 3.6). As for the coupling constant of the $5f$ spin-orbit interaction, ζ_{5f} , however, due to the large atomic nucleus, it has a large value with the same order as that of the rare-earth elements, ζ_{4f} . As a result of these facts, the situation in the U ions do not pertain to the Russell-Saunders case; the condition $|H_{ee}| \gg |H_{so}|$ is not gratified sufficiently. In the limit of strong spin-orbit interaction, ground state is described by the jj -coupling scheme; individual electrons have resultant angular momentum $\mathbf{j} = \mathbf{l} + \mathbf{s}$ with the aid of H_{so} , and then the multipole Coulomb interaction H_{ee} forms total angular momentum $\mathbf{J} = \mathbf{j}_1 + \mathbf{j}_2 + \dots$. Unfortunately, neither the LS -coupling scheme nor jj -coupling scheme explains the actinide system (this situation is known as *intermediate coupling*), and an analytic theory as in the case of the $3d$ and $4f$ ions is not feasible. We should rely on a numerical calculation to get the ground state.

On the analogy of the calculation of the $3d$ ions in O_h crystal field, discussed in Sec. 3.4.2, a good result is expected for HFA since the one-body term H_{so} of the U ions is rather strong. Figure 3.34 shows the way of electron population in $m\sigma$ basis, calculated by the CI and HF methods. In contrast to the case of the free $4f$ ions (see Fig. 3.25), HFA well describes the extension of the population into the minority spin states. Tables 3.12 and 3.13 give the calculated magnetic quantities. One can see that the agreement between the CI and HF results is fairly good; the deviation is less than 15% for all quantities. In conclusion, HFA can be a good starting point to describe the U $5f$ ground state as far as the magnetic moments are concerned.

Table 3.11: Parameter values of the U ions in unit of eV. F^k 's and ζ_{5f} are from Ref. [27], but F^k 's are scaled to 80% of their bare values, to account for the intra-atomic correlation effect.

$5f^N$		F^2	F^4	F^6	ζ_{5f}	Δ_m
f^2	(U ⁴⁺)	7.611	4.979	3.655	0.261	1.0×10^{-4}
f^3	(U ³⁺)	7.086	4.598	3.363	0.235	1.0×10^{-4}

Table 3.12: Calculated results for the free U ions, based on the CI method. S , L , and J are obtained by solving equations such as $S(S+1) = \langle S^2 \rangle$. The magnetic moments μ , μ_{spin} , and μ_{orb} are in unit of μ_B . $R_\mu = \mu_{\text{orb}}/\mu_{\text{spin}}$.

$5f^N$	S	L	J	μ	μ_{spin}	μ_{orb}	R_μ	$\langle J_z \rangle$	$\langle T_z \rangle$
f^2 (U ⁴⁺)	0.93	4.89	4	-3.30	1.40	-4.70	-3.36	4	-0.81
f^3 (U ³⁺)	1.38	5.85	9/2	-3.41	2.18	-5.59	-2.56	9/2	-0.63

Table 3.13: Same as Table 3.12, but calculated by the HF method. Deviations of the HF result from the CI one are represented in parentheses by percentage. The second column ΔE is the energy difference between HF and CI, in unit of meV.

$5f^N$	ΔE	S	L	J	μ	μ_{spin}	μ_{orb}	R_{μ}	$\langle J_z \rangle$	$\langle T_z \rangle$
$f^2 (\text{U}^{4+})$	15.1	0.90	4.85	4.01	-3.26	1.48	-4.74	-3.21	4	-0.81
		(-3)	(-1)	(0)	(-1)	(6)	(1)	(5)	(0)	(0)
$f^3 (\text{U}^{3+})$	52.3	1.35	5.81	4.58	-3.25	2.49	-5.75	-2.30	9/2	-0.60
		(-2)	(-1)	(2)	(-5)	(14)	(3)	(-10)	(0)	(-5)

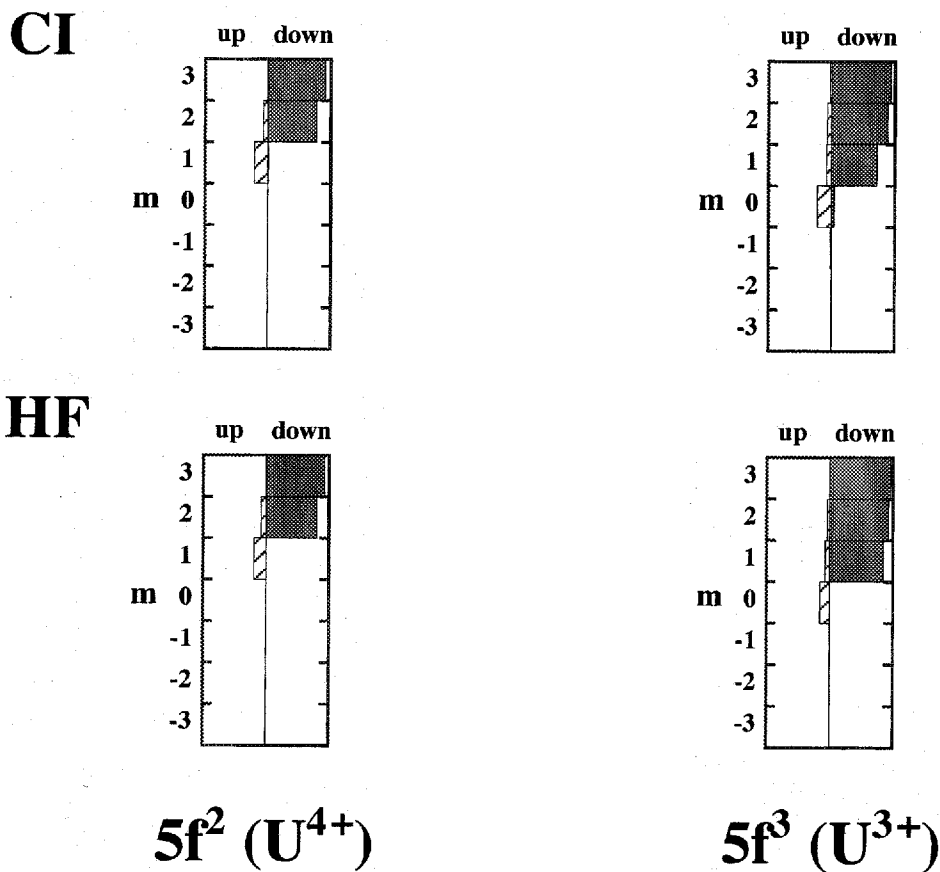


Figure 3.34: Electron population in the $m\sigma$ basis, for the free U ions. In each configuration the upper panel represents the result by the CI method, and lower by the HF method. The shaded or hatched area shows the probability of electron occupation of each state.

3.7 Summary

We have investigated the atomic ground state of the $3d$, $4f$, and U isolated ions, and examined the validity of HFA.

The $3d$ and $4f$ ground states in spherical symmetry are given by the Hund rules and LS -coupling scheme. In the more than half filling case, their wavefunctions are expressed by a single Slater determinant, whereas multi-determinants are needed in the less than half filling. Consequently, HFA, *i.e.*, single-determinant approximation, gives precise results for the more than half filling case but fails in the less than half filling.

Under the realistic O_h crystal field, HFA comes to be a good approximation for the $3d$ states, even in the less than half filling case. This shows that HFA increases its accuracy with sufficiently strong one-body interaction.

The U $5f$ states do not belong to the Russell-Saunders case. H_{so} is so strong that it can mix different LS multiplets deduced from H_{ee} . Because of this strong one-body term, HFA gives a good result for $5f^2$ and $5f^3$ configurations.

The radial wavefunction of the $3d$ and $5f$ orbitals spread rather outside so that considerable solid-state effects, such as hybridization effect and crystal field effect, are anticipated in crystals. It seems reasonable to conclude that HFA is expected to provide a good description for $3d$ or $5f$ substances.

Chapter 4

Tight-binding method

The tight-binding approximation for solids has been developed by Slater and Koster.[28] Originally this method was proposed as an interpolation method since the first-principles band structure calculation with using elaborate technique needs huge computing power; accurate calculations were done only for some points of high symmetry in the Brillouin zone, and they were interpolated by the tight-binding method throughout the Brillouin zone. Owing to the great progress in computational facilities, the interpolation scheme is no longer required, at least for the usual band structure calculation. However, the tight-binding approach is still useful to studies where tremendous computing power is necessary, for instance, large unit cell crystals, defects, disordered materials, surfaces, interfaces, and phonon spectra. Furthermore it is often applied to model calculations to treat excited states or strong electron-correlation effects, which can not be handled by LDA. Although there are some limitations and shortcomings in LDA, it often gives good results as far as ground-state properties or interaction strengths are concerned. Parameters relevant to models are often extracted from converting an LDA band structure into the tight-binding scheme.

In the tight-binding method, the one-electron wavefunction in crystal is approximately expressed by a linear combination of atomic orbitals (LCAO). As in Eq. (3.2), an atomic orbital located at site i can be expressed by

$$\phi_{i\nu}(\mathbf{r} - \mathbf{p}_i) = R_{nl}^i(|\mathbf{r} - \mathbf{p}_i|) Y_{lm} \left(\frac{\mathbf{r} - \mathbf{p}_i}{|\mathbf{r} - \mathbf{p}_i|} \right) \chi_\sigma, \quad (4.1)$$

where ν is the combined label of n , l , m , and σ . From these functions one can construct linear combination

$$u_{i\nu}^{\mathbf{k}}(\mathbf{r}) = \frac{1}{\sqrt{N}} \sum_{\omega} e^{i\mathbf{k} \cdot (\mathbf{R}_\omega + \mathbf{p}_i)} \phi_{i\nu}(\mathbf{r} - \mathbf{R}_\omega - \mathbf{p}_i), \quad (4.2)$$

where \mathbf{R}_ω is a translational vector stretching from the zero point to the ω -th unit cell; \mathbf{p}_i is the position vector of the site i within a unit cell (See Fig. 4.1); N is the number of unit cells in a large box, which is utilized for the periodic boundary condition. The function $u_{i\nu}^{\mathbf{k}}$ satisfies Bloch's theorem

$$u_{i\nu}^{\mathbf{k}}(\mathbf{r} + \mathbf{R}) = e^{i\mathbf{k} \cdot \mathbf{R}} u_{i\nu}^{\mathbf{k}}(\mathbf{r}), \quad (4.3)$$

where \mathbf{R} is any translational vector. Wave vector \mathbf{k} has a meaning as the *crystal momentum*, which is an irreducible representation in periodic system. Eigenfunction of crystal Hamiltonian H , is to be labeled by \mathbf{k} and the band index n , and expressed by a linear combination of $u_{i\nu}^{\mathbf{k}}$'s:

$$\Psi_n^{\mathbf{k}}(\mathbf{r}) = \sum_{i\nu} C_{ni\nu}^{\mathbf{k}} u_{i\nu}^{\mathbf{k}}(\mathbf{r}). \quad (4.4)$$

Table 4.1: Two-center tight-binding energy integrals, expressed in terms of the Slater-Koster integrals and the direction cosines l , m , n ($l^2 + m^2 + n^2 = 1$). The entries not given in the table can be found by cyclically permuting the coordinates and direction cosines. Interchanging the order of the indices has no effect if the sum of the parities of the two orbitals is even, but changes the sign if the sum of the parities is odd.

$E_{s, s}$	$(ss\sigma)$
$E_{s, x}$	$l(sp\sigma)$
$E_{x, x}$	$l^2(pp\sigma) + (1 - l^2)(pp\pi)$
$E_{x, y}$	$lm(pp\sigma) - lm(pp\pi)$
$E_{x, z}$	$ln(pp\sigma) - ln(pp\pi)$
$E_{s, xy}$	$\sqrt{3} lm(sd\sigma)$
E_{s, x^2-y^2}	$\frac{1}{2}\sqrt{3} (l^2 - m^2)(sd\sigma)$
$E_{s, 3z^2-r^2}$	$[n^2 - \frac{1}{2}(l^2 + m^2)](sd\sigma)$
$E_{x, xy}$	$\sqrt{3} l^2 m(pd\sigma) + m(1 - 2l^2)(pd\pi)$
$E_{x, yz}$	$\sqrt{3} lmn(pd\sigma) - 2lmn(pd\pi)$
$E_{x, zx}$	$\sqrt{3} l^2 n(pd\sigma) + n(1 - 2l^2)(pd\pi)$
E_{x, x^2-y^2}	$\frac{1}{2}\sqrt{3} l(l^2 - m^2)(pd\sigma) + l(1 - l^2 + m^2)(pd\pi)$
E_{y, x^2-y^2}	$\frac{1}{2}\sqrt{3} m(l^2 - m^2)(pd\sigma) - m(1 + l^2 - m^2)(pd\pi)$
E_{z, x^2-y^2}	$\frac{1}{2}\sqrt{3} n(l^2 - m^2)(pd\sigma) - n(l^2 - m^2)(pd\pi)$
$E_{x, 3z^2-r^2}$	$l[n^2 - \frac{1}{2}(l^2 + m^2)](pd\sigma) - \sqrt{3} ln^2(pd\pi)$
$E_{y, 3z^2-r^2}$	$m[n^2 - \frac{1}{2}(l^2 + m^2)](pd\sigma) - \sqrt{3} mn^2(pd\pi)$
$E_{z, 3z^2-r^2}$	$n[n^2 - \frac{1}{2}(l^2 + m^2)](pd\sigma) + \sqrt{3} n(l^2 + m^2)(pd\pi)$
$E_{xy, xy}$	$3l^2 m^2(dd\sigma) + (l^2 + m^2 - 4l^2 m^2)(dd\pi) + (n^2 + l^2 m^2)(dd\delta)$
$E_{xy, yz}$	$3lm^2 n(dd\sigma) + ln(1 - 4m^2)(dd\pi) + ln(m^2 - 1)(dd\delta)$
$E_{xy, zx}$	$3l^2 mn(dd\sigma) + mn(1 - 4l^2)(dd\pi) + mn(l^2 - 1)(dd\delta)$
E_{xy, x^2-y^2}	$\frac{3}{2}lm(l^2 - m^2)(dd\sigma) + 2lm(m^2 - l^2)(dd\pi) + \frac{1}{2}lm(l^2 - m^2)(dd\delta)$
E_{yz, x^2-y^2}	$\frac{3}{2}mn(l^2 - m^2)(dd\sigma) - mn[1 + 2(l^2 - m^2)](dd\pi)$ $+ mn[1 + \frac{1}{2}(l^2 - m^2)](dd\delta)$
E_{zx, x^2-y^2}	$\frac{3}{2}nl(l^2 - m^2)(dd\sigma) + nl[1 - 2(l^2 - m^2)](dd\pi)$ $- nl[1 - \frac{1}{2}(l^2 - m^2)](dd\delta)$
$E_{xy, 3z^2-r^2}$	$\sqrt{3} lm[n^2 - \frac{1}{2}(l^2 + m^2)](dd\sigma) - 2\sqrt{3} lmn^2(dd\pi)$ $+ \frac{1}{2}\sqrt{3} lm(1 + n^2)(dd\delta)$
$E_{yz, 3z^2-r^2}$	$\sqrt{3} mn[n^2 - \frac{1}{2}(l^2 + m^2)](dd\sigma) + \sqrt{3} mn(l^2 + m^2 - n^2)(dd\pi)$ $- \frac{1}{2}\sqrt{3} mn(l^2 + m^2)(dd\delta)$
$E_{zx, 3z^2-r^2}$	$\sqrt{3} ln[n^2 - \frac{1}{2}(l^2 + m^2)](dd\sigma) + \sqrt{3} ln(l^2 + m^2 - n^2)(dd\pi)$ $- \frac{1}{2}\sqrt{3} ln(l^2 + m^2)(dd\delta)$
$E_{x^2-y^2, x^2-y^2}$	$\frac{3}{4}(l^2 - m^2)^2(dd\sigma) + [l^2 + m^2 - (l^2 - m^2)^2](dd\pi)$ $+ [n^2 + \frac{1}{4}(l^2 - m^2)^2](dd\delta)$
$E_{x^2-y^2, 3z^2-r^2}$	$\frac{1}{2}\sqrt{3} (l^2 - m^2)[n^2 - \frac{1}{2}(l^2 + m^2)](dd\sigma) + \sqrt{3} n^2(m^2 - l^2)(dd\pi)$ $+ \frac{1}{4}\sqrt{3} (1 + n^2)(l^2 - m^2)(dd\delta)$
$E_{3z^2-r^2, 3z^2-r^2}$	$[n^2 - \frac{1}{2}(l^2 + m^2)]^2(dd\sigma) + 3n^2(l^2 + m^2)(dd\pi)$ $+ \frac{3}{4}(l^2 + m^2)^2(dd\delta)$

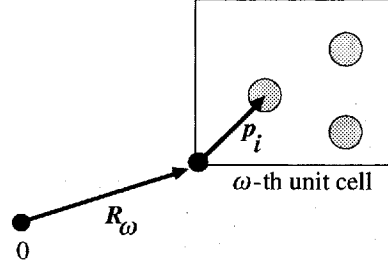


Figure 4.1: Position of a unit cell and site.

Note that the summation over i is taken within a unit cell. It is not assured that the bases $u_{i\nu}^{\mathbf{k}}$'s are orthogonal with each other, since two atomic orbitals, $\phi_{i\nu}$ and $\phi_{j\mu}$, usually have an overlap if they are located on different atoms ($i \neq j$) in a close distance. Such an overlap is often ignored for simplicity, as in the case of this thesis, but we will continue to formulate the tight-binding method with the more general case of non-orthogonal basis.

Matrix element of the crystal Hamiltonian H can be written as follows on the basis of $u_{i\nu}^{\mathbf{k}}$

$$\begin{aligned} H_{i\nu,j\mu}(\mathbf{k}) &\equiv \langle u_{i\nu}^{\mathbf{k}} | H | u_{j\mu}^{\mathbf{k}} \rangle \\ &= \int u_{i\nu}^{\mathbf{k}*}(\mathbf{r}) H u_{j\mu}^{\mathbf{k}}(\mathbf{r}) d\mathbf{r} \\ &= \sum_{\omega} \exp\{i\mathbf{k} \cdot (\mathbf{R}_{\omega} + \mathbf{p}_j - \mathbf{p}_i)\} E_{i\nu,j\mu}(\mathbf{R}_{\omega}), \end{aligned} \quad (4.5)$$

where we have used the periodicity of the Hamiltonian, $H(\mathbf{r} + \mathbf{R}_{\omega}) = H(\mathbf{r})$, and introduced a following matrix:

$$E_{i\nu,j\mu}(\mathbf{R}_{\omega}) \equiv \int \phi_{i\nu}^*(\mathbf{r} - \mathbf{p}_i) H \phi_{j\mu}(\mathbf{r} - \mathbf{R}_{\omega} - \mathbf{p}_j) d\mathbf{r}; \quad (4.6)$$

this matrix represents the interaction between electrons localized at position \mathbf{p}_i and $\mathbf{R}_{\omega} + \mathbf{p}_j$. On the same way, let us define the following "overlap matrix" between the bases:

$$\begin{aligned} S_{i\nu,j\mu}(\mathbf{k}) &\equiv \langle u_{i\nu}^{\mathbf{k}} | u_{j\mu}^{\mathbf{k}} \rangle \\ &= \int u_{i\nu}^{\mathbf{k}*}(\mathbf{r}) u_{j\mu}^{\mathbf{k}}(\mathbf{r}) d\mathbf{r} \\ &= \sum_{\omega} \exp\{i\mathbf{k} \cdot (\mathbf{R}_{\omega} + \mathbf{p}_j - \mathbf{p}_i)\} S_{i\nu,j\mu}(\mathbf{R}_{\omega}), \end{aligned} \quad (4.7)$$

where

$$S_{i\nu,j\mu}(\mathbf{R}_{\omega}) \equiv \int \phi_{i\nu}^*(\mathbf{r} - \mathbf{p}_i) \phi_{j\mu}(\mathbf{r} - \mathbf{R}_{\omega} - \mathbf{p}_j) d\mathbf{r}. \quad (4.8)$$

Having defined these matrices, the Schrödinger equation, $H\Psi_n^{\mathbf{k}} = E_n(\mathbf{k}) \Psi_n^{\mathbf{k}}$, reduces to a secular equation

$$\sum_{j\mu} [H_{i\nu,j\mu}(\mathbf{k}) - E_n(\mathbf{k}) S_{i\nu,j\mu}(\mathbf{k})] C_{nj\mu}^{\mathbf{k}} = 0 \quad (4.9)$$

or

$$\mathbf{H}(\mathbf{k}) \begin{bmatrix} \vdots \\ C_{nj\mu}^{\mathbf{k}} \\ \vdots \end{bmatrix} = E_n(\mathbf{k}) \mathbf{S}(\mathbf{k}) \begin{bmatrix} \vdots \\ C_{nj\mu}^{\mathbf{k}} \\ \vdots \end{bmatrix}, \quad (4.10)$$

for each \mathbf{k} in the Brillouin zone. This is a generalized eigenvalue problem with the overlap matrix, and is solvable by using appropriate computer program.

The main subject in the tight-binding scheme is to determine the atomic-orbital matrices (4.6) and (4.8). The crystal Hamiltonian H , involving a periodic potential, can be written as the sum of a kinetic energy operator, and a potential, which is approximately a sum of spherically symmetrical potential wells located at all the sites of the crystal; $H = -\frac{\hbar^2}{2m} \nabla^2 + \sum_{\eta l} V_l(\mathbf{r} - \mathbf{R}_\eta - \mathbf{p}_l)$. Hence the matrix (4.6) is a linear combination of integrals of a product of an atomic orbital $\phi_{i\nu}^*$ located on the site at position \mathbf{p}_i , another atomic orbital $\phi_{j\mu}$ on the site at $\mathbf{R}_\omega + \mathbf{p}_j$, and a spherical potential function located on still a third site. It is convenient to express them through on-site integral, two-center integral, and three-center integral.

$$\begin{aligned} E_{i\nu,j\mu}(\mathbf{R}_\omega) &= E_{i\nu\mu} \delta_{ij} \delta_{\omega 0} \\ &+ \int \phi_{i\nu}^*(\mathbf{r} - \mathbf{p}_i) V_j(\mathbf{r} - \mathbf{R}_\omega - \mathbf{p}_j) \phi_{j\mu}(\mathbf{r} - \mathbf{R}_\omega - \mathbf{p}_j) d\mathbf{r} \\ &+ \sum'_{\eta,l} \int \phi_{i\nu}^*(\mathbf{r} - \mathbf{p}_i) V_l(\mathbf{r} - \mathbf{R}_\eta - \mathbf{p}_l) \phi_{j\mu}(\mathbf{r} - \mathbf{R}_\omega - \mathbf{p}_j) d\mathbf{r}. \end{aligned} \quad (4.11)$$

The first term, $E_{i\nu\mu}$ represents the "on-site energy" or "orbital energy", and the other terms represent the electron hopping. The primed summation in the third term means that either the case of $\mathbf{R}_\eta + \mathbf{p}_l = \mathbf{p}_i$ or $\mathbf{R}_\eta + \mathbf{p}_l = \mathbf{R}_\omega + \mathbf{p}_j$, namely, the on-site integral or two-center integral, is not included in this sum.

For practical reason, this rigorous expression is simplified by ignoring the three-center integrals, and further retaining only a few two-center integrals; for instance, those between nearest- and next-nearest-neighbor atoms. Since the potential function is assumed to be spherical, the two-center integrals are expressed by a small number of "disposable" parameters. If we consider the vector $\mathbf{R}_\omega + \mathbf{p}_j - \mathbf{p}_i$, stretching from one site to the other, to be an axis like that of a diatomic molecule, we can express each of the function ϕ as a sum of functions quantized with respect to the axis. From this rotation of the axis, a two-center integral becomes a linear combination of numerous integrals. However, the property of the spherical harmonics permits only a few integrals to be non-zero — only when two atomic functions have the same m (magnetic orbital quantum number) the integral can have a finite value. The non-zero components are labeled by σ , π , δ , and ϕ , for $m = 0, \pm 1, \pm 2$, and ± 3 , respectively (these are called Slater-Koster integrals or SK parameters). Now one can express the two-center integrals in terms of a few "disposable" SK parameters and the direction cosines l, m, n of the vector $\mathbf{R}_\omega + \mathbf{p}_j - \mathbf{p}_i$. For convenience, the relations for all combination of s, p , and d orbitals, taken from Ref. [28], are reproduced in Table 4.1. These relations are also applicable to the overlap integrals.

In SK Table 4.1, relations including f orbitals are not given. Our interest in this thesis is the electronic structure of uranium compounds where the $5f$ orbital plays an important role. In spite of using Table 4.1, we will derive the same relations numerically, based on the rotation of the spherical harmonics. This method can be applied to all combinations of atomic functions with any orbital angular momentum.

Rotation of a cartesian coordinate system (x, y, z) can be specified by the Euler angles α, β, γ ($0 \leq \alpha < 2\pi, 0 \leq \beta \leq \pi, 0 \leq \gamma < 2\pi$). These angles relate a final rotated coordinate system (x', y', z') to the initial one in the following three steps:

1. The x_1, y_1, z_1 -axes are rotated about the z -axis through an angle α counterclockwise relative to x, y, z . (The z and z_1 -axes coincide.)
2. The x_2, y_2, z_2 -axes are rotated about the y_1 -axis through an angle β counterclockwise relative to x_1, y_1, z_1 . (The y_1 and y_2 -axes coincide.)
3. The final rotation is through an angle γ counterclockwise about z_2 -axis, yielding the x', y', z' system. (The z_2 and z' -axes coincide.)

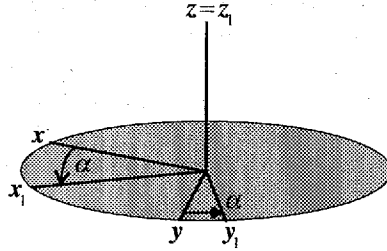


Figure 4.2: Rotation about z through angle α

Spherical harmonics viewed from the new coordinate system x', y', z' , can be related to the one in the original system by a unitary transformation:

$$Y_{lm}(\theta'\varphi') = \sum_{m'} Y_{lm'}(\theta\varphi) D_{m'm}^l(\alpha, \beta, \gamma), \quad (4.12)$$

where the unitary matrix \mathbf{D} is defined by

$$D_{m'm}^l(\alpha, \beta, \gamma) = \sum_{k=0}^{l+m} (-)^k \frac{\sqrt{(l+m)!(l-m)!(l+m')!(l-m')!}}{k!(l-m'-k)!(l+m-k)!(m'-m+k)!} \\ \otimes e^{-im\gamma} \left(\cos \frac{\beta}{2} \right)^{2l+m-m'-2k} \left(-\sin \frac{\beta}{2} \right)^{m'-m+2k} e^{-im'\alpha}. \quad (4.13)$$

Note that this rotation matrix is a general one in the sense that it can be applied to any angular momentum j with integral and half odd integral values ($j = 0, \frac{1}{2}, 1, \frac{3}{2}, \dots$). Angular part appearing in a two-center integral can be considered as the following simplified form:

$$\int Y_{l_1 m_1}^* \left(\frac{\mathbf{r}}{|\mathbf{r}|} \right) Y_{l_2 m_2} \left(\frac{\mathbf{r} - \mathbf{R}}{|\mathbf{r} - \mathbf{R}|} \right) d\Omega \\ = \int Y_{l_1 m_1}^*(\vartheta\varphi) Y_{l_2 m_2}(\vartheta_{\mathbf{R}}\varphi_{\mathbf{R}}) d\Omega, \quad (4.14)$$

where one spherical harmonics is located at zero-point, and the other at position \mathbf{R} . We would make a new coordinated system (x', y', z') or $(r', \vartheta', \varphi')$ so that the z' -axis coincides with the vector \mathbf{R} . In the new system the azimuthal angles of two vectors \mathbf{r} and $\mathbf{r} - \mathbf{R}$ come to be identical (See Fig. 4.3). Using Eq. (4.12), the angular integral reduces to the one expressed by the new coordinate system

$$\int Y_{l_1 m_1}^*(\vartheta\varphi) Y_{l_2 m_2}(\vartheta_{\mathbf{R}}\varphi_{\mathbf{R}}) d\Omega$$

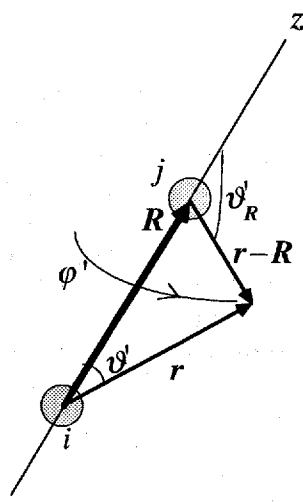


Figure 4.3: Polar and azimuthal angles of vectors \mathbf{r} and $\mathbf{r} - \mathbf{R}$, in the new coordinated system.

$$\begin{aligned}
 &= \int \left(\sum_{m'_1} Y_{l_1 m'_1}(\vartheta' \varphi') D_{m_1 m'_1}^{l_1*} \right)^* \left(\sum_{m'_2} Y_{l_2 m'_2}(\vartheta' \mathbf{R} \varphi') D_{m_2 m'_2}^{l_2*} \right) d\Omega' \\
 &= \sum_{m'_1 m'_2} D_{m_1 m'_1}^{l_1} D_{m_2 m'_2}^{l_2*} \int Y_{l_1 m'_1}^*(\vartheta' \varphi') Y_{l_2 m'_2}(\vartheta' \mathbf{R} \varphi') d\Omega' \quad (4.15)
 \end{aligned}$$

The integral will be zero unless $m'_1 = m'_2$, because of the integral over φ' . Then the expression reduces to

$$\sum_m D_{m_1 m}^{l_1} D_{m m_2}^{l_2+} \int Y_{l_1 m}^*(\vartheta' \varphi') Y_{l_2 m}(\vartheta' \mathbf{R} \varphi') d\Omega'. \quad (4.16)$$

Having known this point about the angular part, the two-center integral in (4.11) can be written as a linear combination of disposable parameters

$$\begin{aligned}
 E_{i\nu, j\mu}(\mathbf{R}_\omega) &= \int \phi_{i\nu}^*(\mathbf{r} - \mathbf{p}_i) V_j(\mathbf{r} - \mathbf{R}_\omega - \mathbf{p}_j) \phi_{j\mu}(\mathbf{r} - \mathbf{R}_\omega - \mathbf{p}_j) dr \\
 &= \sum_m D_{m_\nu m}^{l_\nu}(\omega_{\mathbf{Q}}) V_{|m|}^{i\nu l_\nu j n_\mu l_\mu}(\mathbf{Q}) D_{m m_\mu}^{l_\mu+}(\omega_{\mathbf{Q}}), \quad (4.17)
 \end{aligned}$$

with

$$\mathbf{Q} \equiv \mathbf{R}_\omega + \mathbf{p}_j - \mathbf{p}_i \quad (4.18)$$

$$\begin{aligned}
 V_{|m|}^{i\nu l_\nu j n_\mu l_\mu}(\mathbf{Q}) &\equiv \int R_{i\nu l_\nu}(r) V_j(|\mathbf{r} - \mathbf{Q}|) R_{j n_\mu l_\mu}(|\mathbf{r} - \mathbf{Q}|) r^2 dr \\
 &\quad \otimes 4\pi \int Y_{l_\nu m}^*(\vartheta' \varphi') Y_{l_\mu m}(\vartheta' \mathbf{Q} \varphi') d\Omega'. \quad (4.19)
 \end{aligned}$$

Here $\omega_{\mathbf{Q}}$ represents a set of the Euler angles, which describes the rotation to make the new coordinate system where the z' -axis coincides with \mathbf{Q} . The matrices $V_{|m|}$'s correspond to the SK integrals such as $p d\sigma$.

Tight-binding Hartree-Fock method

The tight-binding Hamiltonian described above, $H_{\text{TB}}(\mathbf{k})$, is considered to represent well the electron kinetic energy. In this thesis, in addition to $H_{\text{TB}}(\mathbf{k})$, we would separately treat the on-site Coulomb interaction, at least for an orbital most relevant to magnetism, by the self-consistent HF procedure. Furthermore the spin-orbit interaction should be added for the discussion of orbital magnetism. These intra-atomic interactions are essentially the same as those of isolated atoms discussed in Chap. 3, but a slight modification is needed for the application to solids. We shall show it in the following, by featuring a simple example where there is only one site in the unit cell and only a single orbital is taken into account. Extension for a general case is straightforward.

The Hamiltonian for a one-electron state with the crystal momentum \mathbf{k} may be expressed by

$$H(\mathbf{k}) = H_{\text{TB}}(\mathbf{k}) + H_{\text{so}} + H_{\text{ee}}^{\text{HF}}, \quad (4.20)$$

with

$$H_{\text{so}} = \sum_{\omega} \sum_{\nu\nu'} \langle \omega\nu | \zeta \mathbf{l} \cdot \mathbf{s} | \omega\nu' \rangle a_{\omega\nu}^+ a_{\omega\nu'} \quad (4.21)$$

$$\begin{aligned} H_{\text{ee}}^{\text{HF}} &= \sum_{\omega} \sum_{\nu\nu'} a_{\omega\nu}^+ a_{\omega\nu'} \sum_{\nu_1\nu'_1} \langle a_{\omega\nu_1}^+ a_{\omega\nu'_1} \rangle \\ &\times [\langle \omega\nu, \omega\nu_1 | v | \omega\nu', \omega\nu'_1 \rangle - \langle \omega\nu, \omega\nu_1 | v | \omega\nu'_1, \omega\nu' \rangle]. \end{aligned} \quad (4.22)$$

Here, $|\omega\nu\rangle$ represents an atomic orbital ϕ_{ν} localized at ω -th unit cell. The on-site matrix elements have no ω -dependence. Furthermore, since we will deal with homogeneous solution, for example, magnetically ordered state, the HF order parameter $\langle a_{\omega\nu}^+ a_{\omega\nu'} \rangle$ do not have ω -dependence. Then the expressions become

$$H_{\text{so}} = \sum_{\nu\nu'} \langle \nu | \zeta \mathbf{l} \cdot \mathbf{s} | \nu' \rangle \sum_{\omega} a_{\omega\nu}^+ a_{\omega\nu'} \quad (4.23)$$

$$\begin{aligned} H_{\text{ee}}^{\text{HF}} &= \sum_{\nu\nu'} \sum_{\nu_1\nu'_1} \langle a_{\nu_1}^+ a_{\nu'_1} \rangle \\ &\times [\langle \nu\nu_1 | v | \nu'\nu'_1 \rangle - \langle \nu\nu_1 | v | \nu'_1\nu' \rangle] \sum_{\omega} a_{\omega\nu}^+ a_{\omega\nu'}. \end{aligned} \quad (4.24)$$

It is necessary to unify the basis of each Hamiltonian. The basis of $H_{\text{TB}}(\mathbf{k})$ is the Bloch orbital

$$u_{\nu}^{\mathbf{k}}(\mathbf{r}) = \frac{1}{\sqrt{N}} \sum_{\omega} \exp(i\mathbf{k} \cdot \mathbf{R}_{\omega}) \phi_{\nu}(\mathbf{r} - \mathbf{R}_{\omega}). \quad (4.25)$$

The inverse transformation yields

$$\phi_{\nu}(\mathbf{r} - \mathbf{R}_{\omega}) = \frac{1}{\sqrt{N}} \sum_{\mathbf{k}} \exp(-i\mathbf{k} \cdot \mathbf{R}_{\omega}) u_{\nu}^{\mathbf{k}}(\mathbf{r}) \quad (4.26)$$

or

$$a_{\omega\nu}^+ = \frac{1}{\sqrt{N}} \sum_{\mathbf{k}} \exp(-i\mathbf{k} \cdot \mathbf{R}_{\omega}) a_{\mathbf{k}\nu}^+. \quad (4.27)$$

Using this relation, the basis of H_{so} and $H_{\text{ee}}^{\text{HF}}$, *i.e.*, the atomic orbital basis, can be converted into the Bloch basis:

$$\begin{aligned}
& \sum_{\omega} a_{\omega\nu}^{\dagger} a_{\omega\nu'} \\
&= \sum_{\omega} \left[\frac{1}{\sqrt{N}} \sum_{\mathbf{k}} \exp(-i\mathbf{k} \cdot \mathbf{R}_{\omega}) a_{\mathbf{k}\nu}^{\dagger} \right] \left[\frac{1}{\sqrt{N}} \sum_{\mathbf{k}'} \exp(i\mathbf{k}' \cdot \mathbf{R}_{\omega}) a_{\mathbf{k}'\nu'} \right] \\
&= \sum_{\mathbf{k}\mathbf{k}'} a_{\mathbf{k}\nu}^{\dagger} a_{\mathbf{k}'\nu'} \left(\frac{1}{N} \sum_{\omega} \exp\{-i(\mathbf{k} - \mathbf{k}') \cdot \mathbf{R}_{\omega}\} \right) \\
&= \sum_{\mathbf{k}\mathbf{k}'} a_{\mathbf{k}\nu}^{\dagger} a_{\mathbf{k}'\nu'} \delta_{\mathbf{k}\mathbf{k}'} \\
&= \sum_{\mathbf{k}} a_{\mathbf{k}\nu}^{\dagger} a_{\mathbf{k}\nu'}. \tag{4.28}
\end{aligned}$$

Then the on-site interactions are rewritten as follows

$$H_{\text{so}} = \sum_{\nu\nu'} \langle \nu | \zeta \mathbf{l} \cdot \mathbf{s} | \nu' \rangle \sum_{\mathbf{k}} a_{\mathbf{k}\nu}^{\dagger} a_{\mathbf{k}\nu'} \tag{4.29}$$

$$\begin{aligned}
H_{\text{ee}}^{\text{HF}} &= \sum_{\nu\nu'} \sum_{\nu_1\nu_1'} \langle a_{\nu_1}^{\dagger} a_{\nu_1'} \rangle \\
&\times [\langle \nu\nu_1 | v | \nu'\nu_1' \rangle - \langle \nu\nu_1 | v | \nu_1'\nu' \rangle] \sum_{\mathbf{k}} a_{\mathbf{k}\nu}^{\dagger} a_{\mathbf{k}\nu'}. \tag{4.30}
\end{aligned}$$

The HF order parameter $\langle a_{\nu}^{\dagger} a_{\nu'} \rangle$ is to be calculated from the eigenvectors of occupied states. As previously described, the eigenfunction of H , labeled by \mathbf{k} and the band index n , is given by a linear combination of Bloch orbitals:

$$\Psi_n^{\mathbf{k}}(\mathbf{r}) = \sum_{\nu} C_{n\nu}^{\mathbf{k}} u_{\nu}^{\mathbf{k}}(\mathbf{r}). \tag{4.31}$$

Inversely the Bloch orbital is given by

$$u_{\nu}^{\mathbf{k}}(\mathbf{r}) = \sum_n C_{n\nu}^{\mathbf{k}*} \Psi_n^{\mathbf{k}}(\mathbf{r}) \tag{4.32}$$

or

$$a_{\mathbf{k}\nu}^{\dagger} = \sum_n C_{n\nu}^{\mathbf{k}*} a_{\mathbf{k}n}^{\dagger}. \tag{4.33}$$

Then

$$\begin{aligned}
\langle a_{\nu}^{\dagger} a_{\nu'} \rangle &= \langle a_{0\nu}^{\dagger} a_{0\nu'} \rangle \\
&= \frac{1}{N} \sum_{\mathbf{k}\mathbf{k}'} \langle a_{\mathbf{k}\nu}^{\dagger} a_{\mathbf{k}'\nu'} \rangle \\
&= \frac{1}{N} \sum_{\mathbf{k}\mathbf{k}'} \sum_{nn'} C_{n\nu}^{\mathbf{k}*} C_{n'\nu'}^{\mathbf{k}'} \langle a_{\mathbf{k}n}^{\dagger} a_{\mathbf{k}'n'} \rangle. \tag{4.34}
\end{aligned}$$

Since we are based on the single-determinant approximation, the ground-state expectation value of $a_{\mathbf{k}n}^{\dagger} a_{\mathbf{k}'n'}$ becomes zero unless the following conditions are satisfied.

- $\mathbf{k} = \mathbf{k}'$
- $n = n'$
- the state $\mathbf{k}n$ is an occupied state ($E_{\mathbf{k}n} \leq E_F$)

Thus we get

$$\langle a_{\nu}^{\dagger} a_{\nu'} \rangle = \frac{1}{N} \sum_{\mathbf{k}n \in \text{occu}} C_{n\nu}^{\mathbf{k}*} C_{n\nu'}^{\mathbf{k}}. \quad (4.35)$$

Chapter 5

Antiferromagnetic structure and orbital magnetism in CoO

Part of this chapter has been published in J. Phys. Soc. Jpn. **67**, 2637 (1998) by Tatsuya Shishidou and Takeo Jo.

Abstract

Possible magnetic structures of CoO, which is known to be the second kind of antiferromagnet, are discussed for the cubic phase on the basis of the extended Hubbard model including the $3d$ spin-orbit coupling and the intra-atomic full $3d$ - $3d$ multipole interaction in the framework of the Hartree-Fock (HF) approximation. In addition to a collinear single-Q structure, a noncollinear quadruple-Q one, both of which are compatible with the neutron diffraction experiment, are obtained as stable HF solutions. The magnitude of the Co orbital magnetic moment is shown to be as large as $\sim 1\mu_B$. Relationship between the orbital magnetism and the band-gap formation is explained.

5.1 Introduction

Electronic structures of transition metal (TM) monoxides NiO, CoO, FeO and MnO, which show antiferromagnetism (AF), have been the subject of continuous debates. Since the insulating property of monoxides both below and above the Néel temperature was pointed out to not be explained by a band model,[29] the importance of electron-electron interaction has been discussed. It is generally agreed that the large Coulomb interaction causes the insulating properties.[30, 31] The electronic structures have also been discussed in terms of the recently developed first-principles band structure calculation on the basis of the local density-functional approximation (LDA); LDA does not give the insulator as long as we assume paramagnetism. Even if we assume AF, the insulating band gap obtained from LDA is known to be too small compared with the experimental result.[32]

Among the monoxides, the magnitude of the orbital magnetic moment μ_{orb} of Co and Fe ions in CoO and FeO, respectively, is well known to be on the order of $1\mu_B$. [33] The large μ_{orb} in CoO and FeO was pointed out by Kanamori[26] to cause the large magnetostriction and by the present authors[34] to be reflected explicitly in the isotropic $L_{2,3}$ x-ray absorption spectrum. Although LDA is successfully applied to discussions of the magnetism of TM systems, success depends on the experimental finding that μ_{orb} is almost quenched in TM

systems; CoO and FeO are examples of exceptions. In LDA, there is no theoretical framework for calculating μ_{orb} self-consistently and we must be satisfied with a perturbational calculation which is known to cause an underestimation of μ_{orb} . Since μ_{orb} is comparable with the spin magnetic moment μ_{spin} in $4f$ rare earth and $5f$ actinide systems, various extensions of LDA, which include current-density-functional formulation,[35, 36, 37, 38] have been attempted. The first-principles calculation of μ_{orb} with the same level as that of μ_{spin} is, however, infeasible at the present stage.

The TM ions in NiO, CoO, FeO and MnO exhibit the second kind of AF structure on the fcc lattice which is, in general, described by the four wave vectors determining the magnetic modulation: $\mathbf{Q}_1 = \pi/a(1,1,1)$, $\mathbf{Q}_2 = \pi/a(-1,-1,1)$, $\mathbf{Q}_3 = \pi/a(1,-1,-1)$ and $\mathbf{Q}_4 = \pi/a(-1,1,-1)$. For NiO, FeO and MnO, it is generally agreed that the single-Q structure is realized, where the magnetic moments within the (111) plane are parallel and they are antiparallel with each other between the adjacent (111) planes. In the case of CoO, which shows tetragonal distortion with $c/a < 1$ below the Néel point, the magnetic structure is still controversial. According to van Laar,[39] a noncollinear magnetic structure is also compatible with the neutron diffraction experiment, in addition to the single-Q structure. The purpose of this work is to discuss possible second-kind AF structures of CoO on the basis of Hartree-Fock (HF) approximation for an extended Hubbard model where the full $3d$ orbitals of the Co atom, the $2p$ orbitals of the O atom, the multipole $3d$ - $3d$ intra-atomic interaction and the $3d$ spin-orbit interaction are taken into account.

HF calculation based on the tight-binding model has been applied to discussions of the electronic structures of TM monoxides[40] and insulating Mn perovskites,[41] and it is known to describe their insulating properties. For systems where μ_{orb} and μ_{spin} are comparable with each other, the HF calculation is shown to give a reasonable value of the ratio $\mu_{\text{orb}}/\mu_{\text{spin}}$ for TM oxides and uranium compounds.[42] We therefore adopt the present model, since the magnitude of μ_{orb} of Co in CoO is expected to affect the stable magnetic structure including the direction of the magnetic moment relative to the crystal axis. The present subject can only be discussed by using a realistic model, taking into account the full orbital degeneracy. Realistic calculations of magnetic quantities have been performed by the first-principles LDA approach, but its main object was a ferromagnet[13] and magnetic properties of noncollinear structures and antiferromagnets have been discussed by only a limited number of researchers.[43, 44] The discussion on possible multiple-Q structures with a large μ_{orb} , which is not reproduced by LDA, therefore seems to be a unique subject.

We first give a brief review on the second kind of AF structure on an fcc lattice. We pick out, from an fcc lattice, a tetrahedron composed of four atoms which are nearest neighbors to one another. This fcc lattice is regarded to be a simple cubic (SC) lattice of the tetrahedron. The second kind of AF on the fcc lattice is described by an "antiferromagnetic" arrangement of the magnetic structure of the tetrahedron.[45] A general structure of the second kind of AF is therefore given by an arbitrary arrangement of magnetic moments of the four atoms within the tetrahedron, which is described by the modulation wave vectors $\mathbf{Q}_1 \sim \mathbf{Q}_4$, i.e., the multiple-Q structure (see Fig. 5.1). If we assume a classical Heisenberg model, each multiple-Q structure is degenerate to one another. The degeneracy is removed either by a quantum effect, which prefers a collinear structure, or the four- and more-spin interactions beyond the two-spin one in the Heisenberg model.[46] The quantum effect is important in the case of a small spin, e.g., $s = 1/2$, while the four- and more-spin effects are for a larger spin. The present HF calculation includes the four- and more-spin effects, which seems to be appropriate for discussing the magnetic structure of the Co ion with a spin magnetic moment of $\sim 3\mu_B$.

A phenomenological discussion of the relative stability among multiple-Q states on an fcc lattice has been given by Jo and Hirai.[46] Although they did not consider any effect of the spin-orbit interaction, the deduced results seem to be useful for carrying forward our discussion. In a general structure of the second kind of AF, the magnetic moment of each

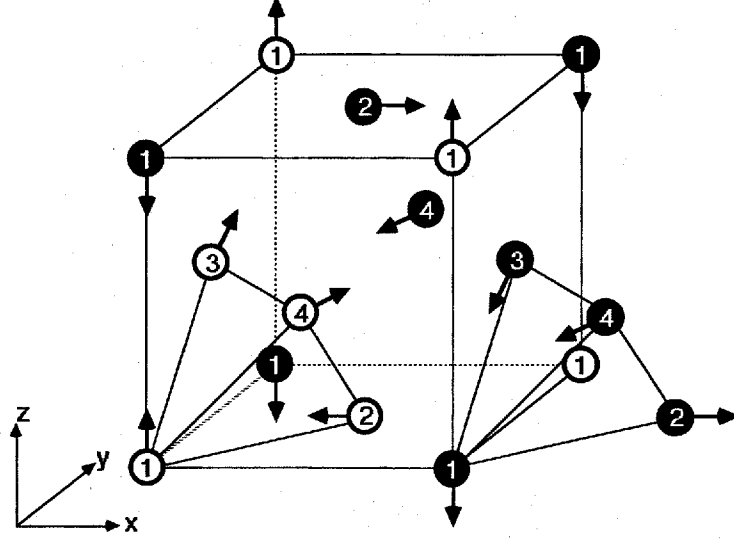


Figure 5.1: A general magnetic structure of the second kind of AF on an fcc lattice. Within a tetrahedron, which is composed of four atoms (sites 1, 2, 3, and 4 shown by open circles), the direction of magnetic moments of each atom is arbitrary, while that of each atom of the tetrahedron with four closed circles is coupled antiferromagnetically to the one with open circles. Then a general structure is given by placing these two types of tetrahedrons alternately at the corners of a simple cubic lattice. See Ref. [46] for a more detailed explanation.

site \mathbf{R}_k can be expressed by

$$\boldsymbol{\mu}_k = \mathbf{A}_1 \exp(i\mathbf{Q}_1 \cdot \mathbf{R}_k) + \mathbf{A}_2 \exp(i\mathbf{Q}_2 \cdot \mathbf{R}_k) + \mathbf{A}_3 \exp(i\mathbf{Q}_3 \cdot \mathbf{R}_k) + \mathbf{A}_4 \exp(i\mathbf{Q}_4 \cdot \mathbf{R}_k). \quad (5.1)$$

To put it another way, this multiple-Q state is formally expressed by

$$\mathbf{A}_1|Q_1\rangle + \mathbf{A}_2|Q_2\rangle + \mathbf{A}_3|Q_3\rangle + \mathbf{A}_4|Q_4\rangle. \quad (5.2)$$

Here \mathbf{A}_i denotes the vector amplitude of the modulated state $|Q_i\rangle$; the direction of \mathbf{A}_i specifies the direction of the magnetic moment of one sublattice and $|\mathbf{A}_i|^2$ represents the weight of the state $|Q_i\rangle$ in the superposition. Magnetic moments of the tetrahedron's four atoms, located at $\mathbf{R}_1 = (0, 0, 0)$, $\mathbf{R}_2 = (a/2, a/2, 0)$, $\mathbf{R}_3 = (0, a/2, a/2)$, and $\mathbf{R}_4 = (a/2, 0, a/2)$ as shown in Fig. 5.1, are represented by

$$\begin{bmatrix} \boldsymbol{\mu}_1 \\ \boldsymbol{\mu}_2 \\ \boldsymbol{\mu}_3 \\ \boldsymbol{\mu}_4 \end{bmatrix} = \begin{bmatrix} 1 & 1 & 1 & 1 \\ -1 & -1 & 1 & 1 \\ -1 & 1 & -1 & 1 \\ -1 & 1 & 1 & -1 \end{bmatrix} \begin{bmatrix} \mathbf{A}_1 \\ \mathbf{A}_2 \\ \mathbf{A}_3 \\ \mathbf{A}_4 \end{bmatrix}. \quad (5.3)$$

Alternatively, $\{\mathbf{A}_i\}$ is given by a linear combination of $\{\boldsymbol{\mu}_k\}$:

$$\begin{bmatrix} \mathbf{A}_1 \\ \mathbf{A}_2 \\ \mathbf{A}_3 \\ \mathbf{A}_4 \end{bmatrix} = \frac{1}{4} \begin{bmatrix} 1 & -1 & -1 & -1 \\ 1 & -1 & 1 & 1 \\ 1 & 1 & -1 & 1 \\ 1 & 1 & 1 & -1 \end{bmatrix} \begin{bmatrix} \boldsymbol{\mu}_1 \\ \boldsymbol{\mu}_2 \\ \boldsymbol{\mu}_3 \\ \boldsymbol{\mu}_4 \end{bmatrix}. \quad (5.4)$$

Jo and Hirai expressed the energy of the system in terms of $\{\mathbf{A}_i\}$ with a consideration of symmetry of the system, and they showed that only limited kinds of superpositions are

candidates within the lowest-order expansion of $\{\mathbf{A}_i\}$ to remove the degeneracy. They are the single-Q, a triple-Q, a collinear quadruple-Q and a noncollinear quadruple-Q state. The single-Q is a familiar structure and is sometimes called the "A-structure", and the collinear quadruple-Q is known as the "B-structure" according to the literature.[47]

5.2 Formulation

We assume the Hamiltonian given by

$$H = H_{\text{TB}} + H_{\text{so}} + H_{\text{ee}}, \quad (5.5)$$

$$H_{\text{TB}} = T_d(E_{3d}, 10Dq) + T_p(E_{2p}) + T_{pd} + T_{pp} + T_{dd}, \quad (5.6)$$

$$H_{\text{so}} = \zeta_{3d} \sum_i \sum_{\nu_1 \nu_2} \langle \nu_1 | \boldsymbol{\ell} \cdot \mathbf{s} | \nu_2 \rangle d_{i\nu_1}^\dagger d_{i\nu_2}, \quad (5.7)$$

$$H_{\text{ee}} = \sum_i \sum_{\nu_1 \nu_2 \nu_3 \nu_4} [g(\nu_1 \nu_2 \nu_3 \nu_4) - g(\nu_1 \nu_2 \nu_4 \nu_3)] \otimes (d_{i\nu_2}^\dagger d_{i\nu_4}) d_{i\nu_1}^\dagger d_{i\nu_3}, \quad (5.8)$$

with

$$g(\nu_1 \nu_2 \nu_3 \nu_4) = \left\langle \nu_1 \nu_2 \left| \frac{1}{r_{12}} \right| \nu_3 \nu_4 \right\rangle. \quad (5.9)$$

H_{TB} represents the kinetic energy. T_d and T_p describe the $3d$ and $2p$ orbital energies, respectively, where we consider point-charge crystal-field splitting ($10Dq$) for the $3d$ level. T_{pd} , T_{pp} , and T_{dd} stand for $2p$ - $3d$, $2p$ - $2p$, and $3d$ - $3d$ electron hopping, respectively. H_{so} represents the $3d$ spin-orbit interaction with coupling constant ζ_{3d} . The operator $d_{i\nu}$ denotes the annihilation of a $3d$ electron in the ν state of Co site i . The symbol ν is the combined index of the spin and orbital magnetic quantum number. H_{ee} represents the intra-atomic $3d$ - $3d$ multipole interaction, which is treated within the HF approximation. The matrix element $g(\nu_1 \nu_2 \nu_3 \nu_4)$ is written in terms of the Slater integrals and Gaunt coefficients. For the parameter values of the Hamiltonian, we adopt those listed in Table 5.1. Here ζ_{3d} is obtained by *ab initio* atomic HF calculation, and the other parameters are from Ref. [40]. For the $3d$ - $3d$ multipole interaction, we calculate the expectation values not only of 10 number operators but also ${}_{10}C_2 = 45$ off-diagonal operators to maintain the rotationally invariant property of the interaction operator. Due to the presence of μ_{orb} , the direction of atomic magnetic moment obtained as the HF solution is restricted. In the iteration process of the HF calculation, we determine the magnitudes of μ_{spin} and μ_{orb} and their directions simultaneously in the following way. First we give the quantization axes of both spin and orbital moments and the expectation values of the above-mentioned operators as input parameters. Then we obtain, as output values, the new expectation values. With these, we obtain the expectation values of the spin components S_x , S_y and S_z and the components of orbital angular momentum L_x , L_y and L_z in the $3d$ state under the given quantization axes; we obtain the directions of μ_{spin} and μ_{orb} . In the next step of iteration, we adopt the obtained directions of μ_{spin} and μ_{orb} as the new quantization axes of μ_{spin} and μ_{orb} , respectively. We repeat the iteration up to several thousand steps until the sufficient convergence is obtained; the directions of μ_{spin} and μ_{orb} can be different from each other.

5.3 Results and Discussions

Single-Q structure

Table 5.1: Parameter values used in the calculation. Except ζ_{3d} , these are from Ref. [40], where the Coulomb interaction parameter were represented by the Racah parameters, $A = F^0 - 49F^4/441$, $B = F^2/49 - 5F^4/441$, and $C = 35F^4/441$. The energy difference between the $2p$ and $3d$ levels is deduced from the charge transfer energy in Ref. [40] defined by $\Delta = E_{3d} - E_{2p} + nU_{dd}$, where n is the $3d$ -electron number in TM^{2+} ion and U_{dd} is the multiplet-averaged $3d$ - $3d$ Coulomb interaction $U_{dd} = A - 14B/9 + 7C/9 = F^0 - 2F^2/63 - 2F^4/63$. All in units of eV.

Parameter	MnO	FeO	CoO	NiO
$pd\sigma$	1.3	1.3	1.3	1.4
$pd\pi$	-0.6	-0.6	-0.6	-0.63
$pp\sigma$	0.55	0.55	0.55	0.60
$pp\pi$	-0.15	-0.15	-0.15	-0.15
$dd\sigma$	-0.23	-0.29	-0.25	-0.23
$dd\pi$	0.025	0.030	0.058	0.10
$dd\delta$	-0.005	-0.004	-0.006	-0.01
$E_{2p} - E_{3d}$	11.3611	27.027	32.314	41.9156
$10Dq$	0.70	0.70	0.70	0.70
F^0	4.474	6.172	5.956	6.440
F^2	8.750	9.730	10.640	10.570
F^4	5.166	6.048	6.804	7.560
ζ_{3d}	0.041	0.052	0.067	0.083

We first start from the ‘‘A-structure’’ obtained for $3d$ spin-orbit coupling $\zeta_{3d} = 0$, where the modulation is given by the wave vector $\mathbf{Q}_1 = \pi/a(1, 1, 1)$ and the direction of μ_{spin} is in the $[001]$ direction and $\mu_{\text{orb}} = 0$. By turning on the $3d$ spin-orbit coupling, μ_{orb} increases with changing its direction within the (110) plane. This causes a similar reorientation of μ_{spin} . We obtain a stable HF solution after several thousand iterations. Figure 5.2 displays this relaxation process. We take the polar axis to be in the $[001]$ direction and specify the direction by (ϑ, φ) using the polar and azimuthal angles ϑ and φ in units of degrees. The solution has the single-Q structure, where, for one of the sublattice, $\mu_{\text{spin}} = 2.81\mu_{\text{B}}$ and its direction is $(36.1, 225)$ and $\mu_{\text{orb}} = 0.84\mu_{\text{B}}$ and its direction is $(35.9, 225)$. For the other sublattice, the directions are obtained by inversion. We note that the $[\bar{1}\bar{1}2]$ direction within the (111) plane corresponds to $(35.3, 225)$. The directions of μ_{spin} and μ_{orb} in our solution are almost in this direction. At present, it is not clear whether the difference between the angles in our solution and 35.3 is significant or not. Even if we start our iteration from the $[\bar{1}\bar{1}0]$ direction, the same solution is obtained. We also note that Solovyev *et al.* recently obtained, by the LDA+ U approach (essentially the same calculation as the present one), a solution with nearly $(35, 225)$ and with similar values for μ_{spin} and μ_{orb} . [48]

Quadruple-Q structure

In the phenomenological discussion by Jo and Hirai[46] on the relative stability among multiple-Q states, in addition to the single-Q structure, the two kinds of quadruple-Q states which are superpositions of the 4 kinds of single-Q states with an equal weight, are found to be stable in a wide parameter region. Following (5.2), we define the state $|B\rangle$ given by $\mathbf{A}_1 = 1/2(0, 0, -1)$, $\mathbf{A}_2 = 1/2(0, 0, 1)$, $\mathbf{A}_3 = 1/2(0, 0, 1)$ and $\mathbf{A}_4 = 1/2(0, 0, 1)$. We also define the state $|C\rangle$ given by $\mathbf{A}_1 = \frac{1}{2\sqrt{3}}(1, 1, 1)$, $\mathbf{A}_2 = \frac{1}{2\sqrt{3}}(1, 1, -1)$, $\mathbf{A}_3 = \frac{1}{2\sqrt{3}}(-1, 1, 1)$ and $\mathbf{A}_4 = \frac{1}{2\sqrt{3}}(1, -1, 1)$. Then $|B\rangle$ and $|C\rangle$ or their equivalent states are the two kinds of stable quadruple-Q states. The former corresponds to the ‘‘B-structure’’ (collinear one) and the

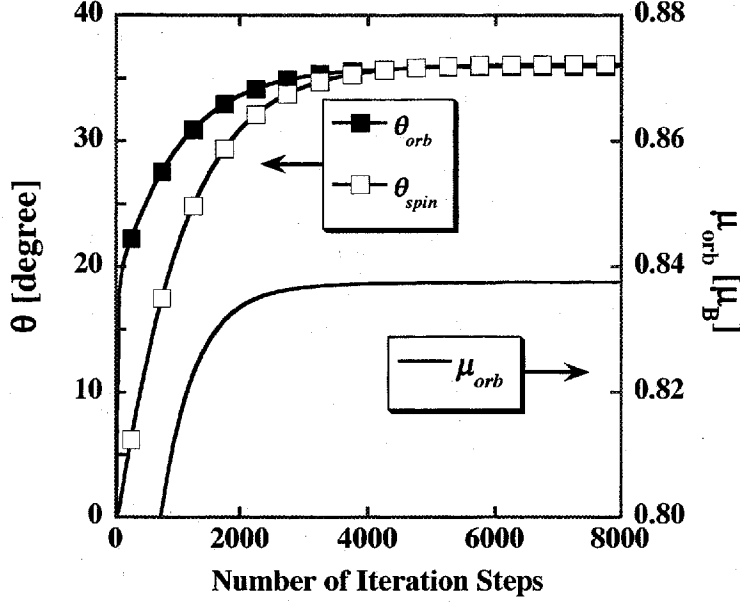


Figure 5.2: Relaxation process to the new equilibrium magnetic state with switching on the spin-orbit interaction. Growth of the orbital magnetic moment (solid line) and deviations of the spin (white squares) and orbital (black squares) magnetic moments from the [001] axis are displayed. No significant change can be seen for the magnitude of μ_{spin} (not shown) in course of the iteration.

latter to the other one where the magnetic moments of four atoms of the tetrahedron are directed towards its center of gravity (see Fig. 5.3).

We next start from the HF solution assuming a “B-structure” with μ_{spin} in the [001] direction for $\zeta_{3d} = 0$. Then by switching on ζ_{3d} , μ_{orb} again increases and we obtain, after several thousand iteration steps, a HF solution, where $|\mu_{\text{spin}}| = 2.81\mu_{\text{B}}$ with $\vartheta = 33.8$ and $|\mu_{\text{orb}}| = 0.92\mu_{\text{B}}$ with $\vartheta = 35.5$ for a tetrahedron. We assume the four atoms of the tetrahedron are at $\mathbf{R}_1 = a/2(0, 0, 0)$, $\mathbf{R}_2 = a/2(1, 1, 0)$, $\mathbf{R}_3 = a/2(0, 1, 1)$ and $\mathbf{R}_4 = a/2(1, 0, 1)$. Then φ is 45 for \mathbf{R}_1 , 225 for \mathbf{R}_2 , 135 for \mathbf{R}_3 and 315 for \mathbf{R}_4 (see Fig. 5.4). The magnetic moments of atoms on the nearest-neighbor tetrahedrons are given by inversion. We consider the quadruple-Q state given by $\sqrt{2/3}|B\rangle + \sqrt{1/3}|C'\rangle$, where $|C'\rangle$ is a noncollinear quadruple-Q state defined by $\mathbf{A}_1 = \sqrt{1/8}(1, 1, 0)$, $\mathbf{A}_2 = \sqrt{1/8}(1, 1, 0)$, $\mathbf{A}_3 = \sqrt{1/8}(1, -1, 0)$ and $\mathbf{A}_4 = \sqrt{1/8}(-1, 1, 0)$.

Table 5.2: Calculated results assuming the single-Q or multiple-Q structure. n_{3d} is the 3d-electron number. Magnetic moments are in unit of μ_{B} , and angles in degree.

	n_{3d}	μ_{spin}	ϑ_{spin}	φ_{spin}	μ_{orb}	ϑ_{orb}	φ_{orb}
Single-Q							
$\zeta_{3d} = 0$	7.1719	2.82	0	—	—	—	—
$\zeta_{3d} \neq 0$	7.1715	2.81	36.1	225	0.84	35.3	225
Multiple-Q							
$\zeta_{3d} = 0$	7.1705	2.82	0	—	—	—	—
$\zeta_{3d} \neq 0$	7.1702	2.81	33.8	45, 225, 135, 315	0.92	35.5	45, 225, 135, 315

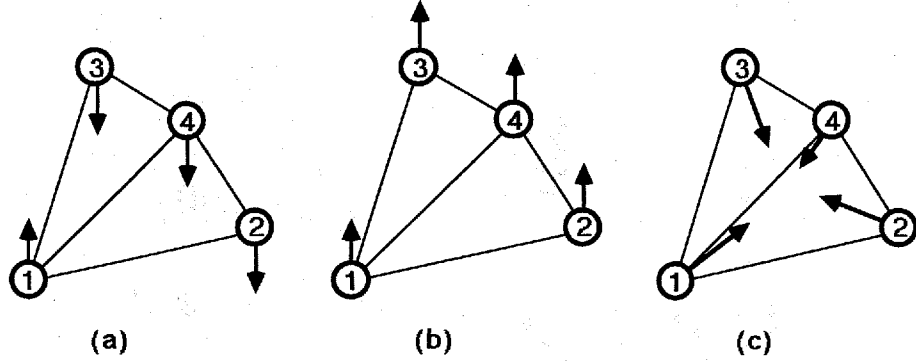


Figure 5.3: Magnetic moment arrangement within a tetrahedron in (a) the single-Q state (so-called A-structure), (b) the collinear quadruple-Q state (B-structure), and (c) the non-collinear quadruple-Q state where the moments are directed towards the center of gravity of the tetrahedron.

Then ϑ is equal to 35.3 at $\mathbf{R}_1 \sim \mathbf{R}_4$ for both μ_{spin} and μ_{orb} and φ 's for the four atoms in tetrahedrons are the same as those of our solution, where the atomic magnetic moment is in the $[112]$, $[\bar{1}\bar{1}2]$, $[\bar{1}12]$ and $[1\bar{1}2]$ directions for \mathbf{R}_1 , \mathbf{R}_2 , \mathbf{R}_3 and \mathbf{R}_4 , respectively. Our solution almost corresponds to this structure. At present, it is not clear whether the small difference in ϑ between our solution and the structure $\sqrt{2/3}|B\rangle + \sqrt{1/3}|C'\rangle$ is significant or not. According to van Laar,[39] the neutron diffraction experiment is compatible with the structure $\sqrt{2/3}|B\rangle + \sqrt{1/3}|C'\rangle$ with $\vartheta = 35.3$ replaced by $\vartheta = 27.4$ in the tetragonal phase. Furthermore, according to Solovyev *et al.*,[48] the single-Q structure with $\vartheta \simeq 35$ in the cubic phase is, by tetragonal distortion, changed to that with $\vartheta \simeq 27.5$. Although we have not performed a calculation including the tetragonal distortion, we expect that our solution in the cubic phase corresponds to that pointed out as a candidate by van Laar.

Orbital magnetism

Although a definite value of μ_{orb} is not yet experimentally determined, the magnitude of $\sim 1\mu_{\text{B}}$ is consistent with the results of various experiments. The calculated magnitude of the total magnetic moment is consistent with the results of experiments.[49, 50, 51] A partial quenching of μ_{orb} , i.e., large residual μ_{orb} of Co^{2+} in the octahedral crystal field, is discussed by Van Vleck,[52] and calculated explicitly in Sec. 3.4.2 of this thesis. Its relation to the branching ratio and spectral shape of the Co L_2 and L_3 x-ray absorption spectrum is also discussed by the present authors on the basis of a single-ion model, where an intuitive discussion is given for the preferential occupation of specific $3d$ magnetic quantum numbers.[34] In the present HF calculation based on the lattice model, although each state with specific symmetry has a finite bandwidth, the essence of the discussion based on the single-ion model is not altered. Namely, due to the fact that our system is a Mott insulator, the occupation of an orbit with a given symmetry raises the energy of orbits with other symmetries to above the band gap through intra-atomic Coulomb repulsion. Solovyev emphasized the F^0 dependence of the orbital moment in solids, by picking up CoO as an example (See Fig. 2 in Ref. [48]). But the scenario of the orbital magnetism in CoO is a simple one as described above; for a sufficiently large F^0 enough to open the band gap, the system is well described by the ligand-field theory and the triply degenerate orbital state under the O_h crystal field is the reason for the large value of the orbital moment. Thus the case of CoO seems to be an exceptional one and a more general discussion is desirable. In the next chapter, by dealing with a *metallic* $3d$ system, we will examine the role of the monopole Coulomb interaction in the orbital magnetism.

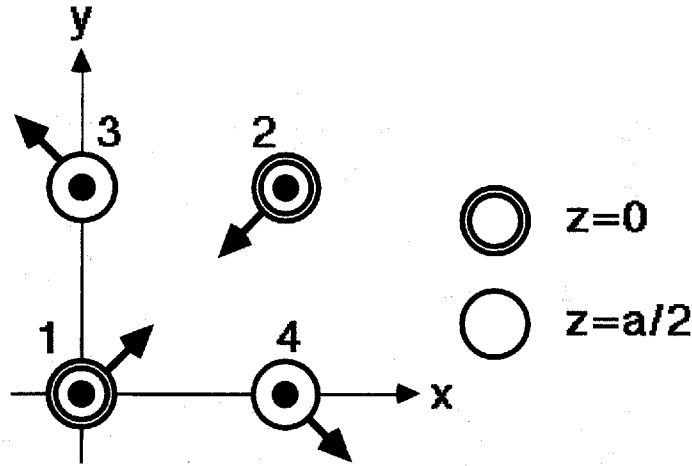


Figure 5.4: The noncollinear multiple-Q structure obtained as a HF solution. The z component of each moment is in the positive z direction.

Relative stability among two solutions

We performed a preliminary calculation of the energy difference between the single-Q and quadruple-Q states obtained as the HF solutions. The electronic energy of the single-Q state is lower than that of the quadruple-Q state by 0.0066 eV per formula unit. The obtained number of $3d$ electrons is 7.1715 for the single-Q state and 7.1702 for the quadruple-Q state. Since the present system is an insulator, we calculated the difference in Madelung energy between the two solutions, assuming the observed lattice constant and the positive charge of 1.8285 ($= 9.0 - 7.1715$) for the Co ion for the single-Q state and of 1.8298 ($= 9.0 - 7.1702$) for the quadruple-Q state; negative charge to guarantee charge neutrality is assumed for the O ion. The result shows that the Madelung energy of the quadruple-Q state is lower than that of the single-Q state by 0.056 eV per formula unit. If we simply sum the electronic energy and the Madelung energy, the total energy of the quadruple-Q state is lower than that of the single-Q state. In the present calculation of the Madelung energy, however, we assume the point-charge model which seems to overestimate the absolute magnitude of Madelung energy. In the present HF calculation, the electron charge distribution is coupled with our Hamiltonian only through the intra-atomic $3d-3d$ interaction. In the actual system, the spatial charge distribution is coupled with the Hamiltonian of electrons through intra- and inter-atomic interactions, the inclusion of which is required in order to discuss the energy, but which is beyond the capacity of the present model. We therefore cannot definitely conclude that the quadruple-Q state is lower than that of the single-Q state at the present stage.

Since our single-Q solution is almost the same as that obtained by the LDA+ U approach, our results, including those for the quadruple-Q state, are expected to be independent to the details of the adopted model. In fact, even if we vary the value of ζ_{3d} near the adopted value, the obtained magnetic structure is the same as that shown above. At present, we have not obtained HF solutions other than the single-Q and quadruple-Q solutions, which are also attained from the initial states of HF iteration other than those discussed above. According to the phenomenological discussion of stable multiple-Q structures, a specific triple-Q structure may be possible under certain conditions. In the present HF iteration, mixing of the triple-Q state is not seen.

5.4 Conclusion

In conclusion, we have shown that, in addition to the well-known single-Q state, the noncollinear quadruple-Q state shown in Fig. 5.4, both of which are expected to be compatible with the neutron diffraction experiment, is a promising candidate of the magnetic structure on the fcc lattice of NaCl-type CoO, on the basis of the HF calculation. We expect that future experiments will yield a conclusive answer. On the theoretical side, more quantitative discussions on the relative stability among candidates including the tetragonal lattice distortion will be needed.

Chapter 6

Orbital magnetism in metallic $3d$ systems

6.1 Introduction

Nowadays, it is a rather easy task to include the effect of the spin-orbit interaction in the modern first-principles band-structure calculation based on the local (spin) density approximation [L(S)DA]. In most cases, however, LSDA seriously underestimates the contribution of μ_{orb} , as discussed in Chap. 1. As far as the spin polarization is concerned, LSDA gives good results for itinerant magnetic materials. But it seems that LSDA has no theoretical framework to determine μ_{orb} self-consistently. A clear explanation for the mechanism of the orbital polarization (OP) in solids has been desired.

In free atoms, the Hund second rule describes the orbital angular momentum L of valence electrons; L has the largest value consistent with the Pauli principle and with the Hund first rule (maximum total spin S). As explained in Chap. 3, this is the consequence of the multipole Coulomb interaction, which is written in terms of the Slater integrals other than the monopole part F^0 . A hypothesis, that is, the mechanism of the OP in *solids* is essentially related to the *atomic* Hund second rule, has been made by Brooks.[20] From the interpretation of the Hartree-Fock (HF) total energy of atoms with open shell, he derived an explicit OP functional form as an additional term in the LSDA total energy. For the $3d$ shell, it is $-\frac{1}{2}B\langle L \rangle^2$ with the Racah parameter B ($= \frac{9}{441}F^2 - \frac{5}{441}F^4$) and the expectation value of L . Its application to several metallic substances shows encouraging results[53] but fails in some cases.[54]

Solovyev *et al.*[48] have pointed out that the Brooks interpretation of the open-shell HF energy is incorrect and proposed a different theory for the OP mechanism. By examining the HF total energy of some simple cases, they analytically showed that, for the proportional constant of $\langle L \rangle^2$, in addition to B , there exist F^0 and other Slater integrals. They criticize the success of the Brooks theory in some metallic magnets as follows: F^0 is strongly renormalized due to the screening effect in metals and F^0 -dependent term will be almost canceling out via other terms, with leaving only the B term alone. Thus the OP mechanism proposed by Brooks is one of the limiting cases of general mechanism and they argued that the “hidden parameter” responsible for the orbital enhancement in solids is the renormalized F^0 .

To emphasize this concept, they demonstrated the F^0 dependence of μ_{orb} of CoO and showed that the orbital magnetism (the magnitude, direction, and localization of the orbital moment) is directly related with the appearance of the band gap caused by the large F^0 . The offered example of CoO, however, seems to be rather exceptional case for the purpose of

Table 6.1: Parameter values used in the calculation. All in units of eV. Parameters for the intra-atomic interactions, ζ_{3d} , F^2 , and F^4 are obtained from the *ab initio* atomic HF calculation with assuming the Fe configuration $(3d)^6(4s)^2$. The Slater integrals, F^2 and F^4 , are renormalized to 80% of their *ab initio* values.

$dd\sigma$	$dd\pi$	$dd\delta$	ζ_{3d}	F^2	F^4
-0.3780	0.1705	-0.0211	0.050	8.5066	5.2724

examining the OP mechanism in solids, because its result is concerned with the discontinuity of the magnetic quantities in the course of the metal-insulator transition. Once the band gap opens, μ_{orb} of the $3d$ electrons is well described by the ligand-field theory and it takes a large magnitude, which can be deduced from the orbital degeneracy in a given crystal field and the spin-orbit interaction. In order to make a more general discussion about the mechanism of OP in solids, a detailed examination in *metallic* phase seems to be desirable.

In this chapter, we would investigate the role of F^0 in the orbital magnetism in solids, by using the tight-binding HF method with preparing *metallic* $3d$ bands. For simplicity, we consider an fcc lattice with single site in the unit cell. As the valence band, only a $3d$ orbital is taken into account. Hence no valence fluctuation occurs; the occupation number of the atomic $3d$ orbital of a specific site, n_{3d} , is always integer. It is shown that μ_{orb} is very sensitive to F^0 even in metallic phase.

6.2 Model

We consider an idealized crystal, whose structure is fcc and unit cell contains single site. The valence band is constructed by a $3d$ orbital alone. The Hamiltonian is given by

$$H = H_{\text{TB}} + H_{\text{so}} + H_{\text{ee}}, \quad (6.1)$$

where H_{TB} is the tight-binding Hamiltonian that expresses the $3d$ -electron hopping in the fcc lattice; H_{so} and H_{ee} are the on-site interactions, i.e., the $3d$ spin-orbit interaction and the multipole $3d$ - $3d$ Coulomb interaction treated by the HF approximation, respectively. For the explicit form of each Hamiltonian, we refer to the previous chapters. Parameter values used in the calculation are summarized in Table 6.1. H_{TB} alone, with the listed hopping integrals, reproduces the typical fcc feature in the density of states (DOS), as shown in Fig. 6.1. As for the parameters concerned about the on-site interactions, we took them from those of the neutral iron atom. For a given F^0 and n_{3d} , the Hamiltonian (6.1) is solved

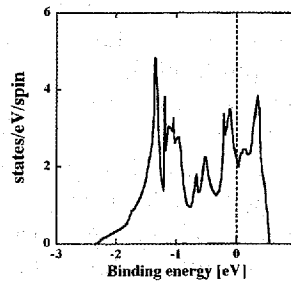


Figure 6.1: Density of states reproduced by H_{TB} for the single-site fcc structure. The Fermi level, denoted by the vertical broken line, is for $n_{3d} = 7$.

in the momentum representation, with assuming the ferromagnetic order. The quantization axis is taken as the z axis (cubic c axis).

6.3 Calculated results

6.3.1 $n_{3d} = 7$

First of all, we would show the calculated results for $n_{3d} = 7$. Figure 6.2 shows the spin-resolved DOS obtained for different values of F^0 . In all cases, the down-spin states

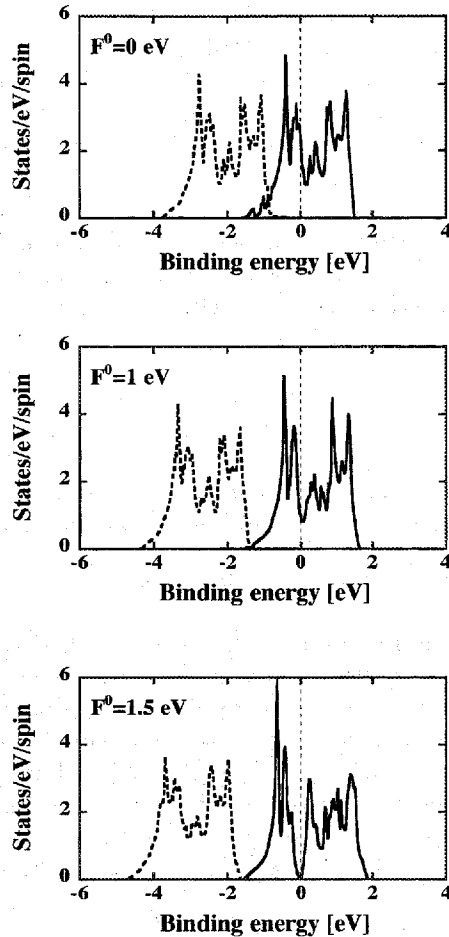


Figure 6.2: Spin-resolved DOS for several F^0 values, with assuming $n_{3d} = 7$. Solid and broken lines refer to the minority (up)-spin DOS and majority (down)-spin DOS, respectively. The Fermi level is denoted by the vertical broken line.

are well pushed below the Fermi level (E_F) and fully occupied. Between the two results of $F^0 = 0$ and 1 eV, no significant change is seen in the shape of DOS except that the down-spin states in $F^0 = 1$ eV located lower in energy than those of $F^0 = 0$ eV. When F^0 exceeds 1 eV, a pseudo gap begins opening in the vicinity of E_F , though there exists a small but finite state density at E_F and it is still remaining for the value of F^0 being up to several electron volts.

Calculated S and L with sweeping F^0 are shown in Fig. 6.3(a). They are obtained by

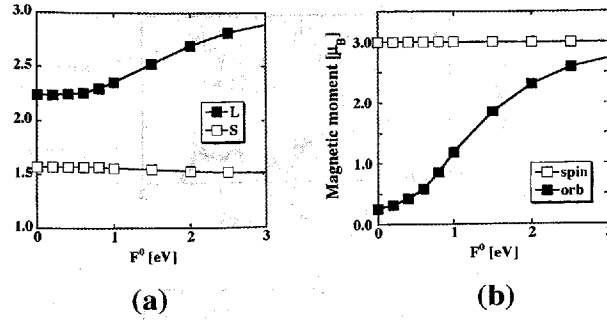


Figure 6.3: Calculated magnetic quantities for $n_{3d} = 7$, with sweeping F^0 : (a) S (open squares) and L (filled squares); (b) μ_{spin} (open squares) and μ_{orb} (filled squares).

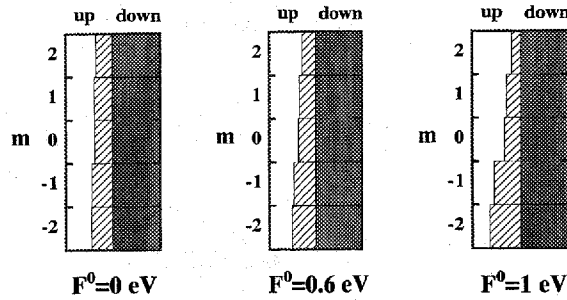


Figure 6.4: The way of electron occupation in the $m\sigma$ basis (m is the orbital magnetic quantum number), for $n_{3d} = 7$ and for several values of F^0 . The shaded or hatched area shows the probability of electron occupation of each $m\sigma$ state.

calculating the expectation values, $\langle S^2 \rangle$ and $\langle L^2 \rangle$, and from the relations $S(S+1) = \langle S^2 \rangle$ and $L(L+1) = \langle L^2 \rangle$. As far as the system keeps the well-metallic behavior ($F^0 \leq 1$ eV), i.e., in the case there is no pseudo gap, L is rather insensitive to the change of F^0 . Once the pseudo gap opens ($F^0 > 1$ eV), L begins to increase toward the atomic Hund rule value $L = 3$. The orbital magnetic moment $\mu_{\text{orb}} = -\mu_B \langle L_z \rangle$, displayed in Fig. 6.3(b), shows a behavior different from that of L . Even in the region of $F^0 \leq 1$ eV, where L is almost constant, μ_{orb} is very sensitive to the change of F^0 and strongly enhanced with increasing F^0 . This clearly indicates that one of the major factors for the orbital polarization in solids, even in the metallic phase, is the enhancement mechanism through the monopole Coulomb interaction.

In the present case, where the electron filling is more than half and the majority-spin states are fully occupied, μ_{spin} is constant and μ_{orb} is determined by the way of electron population in the fivefold minority(up)-spin states. From Fig. 6.4, one can recognize that the symmetry breaking in the electron population among the up-spin states becomes stronger for the larger value of F^0 ; the states with $m = -2$ and -1 come to be occupied preferentially (m is the orbital magnetic quantum number). To see in detail what happens in the course of sweeping F^0 , partial components in the minority-spin DOS, with $m = -2$ substate and its counterpart $m = 2$, are displayed in Fig. 6.5 for several values of F^0 . In the case of $F^0 = 0$ eV, both sub-DOS's are distributed broadly in the wide energy range and overlap with each other, resulting in a considerable cancellation of the orbital moment. In turning on and increasing the value of F^0 , a remarkable change is seen in each sub-DOS while the total DOS does not change its shape greatly. In the limit of the large F^0 , most part of the

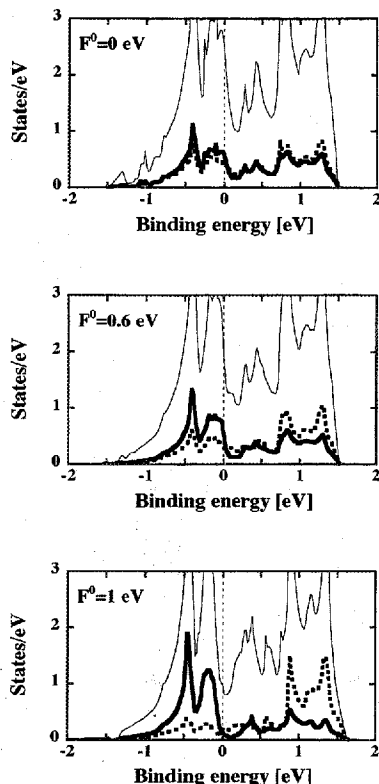


Figure 6.5: Partial DOS specified by the orbital magnetic quantum number $m = -2$ (thick solid line) and $m = 2$ (thick broken line) in the minority-spin state density (thin solid line), for $n_{3d} = 7$ and for several values of F^0 .

$m = 2$ sub-DOS is well pushed up above E_F , while that of the $m = -2$ state is located below E_F . A pair of sub-DOS's with $m = \pm 1$ exhibits almost the same trend.

6.3.2 $n_{3d} = 2$

Calculated magnetic quantities, with assuming $n_{3d} = 2$, are represented in Fig. 6.6, as a function of F^0 . Due to the less than half filling, the directions of μ_{spin} and μ_{orb} are opposite. As enlarging the value of F^0 , the magnitude of μ_{orb} , which is fairly smaller than μ_{spin} for moderately small F^0 , begins increasing and finally overcomes the contribution of μ_{spin} . L and μ_{orb} show the analogous behavior to the case of $n_{3d} = 7$. In the range $0 \leq F^0 \leq 1$ eV, the value of L is rather insensitive to F^0 , whereas μ_{orb} shows the significant change. From Fig. 6.7, one can recognize that the this energy range of F^0 , $0 \leq F^0 \leq 1$ eV, corresponds to the situation that the system reveals the well-metallic behavior, i.e., there is no pseudo gap at E_F . Again, the change of μ_{orb} is interpreted as the redistribution of sub-DOS's between the positive and negative m states while the majority-spin DOS itself, which is the sum of each m -state density, is kept almost unchanged. (See the right hand side figures in Fig. 6.7.)

In the present calculation all of the minority-spin DOS is located above E_F . The mixing of different spin states never occurs. This feature is retained to the infinite limit of F^0 . The atomic electronic structure, which is discussed in detail in Chap. 1, must be recalled here. We have seen that the ground-state electron-population in the $m\sigma$ basis should be distributed into both spin states, for the free 3d ions with the less than half filling. Atomic

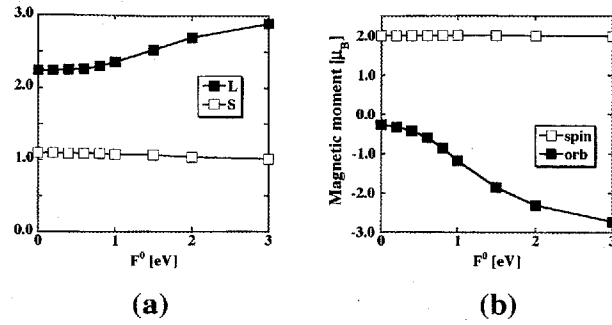


Figure 6.6: Calculated magnetic quantities for $n_{3d} = 2$, with sweeping F^0 : (a) S (open squares) and L (filled squares); (b) μ_{spin} (open squares) and μ_{orb} (filled squares).

HFA fails to describe this spin mixing. In the present solid case, the result for the large F^0 limit is clearly wrong; the calculated magnetic quantities do not approach the corresponding atomic ones. Obviously this is due to the shortcomings of HFA and the many-body effect beyond HFA is necessary to obtain the true ground state. In the range of small F^0 , however, it is not clear whether the present calculation that shows no spin mixing is well describing the real system or not.

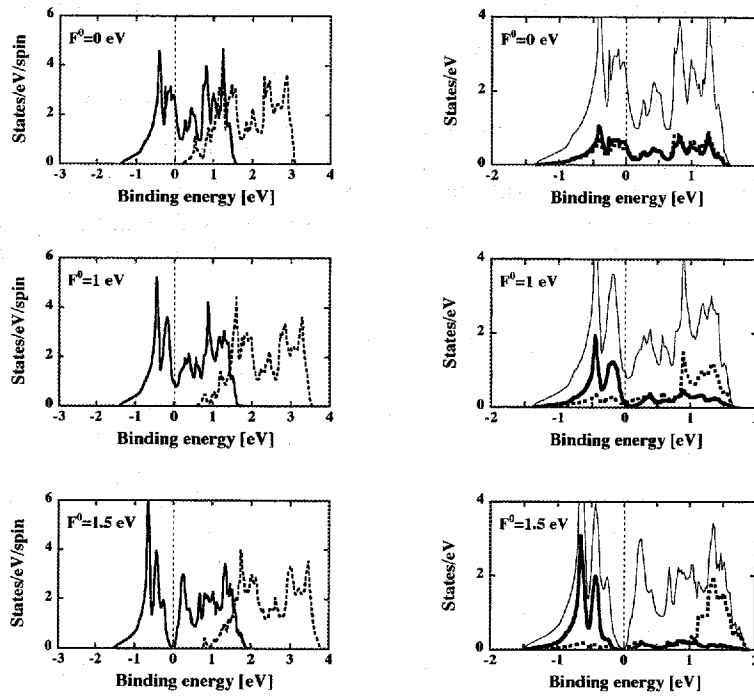


Figure 6.7: Calculated DOS's in the $n_{3d} = 2$ case for various values of F^0 : from the top-side panel, $F^0 = 0, 1,$ and 1.5 eV, respectively. The left hand side figures are the spin-resolved DOS's with solid (broken) line representing the majority (minority)-spin DOS. In the right hand side figures, the majority-spin DOS's are decomposed into the substates with $m = +2$ (thick solid line) and $m = -2$ (thick broken line).

6.3.3 Another filling case

Calculated results for all filling cases are summarized in Figs. 6.8 and 6.9. Here we have just presented the orbital-related quantities, L and μ_{orb} . The spin-related ones are insensitive to the change of F^0 , and we would not show that. The result for $n_{3d} = 8$ shows almost the same one as $n_{3d} = 7$, and $n_{3d} = 3$ case is similar to $n_{3d} = 2$ case.

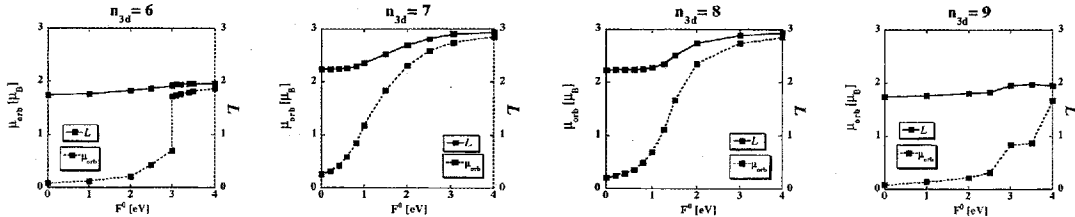


Figure 6.8: Orbital-related magnetic quantities in the more than half filling case. Solid and broken lines refer to the orbital angular momentum L and the orbital magnetic moment μ_{orb} , respectively.

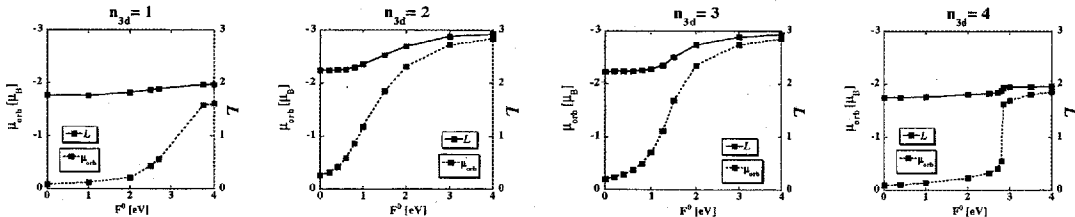


Figure 6.9: Same as Fig. 6.8, but in the less than half filling case.

6.4 Discussions and Conclusions

From the calculations in this chapter, it becomes clear that μ_{orb} in solids is very sensitive to the value of F^0 , even in the metallic phase. It is well known that, among the intra-atomic interactions, the spin-orbit interaction in solids is not so different from the atomic one, and that the screening effect on the Slater integrals is rather weak except F^0 . [55] On the other hand, the monopole Coulomb interaction, expressed by F^0 , is to be greatly screened in solids due to the many-body effect, especially in the metallic phase. [56] The degree of this screening effect is expected to have a strong material-dependence. This effect is to be directly reflected in the orbital moment through its strong sensitivity to the value of F^0 . It can be said that “the way of renormalization of F^0 due to the electron-correlation effect” is one of the significant mechanisms for the enhancement of μ_{orb} in solids, which differs every material.

Is it possible to give an intuitive discussion about the F^0 -driven orbital-enhancement mechanism? If we had treated the present Hubbard model within the many-body scheme, the scenario is rather easy. Roughly speaking, F^0/W , where W is the band width, governs the degree of localization of electrons. In increasing F^0/W , the time scale, for which an electron stays in a specific site, becomes longer. In this period the electron will suffer the spin-orbit interaction and move around the nucleus, resulting in making the orbital moment.

Then the question is whether or not this scenario can be still verified in the mean-field scheme. In our calculations based on HFA, μ_{orb} actually depends on the value of F^0 .

This suggests that the electron-localization mechanism due to F^0 may be reproduced in HFA at least to some extent. In HFA, the exchange interaction is treated exactly, and “the nonphysical self-interaction”, which exists in LDA scheme, is completely excluded. As a result, the electrons in the occupied states feel the electrostatic potential from $N - 1$ electrons other than himself, while the electrons in the unoccupied states feel the potential from total N electrons. This differentiation of Coulomb potential seems to be essential in describing the electron localization in the mean-field scheme.

Chapter 7

Electronic structure of US

Part of this chapter is based on a manuscript by Tatsuya Shishidou, Tamio Oguchi, and Takeo Jo, accepted for publication in *Physical Review B* **59** (1999).

Abstract

The U $5f$ spin (μ_{spin}) and orbital (μ_{orb}) magnetic moments in the ferromagnetic compound US are calculated on the basis of the Hartree-Fock approximation (HFA) for an extended Hubbard model. Our tight-binding model includes the U $6p$, $5f$, $6d$, and $7s$ orbitals and the S $3s$, $3p$, and $3d$ ones, and the intra-atomic $5f$ - $5f$ multipole interaction and the spin-orbit interaction in the $5f$ state are taken into account. Most of parameters involved in the model are determined by fitting with the energy of Bloch electrons in the paramagnetic state obtained by a first-principles calculation based on the local density approximation (LDA). The calculated ratio of the moments $\mu_{\text{orb}}/\mu_{\text{spin}}$ of -2.1 and μ_{orb} of $-3.2\mu_{\text{B}}$ are in good agreement with available experimental results. The calculated magnetic circular dichroism spectrum at the U $3d \rightarrow 5f$ x-ray absorption also agrees with the recent experiment. It is shown that the exact exchange potential gained by HFA mixes different spin states strongly and enhances the effect of the spin-orbit interaction. Problems of LDA in the estimation of μ_{orb} are discussed in detail.

7.1 Introduction

In magnets, the atomic spin (μ_{spin}) and orbital (μ_{orb}) magnetic moments are basic quantities and their separate determination is therefore important. As methods of their experimental determination, the traditional gyromagnetic ratio measurement,[57] the magnetic form factor measurement in the neutron scattering[58] and the magnetic x-ray scattering[59] are known. In addition to these, the recently developed magnetic circular dichroism (MCD) in the core-to-valence x-ray absorption combined with several sum rules[2, 3] has attracted much attention as a method of site- and symmetry-selective determination of μ_{spin} and μ_{orb} . On the theoretical side, the first principles local density approximation (LDA) or local spin-density approximation (LSDA) (Ref. [13]) is known to be a typical method of calculating magnetic quantities and has been successfully applied to various substances. It is, however, known that there are limitations or problems in LSDA.[60]

One of major known problems related to magnetic quantities in LSDA is seen in the underestimation of μ_{orb} in magnets. Even in $3d$ transition metals (Fe, Co, and Ni) where μ_{orb} is quite small compared to μ_{spin} , the LSDA underestimates the contribution of μ_{orb} by about

a factor of 2 especially in Co.[14, 15, 16, 17] The problem becomes more serious in $5f$ systems, i.e., actinide compounds, where the spin-orbit interaction (SOI) among $5f$ electrons is much stronger and μ_{orb} is generally larger. Recent LSDA calculations for uranium compounds seem to underestimate μ_{orb} . [19, 20, 21] In LSDA, the Kohn-Sham equation is described by a local potential including the spin-dependent electron density. The electric current, which describes μ_{orb} , is, however, not included in it. This means that although μ_{spin} is self-consistently determined in LSDA, there is no framework to determine μ_{orb} self-consistently.

In an atom, its ground state of valence shell is, according to Hund's rule, specified by the maximum of the total spin of valence electrons S and the maximum of the total orbital momentum L among the maximum S multiplets. The maximum S is well understood as a consequence of the exchange interaction to align the spin of electrons. The maximum L arises from the multipole exchange interaction represented by the Gaunt coefficient [61] without relying on the SOI, which determines the relative direction between S and L . The local exchange-correlation potential in LSDA seems to be insufficient to describe the maximum L , which is considered to be one of causes of the underestimation of μ_{orb} in solids.

Numerous attempts have been made to estimate μ_{orb} , which are roughly classified into two categories. One is based on the so-called current-density-functional theory [35, 36, 37] that intended to extend the density-functional theory to include the orbital current as an extra degree of freedom, which describes μ_{orb} . Unfortunately an explicit form of the contribution of the current density is at present unknown. Its application to the ferromagnetic Co with the use of a simplified form is, however, not necessarily encouraging. [38] The other category includes the orbital polarization (OP), [20, 53, 54, 62] self-interaction correction (SIC), [63] and LDA+ U (Ref. [48]) approaches, which intended to calculate μ_{orb} practically. For a better description of μ_{orb} , the OP functional form of $-\frac{1}{2}B\langle L_z \rangle^2$ with the Racah parameter B has been deduced [20] from an atomic multiplet ground state without SOI, whose S and L are given by Hund's rules. However, the OP method does not assure us that it will give a good description when the SOI is included and thus S and L are no longer good quantum numbers. A serious problem can be seen in its application to Ce. [54] The $4f$ ground state of magnetic Ce^{3+} ion is, if an infinitesimal magnetic field is applied in the z direction, given by $(j, j_z) = (5/2, 5/2)$, whose wave function is given by a linear combination as $\sqrt{6/7}|3, \downarrow\rangle - \sqrt{1/7}|2, \uparrow\rangle$, where $|m, \sigma\rangle$ denotes the $4f$ state with the magnetic quantum number m and spin σ . The OP result for a large volume limit (i.e., the atomic limit) shows that the $(m = 3, \sigma = \downarrow)$ subband is filled leaving all the other $4f$ states empty; the OP method fails to describe the mixture of the spin states. The same situation is observed in the application of the SIC to Ce. [63] Furthermore, the uncertainty in the application of the OP method to solids is discussed by Solovyev *et al.* with examining the Hartree-Fock (HF) total energy in detail. [48] In solids, as discussed in Chap. 6, μ_{orb} is very sensitive to and dependent on the magnitude of the monopole Coulomb interaction F^0 , while such mechanism is not taken into account in the Brooks formalism.

In the recent LDA+ U approach with the correction term U to LDA, which has the same form as the HF potential and satisfies the rotational invariance, [48] on the other hand, Solovyev *et al.* have succeeded in reproducing a large magnitude of μ_{orb} for Fe and Co atoms ($\sim 1\mu_B$) in the antiferromagnets FeO and CoO, respectively. We have also, by the same HF calculation on the basis of an extended Hubbard model for CoO, succeeded in reproducing μ_{orb} of Co. [64] This means that a faithful HF calculation can be, if an appropriate multi-orbital tight-binding Hamiltonian is prepared, a promising practical method to reproduce the magnitude of μ_{orb} in systems with a large orbital moment. At present, the role of exchange interaction in discussing the magnitude of μ_{orb} , however, does not seem to be discussed from a general point of view.

The purpose of this paper is to investigate how important the exact treatment of the exchange potential is in realizing correct large orbital magnetism in itinerant ferromagnets. For this purpose, ferromagnetic U compounds are the most suitable substances for a severe

test because μ_{orb} is quite large as mentioned above compared with $3d$ compounds. We choose US as a prototype of itinerant U ferromagnets and investigate its magnetic ground state and μ_{orb} under the HF approximation. Our model is the so-called extended Hubbard model, where we consider all the relevant valence-band orbitals and full degeneracy of them. The SOI among the $5f$ electrons is explicitly included and the intra-atomic multipole Coulomb interaction between the $5f$ electrons is treated within the HF approximation.

US is a ferromagnet with Curie temperature being 178 K. Despite rather simple NaCl-type cubic structure, a strong magnetic anisotropy favoring the [111] alignment has been observed.[65, 66, 67] A bulk magnetization measurement[68] shows the ordered moment is $1.55\mu_{\text{B}}$ per unit formula and a neutron scattering measurement[69] shows a slightly larger value of $1.70\mu_{\text{B}}$, which is assigned to the $5f$ magnetic moment. These values are far smaller than that expected for the free ion, indicating that some sort of “solid-state effect” takes place on the $5f$ states. From several experimental results (for instance, photoemission,[70] electrical resistivity,[71] pressure dependence of Curie temperature[72] and specific heat measurements[73, 74]), the $5f$ electrons of US are considered to be itinerant. On the theoretical side, Kraft *et al.* have performed an LSDA calculation with the SOI in a second variational treatment for ferromagnetic U monochalcogenides (US, USe, and UTe), and have shown that the magnitude of the calculated μ_{orb} is larger than that of μ_{spin} and they couple in an antiparallel way to each other.[19] However, the magnitude of the total magnetic moment ($\mu_{\text{spin}} + \mu_{\text{orb}}$) is too small compared to the experimental data, indicating that the calculated μ_{orb} is not large enough. In addition to LSDA, the OP approach[20] and a kind of HF calculation[75] have also been performed for US, about which we will discuss later. We will show that the HF calculation including the expectation values of the off-diagonal operators as well as the number operators with the $|m, \sigma\rangle$ basis in the exchange interaction is crucial in describing the magnetic quantities and wave function.

In Sec. 7.2, we formulate our multiband tight-binding HF model. In Sec. 7.3, calculated results and discussions are presented. To confirm the validity of the $5f$ magnetic state in our model, we also calculate the x-ray MCD spectrum at the U $M_{4,5}$ edge (U $3d \rightarrow 5f$ dipole transition) and compare it with the recent experimental result.[27] The difference in the exchange potential between the HF and LSDA is discussed in detail. Section 7.4 is devoted to conclusions.

7.2 Formulation

7.2.1 Hamiltonian

We consider a realistic multiband Hubbard model defined by

$$H = H^0 + E^0 + Z + H_I, \quad (7.1)$$

where H^0 stands for the electron-hopping energy, which is expressed by the tight-binding method, and the orbital energies other than the $5f$ state. We consider all the valence-band-related orbitals and the full degeneracy of them. We take into account $6p$, $5f$, $6d$, and $7s$ orbitals for the U atom, and $3s$, $3p$, and $3d$ ones for the S atom. The hopping integrals are treated within the Slater-Koster two-center approximation.[28] Other terms in Eq. (7.1) are defined as follows:

$$E^0 = \sum_{i\Gamma\sigma} \sum_{\gamma(\in\Gamma)} \varepsilon_{\Gamma}^0 f_{i\Gamma\gamma\sigma}^+ f_{i\Gamma\gamma\sigma}, \quad (7.2)$$

$$Z = \zeta_{5f} \sum_i \sum_{\nu_1\nu_2} \langle i\nu_1 | \mathbf{l} \cdot \mathbf{s} | i\nu_2 \rangle f_{i\nu_1}^+ f_{i\nu_2}, \quad (7.3)$$

$$H_I = \frac{1}{2} \sum_i \sum_{\nu_1 \nu_2 \nu_3 \nu_4} g(\nu_1 \nu_2 \nu_3 \nu_4) f_{i\nu_1}^+ f_{i\nu_2}^+ f_{i\nu_3} f_{i\nu_4}. \quad (7.4)$$

E^0 describes the $5f$ orbital energy, where ε_Γ^0 stands for the bare on-site energy of the $5f$ state with the orbital symmetry Γ ($\Gamma = T_{1u}, T_{2u}, A_{2u}$). γ is the sub-basis of Γ . The operator $f_{i\Gamma\gamma\sigma}$ denotes the annihilation of a $5f$ electron with the orbital state $\Gamma\gamma$ and the spin σ on the i th U site. Z is the SOI among the U $5f$ electrons with a coupling constant ζ_{5f} . The symbol ν specifies both of the orbital magnetic quantum number (m) and spin one (σ); $\Gamma\gamma$ is a linear combination of m . H_I represents the intra-atomic $5f$ - $5f$ multipole interaction on the U sites. The interaction matrix element $g(\nu_1 \nu_2 \nu_3 \nu_4)$ is written[61] in terms of the Slater integrals F^k 's ($k = 0, 2, 4, 6$) and the Gaunt coefficients $c^k(l_1 m_1, l_2 m_2)$'s as follows:

$$\begin{aligned} g(\nu_1 \nu_2 \nu_3 \nu_4) &= \left\langle \nu_1 \nu_2 \left| \frac{1}{r_{12}} \right| \nu_3 \nu_4 \right\rangle \\ &= \delta_{\sigma_1, \sigma_3} \delta_{\sigma_2, \sigma_4} \delta_{m_1 + m_2, m_3 + m_4} \sum_{k=0,2,4,6} F^k c^k(3 m_1, 3 m_3) c^k(3 m_4, 3 m_2). \end{aligned} \quad (7.5)$$

We employ the HF approximation to the interaction term as

$$H_I^{\text{HF}} = \sum_i \sum_{\nu_1 \nu_2 \nu_3 \nu_4} [g(\nu_1 \nu_2 \nu_3 \nu_4) - g(\nu_1 \nu_2 \nu_4 \nu_3)] \langle f_{i\nu_2}^+ f_{i\nu_4} \rangle f_{i\nu_1}^+ f_{i\nu_3}. \quad (7.6)$$

The expectation value $\langle f_\nu^+ f_\nu \rangle$ is the HF order parameter which should be determined self-consistently. Hereafter we assume a ferromagnetic ordering and drop the site index i from $\langle f_{i\nu}^+ f_{i\nu} \rangle$. We take into account not only the 14 diagonal order parameters but also 91 ($= {}_{14}C_2$) off-diagonal ones. The inclusion of the spin-off-diagonal parts of the HF order parameters and the form of the exchange potential in Eq. (7.6) play an important role in describing the $5f$ state as will be discussed later.

7.2.2 A test of HF approximation in the atomic limit

Before applying the present model to US, we discuss the validity of the HF approximation in describing the $5f$ magnetic ground state. In the limit of the hopping integrals in H^0 being zero, the system becomes isolated atoms (or ions) and we can easily examine the single-determinant HF approximation in the following way. For the electron configuration of $5f^2$ (U^{4+}) or $5f^3$ (U^{3+}), we solve the HF Hamiltonian of a U atom, $Z + H_I^{\text{HF}}$, by the self-consistent iteration to obtain a polarized solution by including a small magnetic field in the first cycle. On the other hand, we can straightforwardly and exactly solve the original Hamiltonian without the mean-field approximation $Z + H_I$ by the configuration-interaction (CI) scheme setting up all the possible many-body bases (all the possible Slater determinants) for a given electron configuration and by performing a numerical diagonalization. Due to the strong SOI, the ground state is not given by the simple Hund rule LS coupling but a mixture of more than one LS multiplet of a given J , i.e., the intermediate coupling. The used parameters[27] and the calculated μ_{spin} , μ_{orb} , and the z component of the magnetic dipole $\langle T_z \rangle$ ($\mathbf{T} = \sum_i [\mathbf{s}_i - 3\mathbf{r}_i(\mathbf{r}_i \cdot \mathbf{s}_i)/r_i^2]$, where \mathbf{s}_i and \mathbf{r}_i are the spin operator and position vector of the i th $5f$ electron, respectively) are listed in Table 7.1. The positive direction of the quantization axis is taken as along the direction of μ_{spin} . Relative deviations of the HF result from the CI one are shown to be less than 15% for all magnetic quantities even though the HF approximation does not consider any correlation effects. Obviously, the HF approximation can be a good starting point for describing the U $5f$ magnetic ground state.

Table 7.1: The $5f$ magnetic state of a free U ion with the $5f^2$ or $5f^3$ electron configuration, calculated by the configuration-interaction (CI) method and HF method. μ_{spin} (μ_{orb}) represents the spin (orbital) magnetic moment, and $\mu_{5f} = \mu_{\text{spin}} + \mu_{\text{orb}}$. $\langle T_z \rangle$ is the expectation value of the z component of the magnetic dipole. The upper panel shows the results for the $5f^2$ configuration, and the middle $5f^3$. Deviations of the HF result from the CI one are represented in parentheses in percentage. Magnetic moments μ_{5f} , μ_{spin} , and μ_{orb} are in units of μ_B . Used parameters (Slater integrals F^k 's, coupling constant ζ_{5f} of the SOI) are also shown in the lower panel in eV.

$5f^2$ (U^{4+})	μ_{5f}	μ_{spin}	μ_{orb}	$\mu_{\text{orb}}/\mu_{\text{spin}}$	$\langle T_z \rangle$
CI	-3.30	1.40	-4.70	-3.36	-0.81
HF	-3.26	1.48	-4.74	-3.21	-0.81
	(-1)	(6)	(1)	(5)	(0)
$5f^3$ (U^{3+})	μ_{5f}	μ_{spin}	μ_{orb}	$\mu_{\text{orb}}/\mu_{\text{spin}}$	$\langle T_z \rangle$
CI	-3.41	2.18	-5.59	-2.56	-0.63
HF	-3.25	2.49	-5.75	-2.30	-0.60
	(-5)	(14)	(3)	(-10)	(-4)
		F^2	F^4	F^6	ζ_{5f}
$5f^2$ (U^{4+})		7.611	4.979	3.655	0.261
$5f^3$ (U^{3+})		7.086	4.598	3.363	0.235

7.2.3 Determination of the parameter values

Let us discuss our method to determine the parameters that appear in the Hamiltonian (7.1). It is well known that one can estimate F^k 's (except F^0) from *ab initio* atomic HF value with an appropriate reduction factor[55, 76] around 0.8 which stems from the intra-atomic correlation (configuration-interaction) effect and that thus the obtained F^k 's are usually usable even in solids. The ordinary *ab initio* atomic values of F^k 's and ζ_{5f} were obtained from Cowan's HF program with relativistic correction,[23] where ζ_{5f} was calculated by the Blume-Watson method.[77, 78] The assumed electron configuration was the neutral atomic one, $5f^3 6d^1 7s^2$, since it may be suitable rather than ionic ones due to the fact that US is a good conductor. Norman[55] has evaluated the reduction factors for each F^k 's in U^{4+} ion in a semiphenomenological manner assuming the Yukawa screened Coulomb interaction. Expecting that such factors will hardly change between the neutral and ionic configurations, we set the reduction factors of our case around Norman's, namely, 0.65, 0.85, and 0.9 for $k=2, 4$, and 6, respectively. Thus determined parameters are $F^2 = 5.530$, $F^4 = 4.669$, $F^6 = 2.881$, and $\zeta_{5f} = 0.226$ in units of eV. Even if we adopt a common reduction factor around 0.8, the essence of calculated results is found to be unchanged. As the monopole integral F^0 , which is associated with the multiplet-averaged effective Coulomb interaction U_{ff} by $U_{ff} = F^0 - 4F^2/195 - 2F^4/143 - 100F^6/5577$, is hard to be evaluated due to a strong screening in solids, we leave it as an adjustable parameter.

H^0 and E^0 in Eq. (7.1) contain a number of parameters which are related to the electron kinetic energies: the hopping integrals and orbital energies. These parameters are determined by fitting with the energy dispersion in the paramagnetic state without the SOI (hereafter we call this the P state) obtained by a first-principles LDA calculation with the full-potential linear augmented plane wave (FLAPW) method.[79] We have mentioned the problems about the LDA, but such problems will be suppressed in the P state, where there is no spin or orbital polarization, and we suppose that the LDA will give a good description.

Table 7.2: The determined orbital energies and Slater-Koster two center hopping integrals in units of eV. Note that the U 5*f* orbital energy is not a *bare* one, i.e., the listed value includes the LDA 5*f*-5*f* potential. See text for details.

		orbital energy						
U 6 <i>p</i>	-2.8632							(<i>T</i> _{1<i>u</i>})
U 5 <i>f</i>	14.1689			13.9655		13.6751		(<i>T</i> _{1<i>u</i>} <i>T</i> _{2<i>u</i>} <i>A</i> _{2<i>u</i>})
U 6 <i>d</i>	17.6525			18.7905				(<i>T</i> _{2<i>g</i>} <i>E</i> _{<i>g</i>})
U 7 <i>s</i>	19.0819							(<i>A</i> _{1<i>u</i>})
S 3 <i>s</i>	-0.6562							(<i>A</i> _{1<i>u</i>})
S 3 <i>p</i>	10.6073							(<i>T</i> _{1<i>u</i>})
S 3 <i>d</i>	22.3455			26.4753				(<i>T</i> _{2<i>g</i>} <i>E</i> _{<i>g</i>})
		1st neighbor			2nd neighbor			
	σ	π	δ	ϕ	σ	π	δ	ϕ
U 6 <i>p</i> -U 6 <i>p</i>	0.2777	0.1475			-1.1020	-0.0099		
U 5 <i>f</i> -U 5 <i>f</i>	0.0728	-0.0366	0.0354	-0.0161				
U 6 <i>d</i> -U 6 <i>d</i>	-0.4291	-0.2321	0.0027		-0.2881	0.0598	0.0372	
U 7 <i>s</i> -U 7 <i>s</i>	-1.0413				0.1603			
S 3 <i>s</i> -S 3 <i>s</i>	0.4011				0.3336			
S 3 <i>p</i> -S 3 <i>p</i>	-0.0082	-0.1497			-0.2205	-0.0499		
S 3 <i>d</i> -S 3 <i>d</i>	0.2779	0.6844	-0.2751		1.1180	0.5992	0.0803	
U 7 <i>s</i> -U 6 <i>p</i>	0.0569				0.7437			
U 7 <i>s</i> -U 6 <i>d</i>	-0.8546				0.2269			
U 7 <i>s</i> -U 5 <i>f</i>	0.3891				0.2523			
U 6 <i>p</i> -U 6 <i>d</i>	-0.1994	-0.2928			0.5572	-0.2317		
U 6 <i>p</i> -U 5 <i>f</i>	-0.2949	-0.3951						
U 6 <i>d</i> -U 5 <i>f</i>	0.3006	0.1199	-0.0058		0.0053	-0.1009	0.0413	
S 3 <i>s</i> -S 3 <i>p</i>	-0.2414				0.3784			
S 3 <i>s</i> -S 3 <i>d</i>	-0.7523				-0.2572			
S 3 <i>p</i> -S 3 <i>d</i>	-0.2674	0.4882			1.3945	0.0573		
S 3 <i>s</i> -U 7 <i>s</i>	1.2161				0.1338			
S 3 <i>s</i> -U 6 <i>p</i>	-1.2198				0.1983			
S 3 <i>s</i> -U 6 <i>d</i>	0.4495				-0.4976			
S 3 <i>s</i> -U 5 <i>f</i>	-0.1444				0.5565			
U 7 <i>s</i> -S 3 <i>p</i>	1.5471				-0.2284			
U 7 <i>s</i> -S 3 <i>d</i>	1.8403				-0.1833			
U 6 <i>p</i> -S 3 <i>p</i>	1.2666	0.6178			-0.2784	0.2641		
U 6 <i>p</i> -S 3 <i>d</i>	-4.7589	-0.4079			-0.5586	-0.3287		
S 3 <i>p</i> -U 6 <i>d</i>	-2.3538	0.5853			0.2697	0.0386		
S 3 <i>p</i> -U 5 <i>f</i>	0.8317	-0.4441			-0.0445	-0.0217		
U 6 <i>d</i> -S 3 <i>d</i>	-1.5566	1.9167	-0.6830		-0.2243	0.3985	-0.1864	
S 3 <i>d</i> -U 5 <i>f</i>	1.1760	-0.6893	-0.4226		0.0573	-0.0589	0.0170	

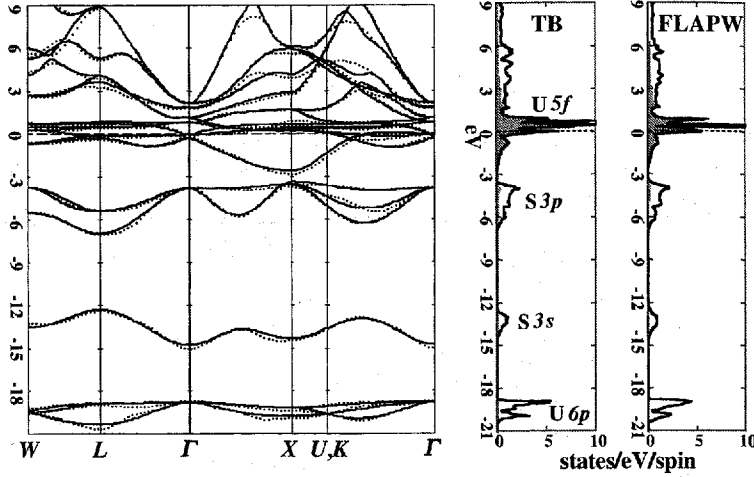


Figure 7.1: Band structure in the paramagnetic state without the SOI (the P state). The left hand side is the band dispersion along the highly symmetric lines of fcc. The solid line shows the FLAPW dispersion and the dotted line represents the fitted one. The vertical axis is the energy measured from the Fermi level in unit of eV. The right hand side is the calculated density of states based on our tight-binding model and also on the FLAPW method. The shaded area represents the U $5f$ partial DOS. See text for details.

To carry out the fitting, we consider the following Hamiltonian in place of Eq. (7.1):

$$H' = H^0 + E, \quad (7.7)$$

here note that Z and H_I are dropped and that the term of the $5f$ orbital energy E differs from E^0 of Eq. (7.2) in the point that ε_Γ^0 is replaced by ε_Γ . Since the symmetry is completely cubic in the P state, the potential energy for the $5f$ state arising from the intra-atomic $5f$ - $5f$ interaction is diagonal in the representation $\Gamma\gamma$ and is included in ε_Γ ; the original ε_Γ^0 is the *bare* on-site energy in the sense that the mean field coming from the interaction among the $5f$ electrons is not counted, whereas ε_Γ includes that. H' is fitted to the FLAPW result for the lowest 20 bands (without spin) at irreducible 29 k points in the Brillouin zone and also at 47 k points along the highly symmetric lines of fcc. A nonlinear least-square fitting problem is solved by the Taylor-series expansion method.[80] The fitted energy dispersion of electrons is shown in Fig. 7.1 and the obtained parameters are listed in Table 7.2. For simplicity, we have ignored the overlap of the atomic orbitals of the tight-binding basis. Nevertheless the fitting quality is rather good. The calculated density of states (DOS) displayed in Fig. 7.1 reproduces the result of FLAPW reasonably. We shall explain the electronic structure in the P state briefly. In the DOS, three lumps can be seen below the Fermi energy (E_F). Each one is mainly composed of the U $6p$, S $3s$, and S $3p$ states, from the deeper binding energy toward E_F , respectively. The sharp structure around E_F is derived from the U $5f$ state, which is embedded in the rather broad U $6d$ DOS and well hybridized with this itinerant state. Although the nearest-neighboring (NN) atom of U is S, the hybridization between U $5f$ and S $3p$ is relatively weak because the energy position of S $3p$ state is detached far from E_F . (However, the U d state is well hybridized with S $3p$ state.) This clearly indicates that the itinerancy of the $5f$ electrons originates from the hybridization with the U $6d$ orbitals of the next-nearest-neighboring (NNN) U atoms. The atomic radius of the chalcogen governs the NNN distance and thus the degree of localization of the $5f$ electrons. This picture explains the experimental fact that for the larger atomic radius of the chalcogen (S, Se, and Te) the saturated magnetic moment becomes larger (1.55 , 1.8 , and $1.9\mu_B$ per unit formula,

respectively), that is, the degree of localization becomes stronger.

For dealing with the ferromagnetic state with the SOI, we should determine the *bare* 5*f* orbital energy ε_{Γ}^0 by subtracting the LDA potential energy, which is arising from the intra-atomic 5*f*-5*f* interaction, from ε_{Γ} . This procedure is to prevent us from double counting the *f*-*f* interaction in the subsequent HF calculation. The LDA potential energy of the *f*-*f* interaction L_{Γ} can be divided into two parts; $L_{\Gamma} = C_{\Gamma} - V$, where C_{Γ} is the classical Coulomb part (i.e., the Hartree part) and is exactly the same as that of the HF [the first term of Eq. (7.6)]. It is written in terms of the order parameters $\langle f_{\nu}^{\dagger} f_{\nu'} \rangle$ in the *P* state, which are already known from H' , and the Slater integrals F^k 's, which are already determined except F^0 . This means that once we choose a specific value for F^0 we can readily evaluate C_{Γ} . The term $-V$ stands for the exchange-correlation part and we assume that it has no Γ dependence. This quantity is hard to be evaluated and we treat it as an adjustable parameter. Moreover, in the ferromagnetic state with the SOI, ε_{Γ}^0 will differ from that of the *P* state to keep the charge neutrality. This change of ε_{Γ}^0 will not be small because the SOI for the 5*f* state is very strong. We impose such change of the 5*f* orbital energy on the unknown parameter V .

Finally our Hamiltonian for US in the ferromagnetic state is given by

$$H = H^0 + E^0(F^0, V) + Z + H_I^{\text{HF}}(F^0), \quad (7.8)$$

where $E^0(F^0, V)$ denotes Eq. (7.2) with $\varepsilon_{\Gamma}^0 = \varepsilon_{\Gamma} - C_{\Gamma}(F^0) + V$, and $H_I^{\text{HF}}(F^0)$ is given by Eq. (7.6) and depends on the unknown parameter F^0 . There are two adjustable parameters, F^0 and V . To determine them we simply assume that the 5*f* electron number n_{5f} shows no change between the *P* and the ferromagnetic state, and we choose V for a given F^0 so that $n_{5f} = 2.88$, which coincides with that of the *P* state obtained from H' . The FLAPW calculation shows a little change in n_{5f} , namely, it increases by only 0.2 from the value in the *P* state. Even if we choose V which gives a difference in n_{5f} between the *P* state and the ferromagnetic one, our main results are found to be insensitive to the choice of V . Then we choose F^0 so as to set the 5*f* magnetic moment to be the experimental value $-1.70\mu_{\text{B}}$. [69] Thus we can determine F^0 and V and examine the individual moments of the 5*f* state, μ_{spin} and μ_{orb} . The adopted assumptions and treatments might be rather reasonable ones for qualitative discussions on whether or not the large μ_{orb} can be obtained with using the HF exact exchange potential and what is absent in the usual LSDA calculation. We believe that the employed assumptions will not affect the essential physics.

Computational details in the self-consistent calculation is as follows. For a given set of parameters, the Hamiltonian (7.8) is solved in the momentum representation. Uniformly spaced 1000 k points are sampled in the Brillouin zone. Interpolation between meshes is done by the tetrahedron method.[81] The convergence of the HF order parameters is that the root mean square sum of the differences of each order parameter between the last two steps is less than 10^{-7} . The quantization axis is taken as along the [111] direction, i.e., the experimental easy axis except for a discussion on the magnetic anisotropy.

7.3 Results and Discussions

7.3.1 Magnetic ground state

Before determining the value of F^0 , variation of the calculated quantities with sweeping F^0 is studied. Figure 7.2 displays (a) the 5*f* magnetic moment μ_{5f} , (b) the ratio of μ_{orb} to μ_{spin} of the 5*f* moment, (c) the individual μ_{spin} and μ_{orb} , (d) the expectation value of the 5*f* magnetic dipole $\langle T_z \rangle$, and (e) the constant potential V for the 5*f* orbital. For a given F^0 , V has been chosen so that the 5*f* electron number n_{5f} becomes 2.88. As shown in (c), the absolute values of the individual μ_{spin} and μ_{orb} increase as a function of F^0 , but

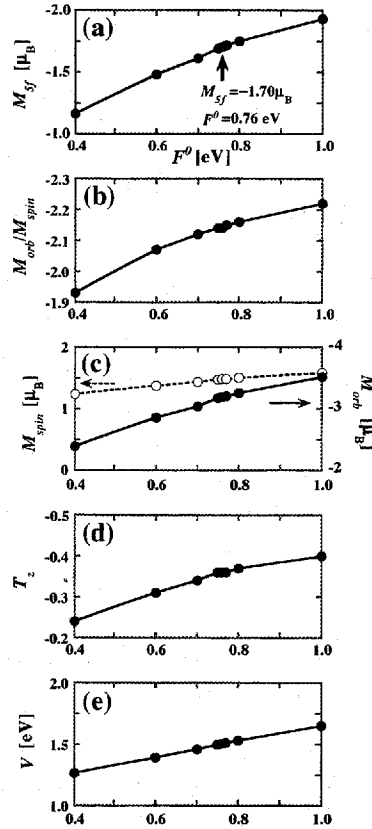


Figure 7.2: The calculated quantities with sweeping F^0 . From the top side of panels, (a) the $5f$ magnetic moment, (b) the ratio $\mu_{\text{orb}}/\mu_{\text{spin}}$ of the $5f$ moment, (c) the individual moments μ_{spin} (open circle with broken line) and μ_{orb} (closed circle with solid line), (d) the $5f$ magnetic dipole (T_z), and (e) the constant potential V .

μ_{spin} is rather insensitive to F^0 , and μ_{orb} almost determines the change of $\mu_{\text{orb}}/\mu_{\text{spin}}$. This tendency is the same as the metallic $3d$ systems discussed in Chap. 6; again, μ_{orb} has a strong F^0 -sensitivity. For $F^0 = 0.76$ eV, μ_{5f} becomes $-1.70\mu_{\text{B}}$ [indicated by an arrow in (a)], which coincides with the result of the neutron scattering,[69] and thus we use this value of F^0 according to our prescription mentioned in the last section. At this point, $\mu_{\text{orb}}/\mu_{\text{spin}}$ is -2.14 , and the individual moments are $\mu_{\text{spin}} = 1.49\mu_{\text{B}}$, $\mu_{\text{orb}} = -3.19\mu_{\text{B}}$, and $\langle T_z \rangle = -0.36$, and the constant potential $V = 1.505$ eV.

For comparison, we list up results of previous band structure calculations for US in Table 7.3. The results based on the conventional LSDA with the SOI through a second variation reveal a too small absolute value of μ_{5f} compared to the experimental $-1.7\mu_{\text{B}}$ and the magnitude of $\mu_{\text{orb}}/\mu_{\text{spin}}$ is smaller than our HF result.[82] Brooks[20] applied the orbital polarization (OP) method and obtained a large magnitude of μ_{orb} and a considerable improvement in μ_{5f} . However, they have stated that the individual magnitudes of μ_{spin} and μ_{orb} are considered to be too large from the analysis of the magnetic form factor.[75] To improve the OP method, Severin *et al.* examined a spin(σ) and magnetic quantum number(m)-diagonal HF exchange potential and scaled it to the size of the corresponding LSDA exchange potential.[75] Their results have a strong resemblance to ours, although they have ignored the spin-off-diagonal elements, which are fully taken into account in our method. This enigma will be discussed later. In the results of the neutron scattering

Table 7.3: Magnetic ground state of the $5f$ orbital by various band structure calculations. Magnetic moments μ_{5f} , μ_{spin} , and μ_{orb} are in units of μ_{B} .

Method		Author	μ_{5f}	$\mu_{\text{orb}}/\mu_{\text{spin}}$	μ_{spin}	μ_{orb}
LSDA+SOI _{2nd}	FLAPW	Oguchi (Ref. [79])	-0.55	-1.33	1.66	-2.21
LSDA+SOI _{2nd}	ASW	Kraft <i>et al.</i> (Ref. [19])	-1.1	-1.73	1.5	-2.6
LSDA+SOI _{2nd}	LMTO	Brooks (Ref. [20])	-1.1	-1.52	2.1	-3.2
OP	LMTO	Brooks (Ref. [20])	-1.8	-1.82	2.2	-4.0
OP (scaled HF)		Severin <i>et al.</i> (Ref. [75])	-1.61	-2.07	1.51	-3.12
HF	TB	present	(-1.70)	-2.14	1.49	-3.19
spin-diag. HF	TB	present	-1.56	-1.87	1.78	-3.34
neutron measurement		Wedgwood (Ref. [69])	-1.7	(-2.3)	(1.31)	(-3.0)

measurement by Wedgwood[69] in Table 7.3, the values in parenthesis are taken from an analysis by Severin *et al.*[75] Our individual moments are in a qualitative agreement with these values.

US is well known to show the largest magnetic anisotropy among cubic materials.[65, 66, 67] It strongly favors a [111] alignment and its saturated moment is about 1.7 times as large as that of the hard axis [001]. We try to examine this anisotropy in the present framework. Table 7.4 shows calculated results (the $5f$ electron number, $5f$ magnetic moment, and total energy) for various quantization axes with the same parameters; F^0 and V are fixed to those determined for the magnetization in the [111] direction. μ_{5f} is strongly dependent on the axis and the calculated tendency about the easy and hard magnetization axis is in accordance with the experimental results, although the change of n_{5f} is less than 0.03. The calculated total energy for each axis shows that the [111] direction is the easy axis as expected from the calculated tendency of μ_{5f} . Even if we determine the value of V so as to give $n_{5f} = 2.88$ for the magnetization in the [001] direction, the tendency of μ_{5f} and the total energy shown in Table 7.4 is found to be unchanged.

Table 7.4: The quantization-axis dependence of the $5f$ electron number, $5f$ magnetic moment, and total energy. The total energy is measured with referring to the energy for the [111] axis.

axis	n_{5f}	μ_{5f} [μ_{B}]	total energy [meV]
[111]	2.88	-1.70	0
[110]	2.87	-1.51	7.5
[001]	2.85	-1.28	12.6

7.3.2 U $M_{4,5}$ MCD spectrum

To see whether or not our model describes the magnetic ground state of US, we investigate magnetic circular dichroism (MCD) in x-ray core-photoabsorption spectroscopy (XAS). Discovery of the so-called orbital[2] and spin[3] sum rules, which directly relate $\langle S_z \rangle$ ($= -\mu_{\text{spin}}/2\mu_{\text{B}}$), $\langle L_z \rangle$ ($= -\mu_{\text{orb}}/\mu_{\text{B}}$) and $\langle T_z \rangle$ of a specific site to simple integrations of measured spectra, have led MCD into a powerful technique for studying ferromagnets. Recently, Collins *et al.* have measured the MCD spectrum of US at the U $M_{4,5}$ edge (U $3d$

core $\rightarrow 5f$ photoabsorption) by using hard x-ray.[27] Their spectra show some characteristic features: (i) pairs of $3d$ core spin-orbit-split peaks (M_4 and M_5 edges) are separated by about 170 eV, which is sufficiently larger than the magnitude of the $3d$ - $5f$ exchange interaction, (ii) the XAS spectrum shows a simple line shape with no clear multiplet or satellite structure, (iii) in both of the M_4 and M_5 regions, the MCD shows positive signals in almost entire photon energies, (iv) the MCD intensity in the M_5 region is very small compared to the M_4 , (v) finally, in the M_5 region, a small negative *splinter* is observed just above the large positive peak in the MCD spectrum.

The feature (i) indicates that the total angular momentum of the $3d$ core spin-orbit multiplet ($j_c = 3/2$ and $5/2$) is a good quantum number in the photoexcited final states. The feature (iii) is considered to be due to the large magnitude of μ_{orb} since the same feature has been seen in the Pt $L_{2,3}$ MCD of CrPt₃, where μ_{orb} dominates the Pt $5d$ magnetic moment.[83, 84, 85] An atomic multiplet calculation[27] can well reproduce the features (ii), (iii), and (iv), but may not explain the feature (v), indicating that some “*solid-state effect*” takes place in the $5f$ state. According to the sum rules,[2, 3] the branching ratio of MCD spectrum in $d \rightarrow f$ transition is related to the ground state magnetic moments by

$$R_{\text{MCD}} \equiv \frac{\int_{M_5} d\omega (I^{-1} - I^{+1})}{\int_{M_4} d\omega (I^{-1} - I^{+1})} = \frac{5}{2} \frac{\langle L_z \rangle}{\langle L_z \rangle - 2\langle S_z \rangle - 6\langle T_z \rangle} - 1, \quad (7.9)$$

where I^κ denotes the absorption coefficient with the photon helicity κ ($\kappa = \pm 1$). If the $\langle T_z \rangle$ term is negligible in Eq. (7.9), one can directly determine $\mu_{\text{orb}}/\mu_{\text{spin}}$ from the experimental integrated intensity ratio R_{MCD} and examine our theoretical value of $\mu_{\text{orb}}/\mu_{\text{spin}}$, but unfortunately, $\langle T_z \rangle$ is generally very large in U systems. Therefore, it could be a severe check for our HF ground state whether our framework can reproduce the value of R_{MCD} itself and the line shape of the U $M_{4,5}$ MCD spectrum, especially the feature (v). The XAS spectrum with the photon helicity κ and energy ω can be calculated as

$$I^\kappa(\omega) = \frac{2\pi}{\hbar} \sum_{E_{kn} > E_F} \sum_c |\langle \psi_{kn} | t^\kappa | \psi_c \rangle|^2 \delta(E_{kn} - E_c - \omega), \quad (7.10)$$

where ψ_{kn} is the HF one-electron valence state with momentum \mathbf{k} , band index n and energy E_{kn} , and ψ_c is the U core $3d$ state with energy E_c , which is split into $j_c = 3/2$ and $5/2$, and the operator t^κ denotes the intra-atomic $3d \rightarrow 5f$ dipole transition with the photon helicity κ . Here, we have ignored the photon energy dependence of t^κ . The summation about ψ_{kn} is taken over all unoccupied states. We have also ignored a core-valence interaction in the final state, which in general leads to a multiplet structure in the spectrum. In our case, however, the feature (ii) indicates that such an interaction is very weak. In fact, the multipole Slater integrals $F^k(3d, 5f)$ and $G^k(3d, 5f)$ are very small,[27] justifying our approximation.

Figure 7.3 shows the calculated XAS and MCD spectra. They have been convoluted by using Lorentzians with FWHM of 4.0 eV, which represent the $3d$ core hole lifetime broadening.[27] The XAS spectra show a simple peak structure, and the MCD spectra reveal positive sign for almost entire photon energies. Note that the intensity of the M_5 MCD is multiplied by 5, namely, it is fairly small compared to the M_4 region. More noteworthy is the appearance of a small negative *splinter* in the M_5 MCD, as experimentally observed as the feature (v), which cannot be obtained by the atomic multiplet calculation. All experimental line shape features can be reproduced well by our present calculation. The experimental branching ratio of the MCD defined by Eq. (7.9), $R_{\text{MCD}} = M_5/M_4$, is 0.13 ± 0.03 , while our result is 0.169. Reasonable agreement for both of the line shape and branching ratio is obtained between our calculation and the experiments by Collins *et al.*[27] It is interesting to clarify the origin of the characteristic features in the MCD line shape, the small branching ratio and the small negative *splinter* in the M_5 region. Both of them can be understood qualitatively by inspecting the $5f$ partial DOS which is projected into the total angular

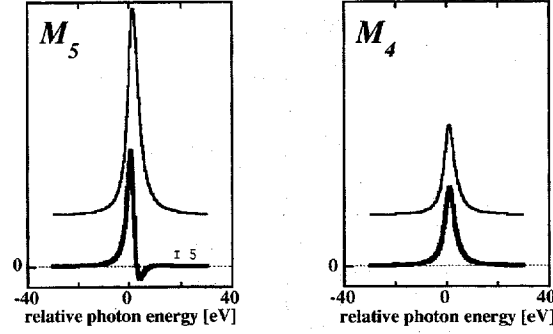


Figure 7.3: Calculated XAS and MCD spectra of US at the U $M_{4,5}$ edge ($3d \rightarrow 5f$). Thin line denotes the polarization-averaged XAS spectrum, $(I^{-1} + I^{+1})/2$. Thick line represents the MCD spectrum, $I^{-1} - I^{+1}$. The left (right) side of figures corresponds to the M_5 (M_4) region. The zero point of the photon energy of each figure is set to $E_F - E_{j_c}$. Lorentzian convolutions with FWHM of 4.0 eV are used to include the core lifetime broadening. Note that the MCD spectrum in the M_5 region is multiplied by 5.

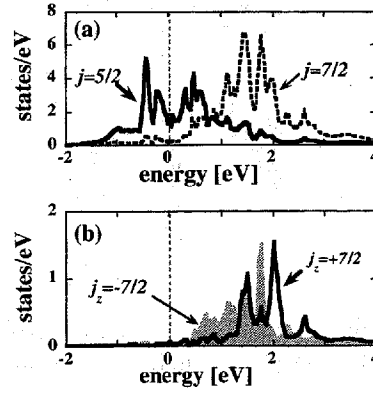


Figure 7.4: The $5f$ partial DOS projected into the j bases: (a) the solid line denotes the $5f$ DOS of $j = 5/2$ and the broken one that of $j = 7/2$, (b) among the $j = 7/2$ states, the individual $j_z = 7/2$ ($j_z = -7/2$) DOS is represented by the solid line (shaded area).

momentum of the $5f$ state, $j = 5/2$ and $7/2$, and the transition probability of the $d \rightarrow f$ dipole excitation. The $5f$ DOS is displayed in Fig. 7.4(a). Although j is not a good quantum number for the $5f$ states, most of the $j = 7/2$ states are well pushed up above E_F and the magnetic $5f$ state is almost determined by an electron population among the sixfold $j = 5/2$ states. Figure 7.5 shows the distribution of the electron population in the j basis. Among the $j = 5/2$ bases, $j_z = 5/2$, $3/2$, and $1/2$ states have large occupations, which leads to the large magnitude of μ_{orb} that is coupled antiparallel to μ_{spin} . Figure 7.6 shows the j_z dependence of weights of the transition probability in the $d \rightarrow f$ photoabsorption. In the $3d_{5/2}$ (M_5) edge, we have a large weight of transition into the $j = 7/2$ states, which are almost unoccupied by electrons, and large absorption intensity is expected for both of I^{-1} and I^{+1} , and the magnitude of their difference $|I^{-1} - I^{+1}|$ becomes small. The small negative *splitter* in the M_5 MCD can be explained by considering the energy position of each DOS among $j = 7/2$ bases. In Fig. 7.4(b), the $j_z = -7/2$ ($+7/2$) state has the largest weight of transition with $\kappa = -1$ ($+1$) photon. DOS for all other bases which have negative

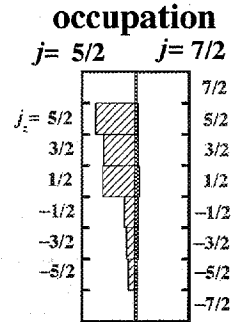


Figure 7.5: The $5f$ electron occupation projected into the j bases. The left side is for $j = 5/2$ (hatched rectangle), and right, $j = 7/2$ (solid rectangle).

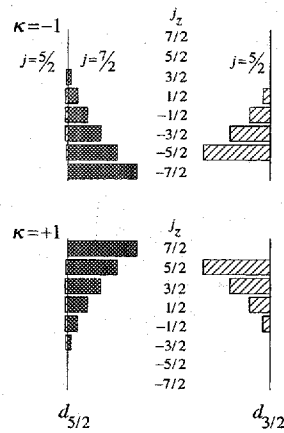


Figure 7.6: The j_z dependence of weights of the transition probability into the f states $|jj_z\rangle$ in the $d \rightarrow f$ photoabsorption by the photon helicity κ ($\kappa = \pm 1$) for each of the core $d_{5/2}$ and $d_{3/2}$ branches.

(positive) j_z , has a strong resemblance to that of $j_z = -7/2$ ($+7/2$). A difference in the energy position between negative and positive j_z DOS causes an asymmetric dispersive MCD line shape; the small negative *splinter* appears just above the positive peak. Next, in the $3d_{3/2}$ (M_4) edge, we have a large weight of transition into the $j = 5/2$ states where $j_z = 5/2$, $3/2$ and $1/2$ are mainly occupied and others are almost empty. In Figs. 7.5 and 7.6, we can expect that the absorption with $\kappa = -1$ is strong because the states with the large weight of transition are almost empty, and that, on the other hand, the absorption with $\kappa = +1$ is weak because vacant seats for the transition are quite few. The MCD, $I^{-1} - I^{+1}$, in the M_4 edge, then, becomes large. Thus the obtained characteristic features in the MCD spectrum are qualitatively understood.

7.3.3 HF and LSDA

We shall discuss in detail the difference between the HF exchange potential and that of the LSDA. From Eqs. (7.5) and (7.6), the exchange part of the HF Hamiltonian can be

Table 7.5: Upper: the absolute values of the spin-off-diagonal matrix elements of the exchange part of the converged HF Hamiltonian in units of eV. Lower: the spin-off-diagonal matrix elements of the spin-orbit interaction among the 5*f* electrons in units of $\zeta_{5f}/2$. The basis of matrices is the spin state σ and the magnetic quantum number m of the 5*f* state.

		↑						
		-3	-2	-1	0	1	2	3
↓	-3	0	0	0.01	0	0	0	0
	-2	0.06	0	0	0.01	0	0	0
	-1	0	0.14	0	0	0.02	0	0
	0	0	0	0.12	0	0	0.01	0
	1	0.04	0	0	0.31	0	0	0.01
	2	0	0.07	0	0	0.25	0	0
	3	0	0	0.04	0	0	0.24	0
	3	0	0	0.04	0	0	0.24	0

		↑						
		-3	-2	-1	0	1	2	3
↓	-3							
	-2	$\sqrt{6}$						
	-1		$\sqrt{10}$					
	0			$\sqrt{12}$				
	1				$\sqrt{12}$			
	2					$\sqrt{10}$		
	3						$\sqrt{6}$	
	3						$\sqrt{6}$	

rewritten as

$$H_X = - \sum_{m_1 m_2 m'_1 m'_2} \left\langle m_1 m_2 \left| \frac{1}{r_{12}} \right| m'_2 m'_1 \right\rangle \sum_{\sigma_1 \sigma_2} \langle f_{m_2 \sigma_2}^+ f_{m'_2 \sigma_1} \rangle f_{m_1 \sigma_1}^+ f_{m'_1 \sigma_2} \quad (7.11)$$

with carrying out the integration in the spin space. Two important aspects about the HF exact exchange potential can be revealed from Eq. (7.11). In the first place, it has a *spin-off-diagonal element (spin-flip term)* $\sigma_1 \neq \sigma_2$, that is, the exchange interaction may mix the spin-up and spin-down states. Since we are considering a situation with the SOI, the self-consistent one-electron state will be a combination of the different spin bases. In such a case, the HF order parameter in Eq. (7.11) in general have a finite value even for $\sigma_1 \neq \sigma_2$. Table 7.5 shows the spin-off-diagonal matrix elements of the converged H_X . Here we simply displayed the absolute values of them although they are actually complex numbers. It can be seen that the columns and rows with larger matrix elements well correspond to those where the spin-off-diagonal matrix element of the SOI has a finite value (the matrix elements of the SOI are displayed also in Table 7.5) and that their magnitude (0.1–0.3 eV) is comparable to that of the SOI, $\sqrt{12} \zeta_{5f}/2 \simeq 0.4$ eV. Thus the exact exchange potential clearly *enhances the effect of the SOI* and *mixes strongly the spin-up and spin-down states*. This feature is not seen in the LSDA exchange potential, since it is a spin-diagonal potential. Needless to say, the effect of the spin-off-diagonal elements, i.e., the correct exchange potential is not taken into account in LSDA, which causes an insufficient mixing between the spin-up and spin-down states. In order to emphasize this point, we shall artificially remove the spin-off-diagonal elements from the HF potential and see what happens. With this restriction and with the same parameters, we calculate again the ground state self-consistently. The results are as follows: $n_{5f} = 2.85$, $\mu_{5f} = -1.56\mu_B$, $\mu_{\text{orb}}/\mu_{\text{spin}} = -1.87$, $\mu_{\text{spin}} = 1.78\mu_B$, $\mu_{\text{orb}} = -3.34\mu_B$,

and $\langle T_z \rangle = -0.22$. A great change can be seen in $\langle T_z \rangle$, that is, its magnitude is about 60% of that of the exact one. μ_{5f} , μ_{spin} and μ_{orb} are quantities which are obtained by the *diagonal* summation in σ and m basis so that they are relatively insensitive to the extinction of the spin-off-diagonal exchange potential. $\langle T_z \rangle$ is, on the other hand, considered to be sensitive to that, because it has a form of $T_z = \sum_i \left\{ \sqrt{3/2} \left[c_1^{(2)}(\mathbf{r}_i) s_{i-} - c_{-1}^{(2)}(\mathbf{r}_i) s_{i+} \right] - 2c_0^{(2)}(\mathbf{r}_i) s_{iz} \right\}$ with $c_m^{(k)}(\mathbf{r}_i) = \sqrt{4\pi/(2k+1)} Y_{km}(\mathbf{r}_i)$ with the spin-flip terms. Thus $\langle T_z \rangle$ will reflect the extent of the spin-up and spin-down mixing in ψ_{kn} . This change in $\langle T_z \rangle$ readily influences the branching ratio of MCD. In fact, R_{MCD} becomes 0.292, which is far larger than the experimental result 0.13 ± 0.03 . Even if the parameters F^0 and V are chosen so that $n_{5f} = 2.88$ and $\mu_{5f} = -1.70\mu_{\text{B}}$, the results of $\langle T_z \rangle$ and R_{MCD} are not improved; $\langle T_z \rangle = -0.24$ and $R_{\text{MCD}} = 0.302$. Severin *et al.* seem to have obtained fairly reasonable results for μ_{5f} and individual moments[75] although they have not considered the spin-off-diagonal terms in the exchange potential. It is debatable whether the character of each one-electron state or $\langle T_z \rangle$ is appropriately described in their framework.

In the second place, there is a strong orbital dependence in the exact exchange potential. In the LSDA, the spin-up and spin-down states are split more or less uniformly, because the exchange potential for the spin σ state has a rather simple form as $n_\sigma^{1/3}(\mathbf{r})$, where $n_\sigma(\mathbf{r})$ is the total charge density with the spin σ , and the corresponding matrix elements within the f states hardly have an orbital dependence. The diagonal matrix element of Eq. (7.11) with respect to m and σ is $(H_X)_{m\sigma, m\sigma} = -\sum_{m'} \langle mm' | 1/r_{12} | m'm \rangle \langle f_{m'\sigma}^+ f_{m'\sigma} \rangle$ and it is m dependent. In fact, the converged H_X for the U $5f$ state of US shows that for the minority spin it varies from -0.3 to -0.4 eV, whereas for the majority spin it varies widely from -0.7 to -1.8 eV, showing the strong m dependence. This is essential in realizing the large orbital magnetic moment.

We conclude that these characteristic features of the exact exchange potential, which are missing in the LSDA, are crucial in the estimation of μ_{orb} . We may say that the underestimation of μ_{orb} in the LSDA approach arises from its insufficient treatment of the exchange interaction and not from its insufficiency in describing the correlation effect.

7.4 Conclusions

We have calculated μ_{spin} and μ_{orb} of the $5f$ state and the MCD spectrum in the U $3d \rightarrow 5f$ x-ray absorption for ferromagnetic US on the basis of the HF approximation for an extended Hubbard model. The model includes the U $6p$, $5f$, $6d$, and $7s$ orbitals and the S $3s$, $3p$, and $3d$ orbitals, and the intra-atomic $5f$ - $5f$ multipole interaction and the $5f$ spin-orbit interaction, most of parameters of which are determined by fitting with the result of the first-principles LDA calculation in the paramagnetic state. The calculated ratio $\mu_{\text{orb}}/\mu_{\text{spin}}$ of -2.1 and μ_{orb} of $-3.2\mu_{\text{B}}$ are in good agreement with available experimental results. The calculated MCD spectrum in the U $3d \rightarrow 5f$ absorption also agrees with the recent experiment.

We have shown that, for the $5f$ electrons specified by the magnetic quantum number m and spin σ , the m -dependent potential and the spin-off-diagonal matrix element, both of which arise from a faithful HF approximation, are crucially important in estimating especially μ_{orb} and $\langle T_z \rangle$ and in obtaining the reasonable wave function. By a comparison between the present HF calculation and LSDA, an insufficiency in describing the exchange interaction in LSDA is pointed out to be a major cause of its underestimation of μ_{orb} , which is seen not only in U compounds but also in transition metals such as Co. Although our model contains the adjustable parameters F^0 and V , we expect that the obtained results are not sensitive to details of adopted models.

In this work, we have not discussed the electron-correlation effect, which is not considered

explicitly in the present calculation. In our calculation, we have set the Slater integral $F^0 = 0.76$ eV so as to obtain $\mu_{5f} = -1.70\mu_B$. The adopted F^0 value, however, seems to be too small. Even itinerant $3d$ transition metals such as Fe and Co are considered to have $F^0 \simeq 1$ eV for the $3d$ - $3d$ intra-atomic interaction.[86, 87] It is well known that the stability of magnetic solution is much emphasized in the HF approximation and that the electron-correlation effect is expected to be a suppression of this tendency.[88, 89] With the correlation effect, the driving force for the polarization will be suppressed and we will need a larger value of F^0 so as to obtain $\mu_{5f} = -1.70\mu_B$. Kanamori has discussed the correlation effect in metal considering the multiple scattering between two electrons in bands.[56] According to his argument, the bare intra-atomic Coulomb integral U is strongly reduced by the correlation effect $U_{\text{eff}} \simeq U/(1 + U/W)$, where W is the band width, and the renormalized U_{eff} cannot exceed W . Then the relatively small value of fitted F^0 is not so surprising because our F^0 is the renormalized effective one, on which all correlation effect is imposed, and the intrinsic $5f$ band width in this case is only about 1.5 eV (see Fig. 7.1). Of course a detailed calculation, in which the correlation effect is explicitly considered in some manner, is preferable and must be interesting, but it is out of the present paper and a future problem. Even if such correlation effect is included, we believe that the role of exchange interaction in obtaining the correct ratio $\mu_{\text{orb}}/\mu_{\text{spin}}$, which is discussed above, is unchanged.

The experimental total magnetic moment per formula unit of US is $-1.55\mu_B$ and the difference from the $5f$ moment $0.15\mu_B$ is supposed to be a contribution from the U $6d$ spin moment, which is coupled parallel to the $5f$ μ_{spin} . [90, 91] In our calculation, since the $5f$ - $6d$ exchange interaction is neglected, the $6d$ state contributes only $0.02\mu_B$. In U chalcogenides, the Kerr spectrum due to the $5f$ - $6d$ optical transition has been observed,[92] which will be a future subject of this study by including the $5f$ - $6d$ interaction.

References

- [1] See, for example, Y. Murakami, J.P. Hill, D. Gibbs, M. Blume, I. Koyama, M. Tanaka, H. Kawata, T. Arima, Y. Tokura, K. Hirota, and Y. Endoh, *Phys. Rev. Lett.* **81**, 582 (1998).
- [2] B.T. Thole, P. Carra, F. Sette, and G. van der Laan, *Phys. Rev. Lett.* **28**, 1943 (1992).
- [3] P. Carra, B.T. Thole, M. Altarelli, and X. Wang, *Phys. Rev. Lett.* **70**, 694 (1993).
- [4] A. Kimura, S. Suga, T. Shishidou, S. Imada, T. Muro, S.Y. Park, T. Miyahara, T. Kaneko, and T. Kanomata, *Phys. Rev. B* **56**, 6021 (1997).
- [5] S. Imada, T. Shishidou, T. Muro, S. Suga, H. Maruyama, K. Kobayashi, H. Yamazaki, and T. Kanomata, *Physica B* **237&238**, 369 (1997).
- [6] T. Muro, T. Shishidou, F. Oda, T. Fukawa, H. Yamada, A. Kimura, S. Imada, S. Suga, S.Y. Park, T. Miyahara, and K. Sato, *Phys. Rev. B* **53**, 7055 (1996).
- [7] Y. Teramura, A. Tanaka, and T. Jo, *J. Phys. Soc. Jpn.* **65**, 1053 (1996).
- [8] Y. Teramura, A. Tanaka, B.T. Thole, and T. Jo, *J. Phys. Soc. Jpn.* **65**, 3056 (1996).
- [9] T. Shishidou, S. Imada, T. Muro, F. Oda, A. Kimura, S. Suga, T. Miyahara, T. Kanomata, T. Kaneko, *Phys. Rev. B* **55**, 3749 (1997).
- [10] See, for example, R. Cowan, *The Theory of Atomic Structure and Spectra* (University of California Press, Berkeley, 1981); I. Lindgren and J. Morrison, *Atomic Many-Body Theory* (Springer-Verlag, New York, 1985); P. Fulde, *Electron Correlations in Molecules and Solids* (Springer-Verlag, New York, 1991).
- [11] See, for example, R. Dreizler and E. Gross, *Density Functional Theory* (Springer-Verlag, New York, 1990).
- [12] P. Hohenberg and W. Kohn, *Phys. Rev.* **136**, B864 (1964).
- [13] See, for example, V.L. Moruzzi, J.F. Janak, and A.R. Williams, *Calculated Electronic Properties of Metals* (Pergamon, New York, 1978).
- [14] M. Singh, J. Callaway, and C.S. Wang, *Phys. Rev. B* **14**, 1214 (1976).
- [15] R. Wu, D. Wang, and A.J. Freeman, *Phys. Rev. Lett.* **71**, 3581 (1993).
- [16] R. Wu and A.J. Freeman, *Phys. Rev. Lett.* **73**, 1994 (1994).
- [17] C.T. Chen, Y.U. Idzerda, H.-J. Lin, N.V. Smith, G. Meigs, E. Chaban, G.H. Ho, E. Pellegrin, and F. Sette, *Phys. Rev. Lett.* **75**, 152 (1995).
- [18] H. Yamagami, *J. Phys. Soc. Jpn* **67**, 3176 (1998).

- [19] T. Kraft, P.M. Oppeneer, V.N. Antonov, and H. Eschrig, *Phys. Rev. B* **52**, 3561 (1995).
- [20] M.S.S. Brooks, *Physica B* **130**, 6 (1985).
- [21] P.M. Oppeneer, M.S.S. Brooks, V.N. Antonov, T. Kraft, and H. Eschrig, *Phys. Rev. B* **53**, R10 437 (1996).
- [22] J.C. Slater, *Phys. Rev.* **49**, 537 (1936).
- [23] R. Cowan, *J. Opt. Soc. Am.* **58**, 808 (1968); *The Theory of Atomic Structure and Spectra* (University of California Press, Berkeley, 1981).
- [24] B. Bleaney and K.W.H. Stevens, *Rep. Progr. Phys.* **16**, 108 (1953).
- [25] J. Kanamori, *J. Appl. Phys. Supplement* **31**, 14S (1960).
- [26] J. Kanamori, *Prog. Theor. Phys.* **17**, 197 (1957).
- [27] S.P. Collins, D. Laundry, C.C. Tang, and G. van der Laan, *J. Phys., Condens. Matter* **7**, 9325 (1995).
- [28] J.C. Slater and G.F. Koster, *Phys. Rev.* **94**, 1498 (1954).
- [29] J. H. de Boer and E. J. W. Verwey, *Proc. Phys. Soc. London* **49**, 59 (1937).
- [30] N. F. Mott and R. Peierls, *Proc. Phys. Soc. London* **49**, 72 (1937).
- [31] N. F. Mott, *Metal-Insulator Transitions* (Taylor & Francis, London, 1974).
- [32] K. Terakura, T. Oguchi, A. R. Williams, and J. Kübler, *Phys. Rev. B* **30**, 4734 (1984).
- [33] C. G. Shull, W. A. Strauser, and E. O. Wollan, *Phys. Rev.* **83**, 353 (1951).
- [34] T. Jo and T. Shishidou, *J. Phys. Soc. Jpn.* **67**, 2505 (1998).
- [35] G. Vignale and M. Rasolt, *Phys. Rev. Lett.* **59**, 2360 (1987).
- [36] P. Skudlarski and G. Vignale, *Phys. Rev. B* **48**, 8547 (1993).
- [37] M. Higuchi and A. Hasegawa, *J. Phys. Soc. Jpn.* **66**, 149 (1997).
- [38] H. Ebert, M. Battocletti, and E.K.U. Gross, *Europhys. Lett.* **40**, 545 (1997).
- [39] B. van Laar, *Phys. Rev.* **138**, A584 (1965).
- [40] M. Takahashi and J. Igarashi, *Phys. Rev. B* **54**, 13 566 (1996).
- [41] T. Mizokawa and A. Fujimori, *Phys. Rev. B* **51**, 12 880 (1995).
- [42] T. Shishidou, T. Oguchi, and T. Jo to be published in *Phys. Rev. B* **59** (1999).
- [43] L. M. Sandratskii and J. Kübler, *Phys. Rev. B* **55**, 11 395 (1997).
- [44] K. Hirai, *Physica B* **237&238**, 440 (1997).
- [45] Y. Yamamoto and T. Nagamiya, *J. Phys. Soc. Jpn.* **32**, 1248 (1972).
- [46] T. Jo and K. Hirai, *J. Phys. Soc. Jpn.* **53**, 3183 (1984).
- [47] See, for example, J. Kanamori, *Prog. Theor. Phys.* **17**, 197 (1957).
- [48] I.V. Solovyev, A.I. Liechtenstein, and K. Terakura, *Phys. Rev. Lett.* **80**, 5758 (1998).

- [49] W. L. Roth, *Phys. Rev.* **110**, 1333 (1958).
- [50] D. Herrmann-Ronzaud, P. Burlet, and J. Rossat-Mignod, *J. Phys. C* **11**, 2123 (1978).
- [51] D. C. Khan and R. A. Erickson, *Phys. Rev. B* **1**, 2243 (1970).
- [52] J. H. Van Vleck, *Phys. Rev.* **41**, 208 (1932).
- [53] O. Eriksson, B. Johansson, R.C. Alberts, A.M. Boring, and M.S.S. Brooks, *Phys. Rev. B* **42**, 2707 (1990).
- [54] O. Eriksson, M.S.S. Brooks, and B. Johansson, *Phys. Rev. B* **41**, 7311 (1990).
- [55] M.R. Norman, *Phys. Rev. B* **52**, 1421 (1995).
- [56] J. Kanamori, *Prog. Theor. Phys.* **30**, 275 (1963).
- [57] See, for example, G.G. Scott, *J. Phys. Soc. Jpn.* **17**, 372 (1962).
- [58] W. Marshall and S.W. Lovsey, *Theory of Thermal Neutron Scattering* (Oxford University Press, Oxford, 1971).
- [59] M. Blume, *J. Appl. Phys.* **57**, 3615 (1985).
- [60] R.O. Jones and O. Gunnarsson, *Rev. Mod. Phys.* **61**, 689 (1989).
- [61] See, for example, E.U. Condon and G.H. Shortley, *The Theory of Atomic Spectra* (Cambridge University Press, Cambridge, 1935).
- [62] M.R. Norman, *Phys. Rev. B* **44**, 1364 (1991).
- [63] S.V. Beiden, W.M. Temmerman, Z. Szotek, and G.A. Gehring, *Phys. Rev. Lett.* **79**, 4970 (1997).
- [64] T. Shishidou and T. Jo, *J. Phys. Soc. Jpn.* **67** 2637 (1998).
- [65] D.L. Tillwick and P. de V. du Plessis, *J. Magn. Magn. Mater.* **3**, 319 (1976).
- [66] D.L. Tillwick and P. de V. du Plessis, *J. Magn. Magn. Mater.* **3**, 329 (1976).
- [67] G.H. Lander, M.S.S. Brooks, B. Lebech, P.J. Brown, O. Vogt, and K. Mattenberger, *J. Appl. Phys.* **69**, 4803 (1991).
- [68] G. Busch, O. Vogt, A. Delpalme, and G.H. Lander, *J. Phys. C* **12**, 1391 (1979).
- [69] F.A. Wedgwood, *J. Phys. C* **5**, 2427 (1972).
- [70] B. Reihl, *J. Less-Common Met.* **128**, 331 (1987).
- [71] J. Schoenes, B. Frick, and O. Vogt, *Phys. Rev. B* **30**, 6578 (1984).
- [72] C.Y. Huang, R.J. Laskowski, C.E. Olsen, and J.L. Smith, *J. Physic* **40**, 26 (1979).
- [73] H. Rudigier, H.R. Ott, and O. Vogt, *Phys. Rev. B* **32**, 4584 (1985).
- [74] E.F. Westrum, R.R. Walters, H.E. Flotow, and D.W. Osborne, *J. Chem. Phys.* **48**, 155 (1968).
- [75] L. Severin, M.S.S. Brooks, and B. Johansson, *Phys. Rev. Lett.* **71**, 3214 (1993).
- [76] B.T. Thole, G. van der Laan, J.C. Fuggle, G.A. Sawatzky, R.C. Karnatak, and J.-M. Esteve, *Phys. Rev. B* **32**, 5107 (1985).

- [77] M. Blume and R.E. Watson, Proc. Roy. Soc. London, Ser. A **270**, 122 (1962).
- [78] M. Blume and R.E. Watson, Proc. Roy. Soc. London, Ser. A **271**, 565 (1963).
- [79] T. Oguchi (unpublished).
- [80] L.F. Mattheiss, Phys. Rev. B **5**, 290 (1972).
- [81] P.E. Blöchl, O. Jepsen, and O.K. Andersen, Phys. Rev. B **49**, 16 223 (1994).
- [82] The first three lines of Table 7.3 show rather different results although they are equally based on the same LSDA+SOI scheme. These discrepancies may be attributed to the following reasons. First, the spatial region in which the moments are calculated is different for each method. The FLAPW method employs the muffin-tin sphere to calculate the moments, whose volume is smaller than that of the atomic sphere in the ASW and LMTO methods. The different results between the ASW and LMTO methods may be owing to the difference in the atomic sphere radius, because US is a compound and how to take the radius of the U sphere is not unique. Second, the ASW and LMTO methods apply the spherical approximation to the potential so that the quenching effect on the orbital momentum is artificially suppressed, which leads to a relatively larger magnitude of M_{orb} than that of the FLAPW method. Anyway, regardless of the detailed differences in method, the common feature of the LSDA+SOI calculations is that the magnitudes of M_{5f} and $M_{\text{orb}}/M_{\text{spin}}$ are considerably small compared with the corresponding experimental results, which clearly indicates the intrinsic problem of the LSDA+SOI approach to the orbital magnetism.
- [83] H. Maruyama, F. Matsuoka, K. Kobayashi, and H. Yamazaki, Physica B **208&209**, 787 (1995).
- [84] T. Oguchi, K. Iwashita, and T. Jo, Physica B **237&238**, 374 (1997).
- [85] K. Iwashita, T. Oguchi, and T. Jo, Phys. Rev. B **54**, 1159 (1996).
- [86] E. Antonides, E.C. Janse, and G.A. Sawatzky, Phys. Rev. B **15**, 1669 (1977).
- [87] G. Trégliat, M.C. Desjonquères, F. Ducastelle, and D. Spanjaard, J. Phys. C **14**, 4347 (1981).
- [88] D. Pines, Phys. Rev. **95**, 1090 (1954).
- [89] K.A. Brueckner and K. Sawada, Phys. Rev. **112**, 328 (1958).
- [90] M. Erbudak, F. Greuter, F. Meier, B. Reihl, and J. Keller, Solid State Commun. **30**, 439 (1979).
- [91] F. Greuter, W. Eib, M. Erbudak, F. Meier, and B. Reihl, J. Appl. Phys. **50**, 7483 (1979).
- [92] J. Schoenes, in *Handbook on the Physics and Chemistry of the Actinides*, edited by A.J. Freeman and G.H. Lander (North-Holland, Amsterdam, 1984), Vol. 1, p. 341.

Acknowledgments

First, I would like to present my sincere thanks to Prof. Takeo Jo. He has invited me to this interesting subject and kept encouraged me.

I would also like to thank Prof. Tamio Oguchi for valuable and helpful discussions. I benefited greatly from his expertise and deep insight in the field of band structure calculations. He really helped me in many ways. For instance, making comfortable atmosphere with a good sense of humor and sometimes instructing me in skiing. I also want to acknowledge his family.

I would like to thank Dr. Arata Tanaka. He is a research associate of the Jo laboratory and has been sharing a room with me. I respect his enthusiasm and positive spirit. It was exciting and fruitful to discuss physics with him.

I also appreciate the support and kindness of all members of the Jo and Oguchi laboratory.

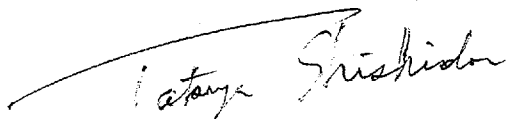
Last summer, in 1998, I have been in France. I would like to thank Dr. Paolo Carra, who helped me during my stay in Grenoble. I'll never forget the great taste of his hand-made Italian seafood pasta.

I would like to thank Dr. J.-C. Parlebas for warm hospitality during my stay in Strasbourg.

When I was a master course student, I worked as an experimenter. I would like to thank Prof. Shigemasa Suga at Osaka University, who was my boss at that time and let me know the delight of physical research. I would thank Dr. Shin Imada, who is a research assistant of the Suga laboratory and told me a lot about the multiplet calculations. I want to thank Drs. A. Kimura, T. Okuda, and T. Muro, who worked together in the Suga laboratory and still give attention to me.

Last, not least, thanks to my parents and my sister who have supported me in many ways.

Higashi-Hiroshima, January 1999,

A handwritten signature in cursive script, reading "Taro Shishido". The signature is written in dark ink and is positioned below the date and location of the letter.